INVESTIGATIONS ON THE RADIATION CHARACTERISTICS OF PLANAR PRINTED UWB ANTENNAS WITH MODIFIED GROUND PLANES

by

Gopikrishna M.

A thesis submitted to

Cochin University of Science and Technology
in partial fulfilment of the
requirements for the degree of
Doctor of Philosophy

Cochin, India

July 2010

Investigations on the Radiation Characteristics of Planar Printed UWB Antennas With Modified Ground Planes

Author:

Gopikrishna M.

Research Fellow

Centre for Research in Electromagnetics and Antennas

Department of Electronics

Cochin University of Science and Technology,

Kochi, 682022, India

E-mail: gopiikrishna@gmail.com

Research Advisor:

Prof. C. K. Aanandan

Department of Electronics

Cochin University of Science and Technology,

Kochi, 682022, India

E-mail: anand@cusat.ac.in

CERTIFICATE

I certify that the research work presented in the thesis entitled ***Investigations on the radiation characteristics of planar printed UWB antennas with modified ground planes*** is based on the original work done by Mr. Gopikrishna M. under my guidance at the Centre for Research in Electromagnetics and Antennas, Dept. of Electronics, Cochin University of Science and Technology, Cochin–22 and has not been included in any other thesis submitted previously for the award of any degree.

Prof. C. K. Aanandan

(Research Advisor)

Department of Electronics

Cochin University of science and Technology

Cochin 682022

DECLARATION

I declare that the work presented in the thesis entitled ***Investigations on the radiation characteristics of planar printed UWB antennas with modified ground planes*** is based on the original work done by me under the guidance and supervision of Dr. C. K. Aanandan, Professor, Department of Electronics, Cochin University of Science and Technology, Cochin–22, India and has not been included in any other thesis submitted previously for the award of any degree.

Gopikrishna M.
Department of Electronics
Cochin University of science and Technology
Cochin 682022

Acknowledgements

The work presented in this thesis would not have been possible without the support of a number of individuals and organizations and I gratefully acknowledge all of them.

I express my sincere thanks to my supervisor Prof. C. K. Aanandan for his insightful advice, consistent encouragement and understanding throughout my doctoral research. My heartfelt thanks are also due to Prof. K. Vasudevan, Prof. P. Mohanan and Prof. P. R. S. Pillai for all genuine guidelines and for providing the perfect milieu for academic activities at Department of Electonics, CUSAT.

Credit for this work must, of course, be shared with people who helped me along the way. Special thanks to Ms. Deepti Das Krishna and Mr. Anupam R. Chandran for all timely help and discussions. My thanks are also due to Mr. Anantha Krishnan, Mr. Paulbert Thomas, Mr. Lindo, Mr. Sujith, Mr. Sarin, Ms. Shameena and Ms. Anju of Department of Electronics; Mr. Manu Punnen John and Mr. Radha Krishnan of Department of Photonics and Department of Physics respectively. I express my gratitude to Mr. Mohanan, Mr. Siraj, Mr. Rajeev, Mr. Nouruddein, Mr. Ibrahim Kutty and Ms. Sudha for providing a harmonious environment for work at the Department of Electronics.

Throughout the course of my research work, I received financial support from the University Grants Commission, India and it is duly acknowledged.

Last, but definitely not least, I thank my parents for all their sacrifices and moral support and my wife Praveena for her encouragements and understanding.

Gopikrishna M.

Abstract

A major challenge in the transmission of narrow pulses is the radiation character-
istics of the antenna. Designing the front ends for UWB systems pose challenges
compared to their narrow and wide band counterparts because in addition to
having electrically small size, high efficiency and band width, the antenna has
to have excellent transient response. The present work deals with the design
of four novel antenna designs- Square Monopole, Semi-Elliptic Slot, Step and
Linear Tapered slot - and an assay on their suitability in UWB systems. Multiple
resonances in the geometry are matched to UWB by redesigning the ground-patch
interfaces. Techniques to avoid narrow band interference is proposed in the
antenna level and their effect on a nano second pulse have also been investigated.
The thesis proposes design guidelines to design the antenna on laminates of any
permittivity and the analyzes are complete with results in the frequency and time
domains.

Table of Contents

List of Tables

List of Figures

Acronyms

AUT	Antenna Under Test
BPSK	Binary Phase Shift Keying
CDMA	Code Division Multiple Access
CPW	Coplanar Waveguide
CREMA	Centre for Research in Electromagnetics and Antennas
DAA	Detect And Avoid
EIRP	Effective Isotropically Radiated Power
FCC	Federal Communication Commission
FDMA	Frequency Division Multiple Access
FWHM	Full Width Half Maxima
GPS	Global Positioning System
HP	Hermite Polynomial
ISI	Inter Symbol Interference
LTCC	Low Temperature Cofired Ceramic
MAI	Multiple Access Interference
MB-OFDM	Multi Band Orthogonal Frequency Division Multiplexing
MIMO	Multiple Input Multiple Output
NBI	Narrow Band Interference
OFDM	Orthogonal Frequency Division Multiplexing
PAM	Pulse Amplitude Modulation
PCB	Printed Circuit Board
PCS	Personal Communications Service
PEC	Perfect Electric Conductor
PNA	Programable Network Analyzer

PPM	Pulse Position Modulation
PRF	Pulse Repetition Frequency
PSD	Power Spectral Density
PSF	Pattern Stability Factor
PTFE	Poly Tetra Flouro Ethylene
QPSK	Quadrature Phase Shift Keying
RCS	Radar Cross Section
RMS	Root Mean Square
SIR	Signal to Interference Ratio
SMA	Sub Miniature Architecture
THSS	Time Hopping Spread Spectrum
TSA	Tapered Slot Antenna
UWB	Ultra Wide Band
VNA	Vector Network Analyzer
VSWR	Voltage Standing Wave Ratio
WBAN	Wireless Body Area Network
WLAN	Wireless Local Area Network
WPAN	Wireless Personal Area Network

Chapter 1

Introduction

Ultra–wideband (UWB) technology for communications and radar has been a topic of research since the early 1960s. However, research and development in this area gained momentum only in recent years for several reasons. The primary reason is the availability of high-speed semiconductor switching device technology. Another reason is that these systems were approved for the first time only in 2002 for unlicensed use under the Federal Communications Commission Part 15 (Title 47 of the Code of Federal Regulations) [FCC, 2002]. This permitted the unlicensed use of intentional UWB wireless emissions within restricted frequency bands at very low power spectral–density and is historical from the viewpoint of frequency overlay. Finally, as the wireless spectral bands are getting crowded with the proliferation of wireless devices, the need for high–bandwidth wireless communications is also pushing the development of UWB communication systems.

1.1   Ultra Wide Band Technology

UWB is any radio transmitter with a spectrum that occupies more than 20% of the center frequency or a minimum of 500 MHz and that conforms to the power limits assigned by the regulatory bodies to minimize threat to legacy systems. UWB reaps benefits of broad spectrum in terms of the bit rates it can handle. By Shannon's theorm, the channel capacity C is given by,

$$C = W \cdot log_2(1 + \frac{S}{N}) \tag{1.1}$$
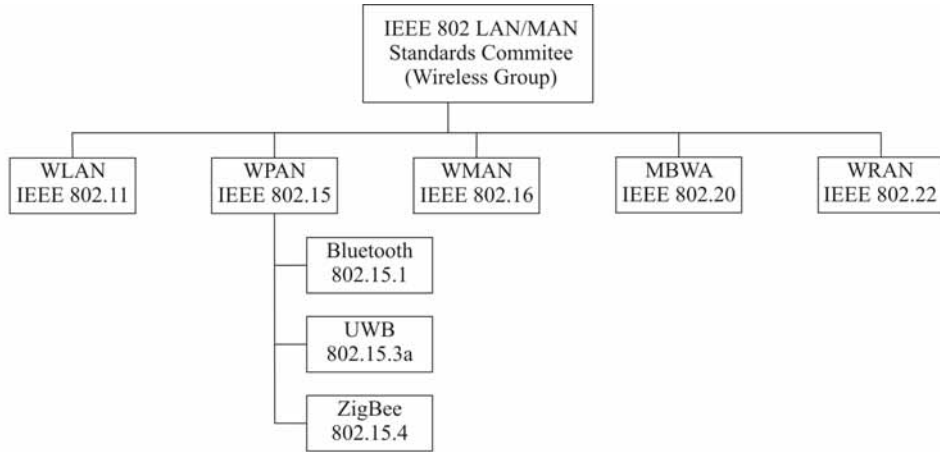
Figure 1.1: Various IEEE 802 standards

where W is the bandwidth and S/N is the signal–to–noise ratio. It can be seen that the bit rate (capacity) can be easily increased by increasing the bandwidth instead of the power, given the linear–versus–logarithmic relationship. Range of operation of such systems are determined by the Friis formula,

$$d \propto \sqrt{\frac{P_t}{P_r}} \tag{1.2}$$

d being the distance, P_t the transmit power and P_r the receive power. Equations 1.1 and 1.2 together suggests that it is more efficient to achieve higher capacity by increasing bandwidth instead of power, while it is equally difficult to achieve a longer range. Thus, UWB primarily is a high–bit, short–range system.

UWB technology is a derivative of the time hopping spread spectrum (THSS) technique, a multiple access technology particularly suited for the transmission of extremely narrow pulses. It has been standardized in IEEE 802.15.3a as a technology for Wireless Personal Area Networks (WPANs) as shown in Figure 1.1 and offers attractive solutions for many wireless communication areas as in Table 1.1.

1.2 Signaling Schemes

There are two general ways to use the available UWB. Impulse Radio, the original approach to UWB, involves the use of very short-duration baseband pulses that occupy bandwidth of several Gigahertz. Data is modulated by pulse amplitude

Table 1.1: UWB advantages, disadvantages and applications

UWB property	Advantages	Disadvantages	Applications
Very wide fractional and absolute RF bandwidth	High rate communications Potential for processing gain Low frequencies penetrate walls, ground	Potential interference to/ from existing systems	High-rate WPAN Low-power, stealthy communications Indoor localization Multiple access
Very short pulses	Direct resolvability of discrete multipath components Diversity gain	Large number of multipaths Long synchronization times	Low-power combined communications and localization
Persistence of multipath reflections	Low fade margins Low power	Scatter in angle of arrival	NLOS communications indoors and on ships
Carrier-less transmission	Hardware simplicity Small hardware	Inapplicability of super-resolution beam-forming	Smart sensor networks

modulation (PAM) or pulse-position modulation (PPM), multiple users being supported by time-hopping [Win M. Z., 1998].

Multi band scheme is a recent approach, where the available band is divided into several sub bands with bandwidth greater than 500MHz. Within the bands, a variety of modulation methods such as BPSK, QPSK, OFDM, etc. are used for data transmission. Multi band signaling is shown in Figure 1.2.

Impulse radio faces the very important challenge of coexisting with existing narrowband systems. To mitigate the effects of narrow band interferers, notch filters are required in impulse radios. However, use of such filters may distort a received signal. Multi banded UWB on the other hand, can avoid transmitting on the frequency bands where other wireless systems like 802.11a are present by
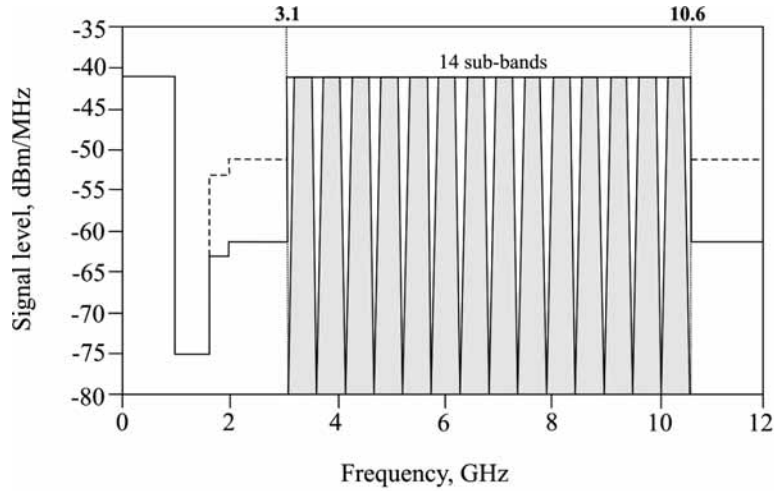
Figure 1.2: Multiband break up of the UWB spectrum.

not using those frequency bands. This approach has the additional benefit of being able to adapt to the different regulatory requirements of various countries due to the flexibility of multi band allocation.

Short duration of the pulses in impulse radio presents several technical challenges as well. The generation of pulses that fit into the spectral mask imposed by regulatory bodies is difficult and their short duration makes them more susceptible to timing jitter. Supporting higher data rates will involve increasing the pulse PRF either by using higher-order modulation or by using spread spectrum technology. The first option makes the system more vulnerable to ISI. The second would increase the peak-to-average power ratio and impose greater linearity requirements on the circuits. The last option requires careful selection of the properties of the codes.

In multi banded UWB, the pulses are not as short. So, the PRF can be lower than that of impulse radio at the same peak power, diminishing the effects of ISI and timing jitter. This approach also eases the requirements of pulse shaping filters and avoids the use of notch filters. Scaling can be achieved by simply adding more bands. Furthermore, more multiple access schemes like FDMA and CDMA are available.

Two other important issues in the design of UWB systems are timing acquisition and multi path effects. For a high data rate system, fast acquisition of a signal is very important and the preamble overhead should be minimized. The wide bandwidth also allows the resolution of several multipath components,

implying the use of a rake receiver for reliable detection.The wider bandwidth of impulse radio leads to more resolvable multipath components, but this also implies less energy per pulse. This increases the acquisition times of the impulse-based system. Furthermore, The RMS delay spread of an indoor environment ($\sim$25 ns [Rappaport, 2001]) is comparable to the symbol duration, leading to ISI spanning several symbols which demand equalization.

The longer duration of the pulses in a multi banded system lead to milder ISI and equalization requirements, but may also require the suppression of adjacent channel interference. In addition, the number of resolved multipath components increases as the bandwidth increases. Thus, the number of rake fingers needed for the impulse-based approach is around ten times more than the multi banded approach for a given signal to interference ratio (SIR), leading to a more complex receiver.

These challenges faced by impulse radios have made UWB solution providers and developers to look toward to a multiband approach for their systems. This approach has much greater flexibility in coexisting with other wireless systems and is based on more conventional technology.

1.3 Pulse Waveform for UWB transmission

For UWB systems to co–exist with existing wireless systems such as GPS, WiMAX, WLAN etc., EIRP regulations are imposed which in turn define the general characteristics of UWB signals and signal systems [Kazimierz Siwiak, 2005]. Table 1.2 shows the international picture of the imposed EIRP regulations.

It is desirable for UWB signals to spread the energy as widely in frequency as possible to minimize the PSD and hence the potential for interference to other user systems. For intentional UWB radiators the –10 dB bandwidth should ensure compliance with minimum bandwidth requirements. The –20 dB bandwidth should make certain that the signal remains below the 20 dB band edge corners on the UWB communications power spectrum density (PSD) mask as in Figure 1.3. The first regulation protects GPS and second one protects PCS transmission.

The UWB pulse wave form can be any function which satisfies the spectral mask regulatory requirements. Gaussian monocycle has been the original proposal for UWB radar and communication systems [Taylor, 1995]. A review on the

Table 1.2: International picture of the UWB regulation

Category	Region	Frequency Bands and Additional Requirements
Full Band	United States	▷ 3.1– 10.6 GHz
		▷ -41.3 dBm/MHz
Low Band	European Union	▷ 3.1 to 4.95 GHz
		▷ -41.3 dBm/MHz with either protection mechanism:
		▷ Using DAA with transmit level reduced to –70 dBm/MHz in the presence of other services that require protection
		▷ Restricting duty cycle to a maximum of 5 percent over 1 second and 0.5 percent over 1 hour
		▷ 4.2 to 4.8 GHz
		▷ No limitation until 2010
	Japan	▷ 3.4 to 4.8 GHz
		▷ -41.3 dBm/MHz with DAA with transmit level reduced to –70 dBm/MHz in presence of other services that require protection
High Band	European Union	▷ 6 to 8.5 GHz
		▷ -41.3 dBm/MHz
	Japan	▷ 7.25 to 10.25 GHz
		▷ -41.3 dBm/MHz

works carried out on Monocycle pulses can be found in [Xiaomin Chen, 2002], [Bo Hu, 2005] and [Weihua Gao, 2007]. However, the PSD of Monocycle has direct current offset and hence will not radiate effectively via antennas. In addition, the PSD does not fit in to the emission mask no matter the value of the pulse width. One possible solution for this is to shift the centre frequency and adjust the bandwidth so that the requirements are met. This could be done by modulating the monocycle with a sinusoid to shift the centre frequency and by varying the pulse width. However, impulse radio being a carrier less system, modulation will increase the cost and complexity. Higher order derivatives of the Gaussian pulse resemble sinusoids modulated by a Gaussian pulse–shaped envelope and in [Win M. Z., 2000], use of second derivative of the Gaussian pulse is proposed as a solution. The fifth derivative of the Gaussian pulse offers even more compliance with emission masks and can be transmitted without any extra filtering [Hongsan Sheng, 2003]. A pulse generator based on CMOS is proposed
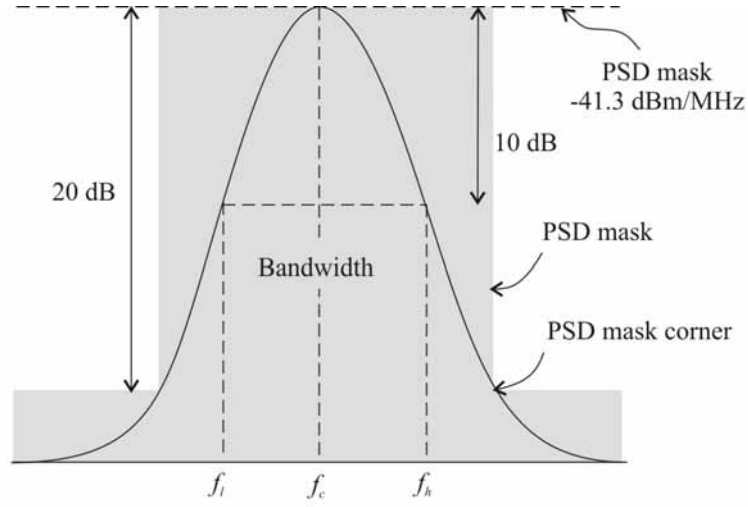
Figure 1.3: UWB signal design points.

for this pulse in [Hyunseok Kim, 2005].

Equation 1.3 gives the general form of a Gaussian wave. In Figure 1.4, derivatives of this signal and the corresponding PSD are shown. As the order of the derivative pulse increases, energy moves to higher frequencies and by choosing the order of the derivative and a suitable pulse width, a pulse that satisfy the regulatory masks can be designed.

$$v(t) = A \ \ exp[-2\pi(\frac{t}{T})^2] \tag{1.3}$$

Pulse set based on the modified Hermite polynomials (HP) are orthogonal to one another[Michael L. B., 2002], but frequency shifting is necessary for the original and 1st order HP pulses to meet the FCC spectral masks. Higher order HP pulses are susceptible to timing jitter and noise, and they also need bandpass filters to fit their PSD into the FCC masks [Bo Hu, 2005]. Pulse designed utilizing the ideas of prolate spheroidal (PS) functions can satisfy the FCC masks [Parr B., 2003], but they do not effectively exploit the allowable bandwidth and power. The orthogonality of both HP pulses and PS pulses is preserved only when each user is assigned a unique pulse in a perfect synchronous multi-user UWB system without considering the channel distorting effect and antenna response characterization, which is not practical in real implementations. Pulses based on linear combination of a set of base waveforms obtained by the differentiation of the Gaussian pulse can be found in [De Nardis L., 2004; Weihua Gao, 2007].
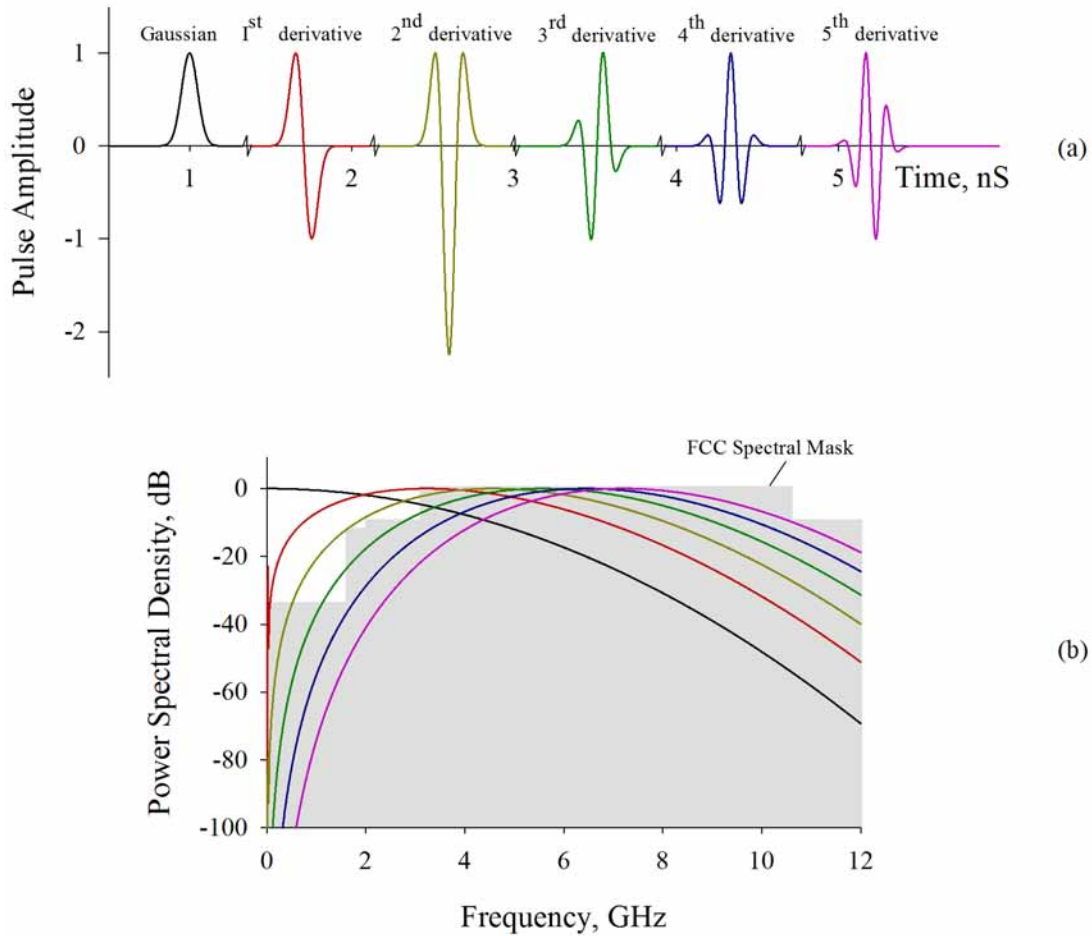
Figure 1.4: Gaussian Pulse and its derivatives (a) waveforms in the time domain (b) power spectral density.

1.4 Research Interests

In spite of all the advantages of UWB, there are several fundamental and practical issues that need to be carefully addressed to ensure the success of this technology in the wireless communication market. Multi access code design, multiple access interference (MAI) cancelation, narrow band interference (NBI) detection and cancellation, synchronization of the receiver to extremely narrow pulses, accurate modeling of UWB channels, estimation of multi path channel delays and coeffi-cients, and adaptive transceiver design are some of the issues that still require a great deal of investigation. In addition to the above physical layer issues, the fundamental role of UWB technology in wireless networks is still open, and a wide

range of research questions continue to present challenges, such as the particular role of UWB in wireless ad-hoc and sensors networks.

A major challenge in the transmission of narrow pulses is the radiation characteristics of the antenna and is an active field of research by both academia and industry. Antenna design considerations in general are strongly dependent on the modulation scheme and applications [Chen, 2007]. Table 1.3 compares the requirements for UWB systems which are based on MB-OFDM and pulse. It is found that the important difference of the requirements between two types of systems is the bandwidth of impedance and phase response.

Table 1.3: A comparison of the design considerations for UWB antennas

Constituent	MB-OFDM	Pulse-based
Electrical	▷ wide impedance bandwidth covering all operating sub-bands	▷ wide impedance bandwidth covering the bandwidth where majority of the source pulse energy falls in
	▷ steady radiation patterns	▷ constant gain at desired directions
	▷ constant gain at directions of interest	▷ linear phase response
	▷ constant desired polarization	▷ constant desired polarization
	▷ high radiation efficiency	▷ high radiation efficiency
Mechanical	▷ small size, low profile, easy integration for portable devices	
	▷ compact but robust especially for fixed devices	
	▷ low cost	

In addition, UWB antenna design is also determined by the applications. For specific applications, systems usually have some requirement for specific parameters. For example, for portable devices, the antennas must be small in size and embeddable with 3–dimensional omni–directional radiation. However, the antennas installed at fixed devices, such as requestors in UWB location systems, the antenna can be a little big but must have high and consistent radiation gain with stable beam widths.

1.5 Antennas for UWB systems

For UWB radio systems, a wide variety of antennas have been developed over the last several decades which can be roughly categorized in to four as shown

in Table 1.4. In general, UWB radiation can be accomplished via the following
three approaches.

Table 1.4: Category of UWB Antennas

	Directional	**Omni-directional**
Two Dimensional	Vivaldy Antenna Tapered Slot Antenna Log-periodic Antenna Planar log-periodic Antenna Conical Spiral Antenna	Planar Dipole Slot Antennas Printed Antenna on PCB
Three Dimensional	TEM Horn Antenna Ridge Horn Antenna Reflector Antenna	Loaded Cylindrical Dipole Bi-conical Antenna Disc-cone Antenna Roll Antenna

Perturbing electromagnetic resonance to broaden the resonant peak : This type
of UWB antenna achieves bandwidth by introducing incoherent resonance and
effectively lowering the quality factor of the electromagnetic resonance. Majority
of these antennas are variations of dipoles or monopoles.

*Allowing only one dominant radiation region that is physically small compared
with wavelengths* : In this approach, multiple diffractions in the antenna structure
are minimized by suitable techniques. A tapered antenna geometry can avoid
strong localized diffractions and allow gentle and continuous diffractions. The
low–frequency limit of this design occurs when the arm length is less than half of
the wavelength. The high–frequency limit is determined by the pattern distor-
tions caused by the curvature smoothness and the starting curvature. Common
examples include tapered-slot antennas, rolled-edge horns and ridged horns.

Absorptive loading is another effective way to achieve wide bandwidth without
multiple diffractions at the price of lower antenna efficiency. Both electric and
magnetic absorptive materials can be used. Resistively loaded dipoles and
resistively loaded horns are well–known examples.

Both curved–arm and absorptive loading can also be applied simultaneously

to further reduce antenna size and to achieve a better pattern stability at the expense of antenna efficiency.

Maintaining a similar radiation/scattering geometry (shape and dimension) in terms of wavelength : This type of antenna adopts frequency–independent or frequency–scaled geometries. Among them, angle–defined geometry, complementary geometry, and log–periodic geometry are the best known.

1.6 Concerns of the present thesis

For application in portable systems, compact, radiation efficient, omni directional printed antennas are desired. In addition, antennas intended for UWB systems should faithfully replicate the transmitted pulse at the receiving end. If propagation delay and retardation time of the pulse in the antenna becomes comparable to its rise time or duration, significant pulse dispersion can result. Hence, UWB antennas are designed with a specification of flat amplitude and linear phase response over the desired bandwidth without regard to the out–of–band performance. Studies have shown that multi resonant antennas introduce ringing to the baseband pulses due to multiple reflections occurring within the geometry. Even though log–periodic, self–complementary geometries offer bandwidths in excess of 110%, they have detrimental effects on baseband pulses due to this.

In this thesis, we have designed different antenna configurations with bandwidths of 110% and excess and their radiation characteristics are studied in frequency and time domains. In all the antennas, ultra wide bandwidth is achieved by redesigning the ground plane to modify the ground–patch interaction. The configurations obtained are square monopole, semi–elliptic slot, step slot and tapered slot antennas which are shown in Figure 1.5.

1.7 Thesis Organization

This thesis presents an exhaustive study carried out on the radiation characteristics of printed UWB antennas designed by ground plane modifications which have different radiation mechanisms.

Chapter 1 of this thesis has presented an overall introduction to UWB systems
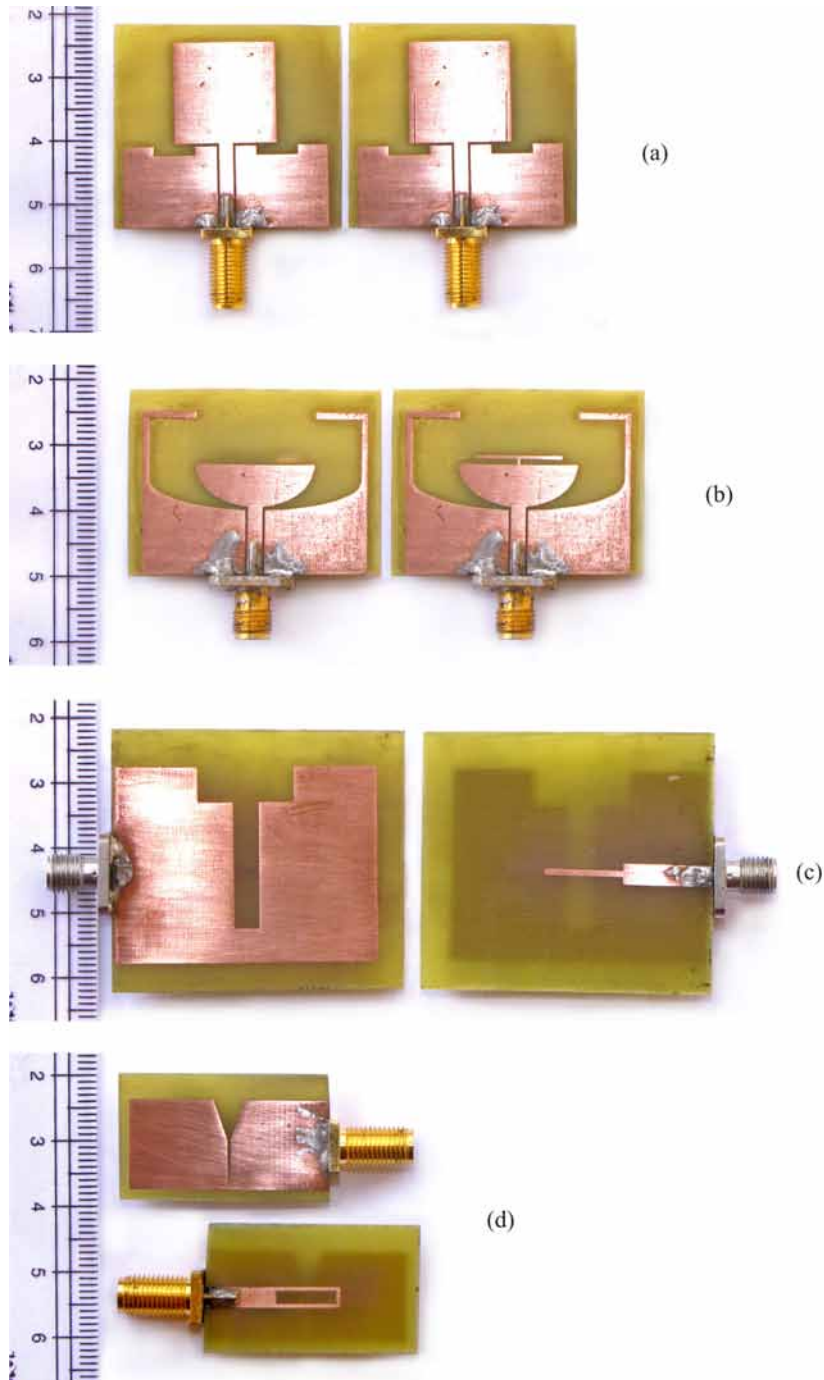
Figure 1.5: Antenna prototypes (a) Square Monopole antenna (b) Semi–Elliptic Slot antenna (c) Step–Slot antenna (d) Linear tapered Slot antenna.

and discussed research interests in this field, antennas for UWB and issues in their engineering. The chapter has also presented the concerns of the present

thesis.

Chapter 2 presents the methodology used for developing the present antennas. Simulation settings in CST Microwave Studio and fabrication steps are explained. Measurements in the frequency domain such as return loss, radiation pattern, gain and the relevant theory behind time domain measurements and the quantification of measurement results are explained.

Chapter 3 deals with the design and characterization of the Square Monopole Antenna. This chapter begins with an exhaustive literature survey on volumetric and non-volumetric monopole antennas for UWB systems. Evolution of the present design is explained and design guidelines are proposed with appropriate equations. A technique to prevent Narrow Band Interference (NBI) is also presented. Experimental results in the frequency domain are presented followed by conclusions.

Chapter 4 deals with the Semi-Elliptic Slot Antenna. The literature survey on Slot Antennas for UWB systems is given at the beginning of the chapter. Geometry, design and optimization of the proposed design are explained along with techniques to prevent Narrow Band Interference. Experimental results in the frequency domain are presented followed by conclusions.

Chapter 5 deals the the Step and Linear Tapered Slot Antennas. This chapter addresses yet another class of slot antennas known as monopole slot antennas whose detailed literature survey is presented at the beginning of the chapter. Antenna geometry, design and optimization are explained and experimental results in the frequency domain are presented.

Chapter 6 considers the transfer property characterizations of the above antennas in the frequency and time domains. Measurements are performed for the azimuthal and elevation planes and are verified using the time domain capabilities of CST Microwave Studio. From the measured impulse response, parameters such as FWHM, Ringing, pulse Fidelity etc. are computed and are compared. Conclusions of the present study are presented.

Chapter 7 gives the summary and conclusion of the overall work and a brief description on the scope for future investigations.

In the Appendix, design of a Compact Rectangular Strip Monopole Antenna is presented which consists of a rectangular radiating patch and a novel impedance transformer in the ground plane.

References

Bo Hu, Norman C. Beaulieu. 2005. Pulse shapes for ultrawideband communication systems. *IEEE Transaction on Antennas and Propagation*, **4**(July), 1789–1797. 6, 7

Chen, Zhi Ning. 2007 (December). UWB Antennas: Design and Application. *Pages 1–5 of:* 6th *International Conference on Information, Communications & Signal Processing.* 9

De Nardis L., G. Giancola, D. B. M.-G. 2004 (June). Power limits fulfilment and mui reduction based on pulse shaping in UWB networks. *Pages 3576–3580 of: IEEE International Conference on Communications (ICC'04)*, vol. 6. 7

FCC. 2002. First report and order in ET Docket No. 98-153, 17 FCC Rcd 7435. April, 22. 1

Hongsan Sheng, Philip Orlik, Alexander M. Haimovich Leonard J. Cimini Jinyun Zhang. 2003 (March). On the spectral and power requirements for ultra-wideband transmission. *Pages 738–742 of: IEEE International Conference on Communications*, vol. 1. 6

Hyunseok Kim, Youngjoong Joo. 2005 (June). Fifth–derivative gaussian pulse generator for uwb system. *Pages 671–674 of: Radio Frequency Integrated Circuits (RFIC) Symposium.* 7

Kazimierz Siwiak, Debra McKeown. 2005. *Ultra–wideband radio technology.* John Wiley & Sons Inc., New York. 5

Michael L. B., M. Ghavami, R. Kohno. 2002 (March). Multiple pulse generator for ultra–wideband communication using hermite polynomial based orthogonal pulses. *Pages 47–51 of: IEEE Conf. Ultra Wideband Systems and Technologies*, vol. 48. 7

Parr B., B. Cho, K. Wallace Z. Ding. 2003. A novel ultra–wideband pulse design algorithm. *IEEE Commununication Letters*, 219–221. 7

Rappaport, T. S. 2001. *Wireless Communications.* Prentice Hall. 5

Taylor, J. D. 1995. *Introduction to ultra wideband radar systems.* Boca Raton, FL: CRC. 5

Weihua Gao, R. Venkatesan, Cheng Li. 2007 (March). A pulse shape design method for ultra–wideband communications. *Pages 2800–2805 of: Wireless Communications and Networking Conference.* 6, 7

Win M. Z., R. A. Scholtz. 1998. Impulse Radio: How it works. *IEEE Communications Letters*, **2**(2), 36. 3

Win M. Z., R. A. Scholtz. 2000. Ultra–wide bandwidth time–hopping spread–spectrum impulse radio for wireless multiple–access communications. *IEEE Transactions on Communication*, **48**(April), 679–691. 6

Xiaomin Chen, Sayfe Kiaei. 2002 (May, 20–23). Monocycles shapes for ultra wideband system. *Pages 597–600 of: IEEE Conf. Ultra Wideband Systems and Technologies*, vol. 48. 6

Chapter 2

Methodology

This chapter presents a detailed account of the simulation, fabrication and experimental studies done in characterizing the antennas discussed in Chapters 3–5. Pre–fabrication studies of these antennas are done in CST Microwave Studio. From the parametric analysis done using the software, a design guideline is formulated. Resonances in the antenna are quantified and are arranged in the frequency domain to result in UWB. The antennas are fabricated on microwave laminates by photolithography and measurements are carried out at the test facility consisting of Vector network Analyzer and anechoic chamber. A detailed account of the measurement techniques for frequency and time domains is presented in this chapter.

2.1   Pre–fabrication studies in CST

Printed antennas have categorization as dipole, monopole and slot types. Guided signals are transmitted to free space by these structures whose impedance to the guided signals should be properly optimized by suitable techniques for the desired bandwidth. Generally, multiple frequencies are impedance matched and merged to result in UWB. In this work, for obtaining multiple resonances/ impedance matching that result in UWB, ground planes of the antennas are redesigned and the design practices suitable for each category of antennas are discussed in detail in Chapters 3–5.

The antenna structure is obtained in CST by specifying the coordinates

for each point of the structure. When the structure is drawn, dielectrics and metallizations are assigned. To accurately account for the losses, metallizations are taken to be Copper. A finite metal thickness of 10 μm is assigned in all the simulations. CST provides pre–defined templates that suit a problem in which parameters such as boundary conditions, mesh size, type etc. are pre–defined or they can be user defined. The frequency sweep is then defined to get solutions for all wanted frequencies and a waveguide port is assigned to excite the antennas.

To study the return loss, radiation pattern, gain etc., antennas are simulated in this manner. Electric fields in the near/far fields can be probed by inserting virtual probes in the problem space as shown in Figure 2.1(b). This is done for studying the time domain performance of the antenna and is explained in detail in the later sections of this chapter.

2.2   Fabrication

Microwave circuits need to be fabricated on low loss, thermally stable substrates with constant permittivity across the operating band. Poly–tetra–flouro–ethylene (PTFE) and Epoxy based laminates are commercially available in various brand names for microwave applications. Prototypes of the antennas for this thesis have been realized on FR4 Glass Epoxy since it is economic and also radiation characteristics can be analyzed in the worst case scenario (material properties can be found in Table 3.2 in Chapter 3).

Antennas are printed on the laminates by photolithography. A negative mask of the desired geometry is created first. An oxide removed single/double sided copper clad lamination of suitable dimension is dipped in the negative photo resist and dried to get a thin film of the photo–resist on the laminate. It is then exposed to ultra violet radiation through the negative mask for 2 minutes. The layer of photo–resist material in the exposed portions hardens. This board is immersed in the developer solution and agitated for a few minutes. It is then washed in Ferric Chloride ($FeCl_3$) solution to remove the unwanted metal portions. $FeCl_3$ dissolves the copper parts except underneath the hardened photo resist layer. Finally, the laminate is washed in Acetone solution to remove the hardened negative photo resist.
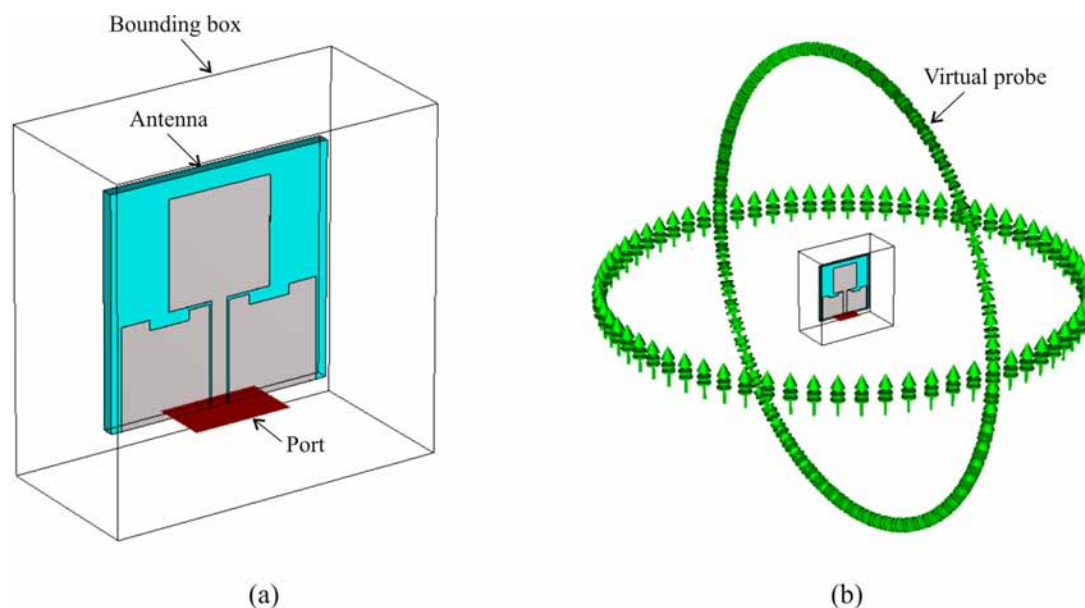
Figure 2.1: CAD of the antenna in CST

2.3 Antenna Measurements

In general, the electrical properties of antennas are characterized by input impedance, efficiency, gain, effective area, radiation pattern, and polarization properties [Balanis, 1996]. For narrow band applications, these are analyzed at the center frequency of the system. For wider bandwidths, the parameters become strongly frequency dependent and a straightforward evaluation of these as functions of frequency is not sufficient to characterize their transient radiation behavior. Measurement of the antenna's transient response can be performed either in time domain or in frequency domain. Measurements in time domain, using very short pulses or step functions as driving voltage, can be faster than measurements in frequency domain and the following Fourier transform. However, Frequency domain measurements take advantage of the high dynamic range and the standardized calibration of the vector network analyzer [Sorgel W., 2003]. The results presented in this thesis follows the latter method.

Frequency domain measurements of the antennas are carried out at the antenna research facility at CREMA, Dept. of Electronics, CUSAT. The test facilities available include Network Analyzers (HP8510C, R&S ZVB20 and Agilent PNA 8362), spectrum analyzer, automated antenna positioner, broadband double–

ridged horn antennas (2-20 GHz) and anechoic chamber.

2.3.1   In the frequency domain

The Network Analyzer is calibrated using the standard calibration kit before performing the measurements. The calibration information can be stored and recalled for performing another set of experiments. Details of the analyzer calibration is provided in Table 2.1 .

Impedance and VSWR

Impedance of the antenna is a measure of the efficiency with which it acts as a transducer between the source and the propagating medium. Antenna impedance is a complex quantity with a real part called the antenna resistance and the imaginary part, called the antenna reactance. When there is an impedance mismatch between the antenna and the source line, a part of the incident energy is reflected back to the source. The ratio of the reflected voltage (or current) to the incident voltage (or current) is termed as the input reflection coefficient (Γ). (S_{11}) is the reflection coefficient expressed in dB.

$$S_{11} = 20 log_{10}(|\Gamma|) \tag{2.1}$$

The level of mismatch is also defined in terms of the voltage standing wave ratio (VSWR) defined as the ratio of the voltage maximum to minimum of the standing wave existing on the antenna input terminal.

The AUT is connected to the input port of the analyzer and reflection mode is selected from the parameter menu. The display then gives the return loss of the AUT as a function of the frequency. By using markers, the resonant frequency, bandwidth etc. can be observed. Bandwidth is measured between the 2:1 VSWR or -10 dB $|S_{11}|$ points of the plot. From the format menu, plots of phase of S_{11}, VSWR, real and imaginary parts of the input impedance etc. can also be obtained.

Antenna Gain

Gain is the ratio of the intensity of an antenna's radiation in the direction of strongest radiation to that of a reference antenna, when both antennas are fed

Table 2.1: Details of Analyzer calibration

Test Port connector	3.5 mm, SMA
Connector for AUT	3.5 mm SMA
Calibration type	TOSM
Frequency range	2- 12GHz, 2-20 GHz
Number of measurement points	801, 1601 (per trace)
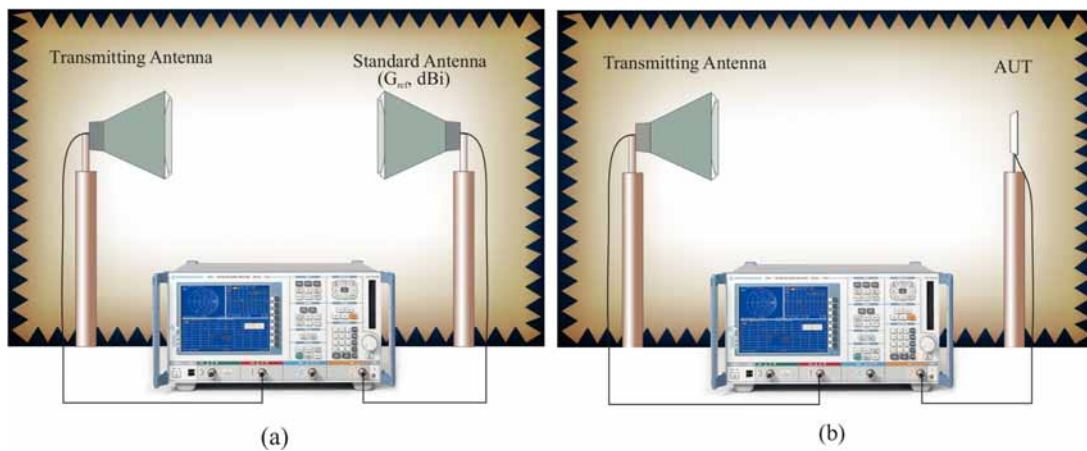
Figure 2.2: Antenna gain measurement set up

with the same input power. If the reference antenna is an isotropic antenna, the gain is expressed in units of dBi. The gain of an antenna is a passive phenomenon – power is not added by the antenna, but simply redistributed to provide more radiated power in a certain direction than would be transmitted by an isotropic antenna.

In this thesis, the gain transfer method is used to calculate the absolute gain of the AUT. The measurement set up is shown in Figure 2.2. There are three antennas; two wide band ridged horns and the antenna under test. Gain chart of the ridged horn antenna is available (G_{ref}, dBi). Initially, the ridged horns are positioned for bore-sight radiation and the transmission coefficient $|S_{21}|_{ref}$ (dB) is read on the analyzer display. A THRU calibration is performed and the data is stored in the analyzer. This is the reference gain for the AUT. Now the AUT replaces the reference antenna and the transmission coefficient $|S_{21}|_{AUT}$ (dB) is recorded, which gives the relative gain. The absolute gain can then be calculated

as,

$$G(dBi) = G_{ref}(dBi) + |S_{21}|_{AUT} \qquad (2.2)$$

Radiation Efficiency

The IEEE definition of antenna radiation efficiency is the ratio of the total power radiated by the antenna to the net power accepted by the antenna at its terminals during the radiation process [IEEE, 1979]. A more reasonable definition of antenna efficiency would include mismatch reflected power as an explicit loss, and define efficiency as the ratio of the total power radiated by the antenna to the net power applied at it's terminals. A method for assessing UWB antenna efficiency that explicitly include mismatch reflected power as a loss term is presented in [Schantz, 2002]. This method is a modification of the Wheeler Cap method conventionally used to measure radiation efficiency of narrow band antennas. Rather than inhibiting radiation from the antenna to a radiation sphere $r \approx \lambda/2\pi$ as in the narrow band approach, UWB Wheeler Cap allows the antenna to radiate freely and then receive its own transmitted, reflected signal.

The power budget for a transmit antenna may be expressed in terms of power fractions. A fraction of the incident energy is dissipated in losses ($l \equiv \frac{P_{loss}}{P_{in}}$), a fraction is reflected away due to mismatch ($m \equiv \frac{P_{refl}}{P_{in}}$), and a fraction is radiated ($\eta \equiv \frac{P_{rad}}{P_{in}}$). Averaging over a suitable time interval and applying conservation of energy yields:

$$l + m + \eta = 1 \qquad (2.3)$$

A number of interesting phenomena manifest in the UWB Wheeler cap. The spherical shell surrounding the antenna under test enforces a near ideal time reversal of the transmitted signal. Thus the antenna receives the reflected signal with negligible structural scattering, and the antenna mode scattering term is simply the mismatch fraction ($m = |S_{11-FS}|^2$). The receive and transmit efficiencies (η) are identical by reciprocity. The scattering coefficient inside the UWB Wheeler Cap becomes:

$$|S_{11-WC}|^2 \;=\; m + \eta^2 + \eta^2 m^1 + \eta^2 m^2 + \eta^2 m^3 ...$$

$$\begin{aligned}
&= |S_{11-FS}|^2 + \eta^2 \sum_{n=0}^{\infty} |S_{11-FS}|^{2n} \\
&= |S_{11-FS}|^2 + \eta^2 \frac{1}{1 - |S_{11-FS}|^2}
\end{aligned} \tag{2.4}$$

which solves to yield the following result for the radiation efficiency:

$$\eta = \sqrt{(1 - |S_{11-FS}|^2)(|S_{11-WC}|^2 - |S_{11-FS}|^2)} \tag{2.5}$$

For measurements, an oblate metallic chamber with diameter 70cm is used. First, the antenna under test is placed in free space and the return loss S_{11-FS} is measured. It is then placed at the center of the closed metallic chamber and the return loss S_{11-WC} is measured. Finally, Equation 2.5 is employed to calculate the radiation efficiency. The measurement is repeated several times and the average value at discrete frequency intervals is computed.

Radiation Pattern

Radiation pattern of an antenna is the graphical representation of its radiation properties as a function of the space co-ordinates. This assumes a three dimensional pattern. Because of the limits set by a practical measurement setup for measuring the 3-D pattern, usually two principal plane patterns are specified for directional antennas and three patterns for those with omni-directional patterns. Generally, far-field patterns are specified for an antenna where the pattern is measured at a distance, $d > 2D^2/\lambda$, where D is the largest dimension of the antenna and λ is the operating wavelength.

As shown in Figure 2.2(b), the AUT is connected to Port 1 and the standard ridged horn is connected to Port 2. The height and polarization of both antennas are aligned for maximum transmission ($|S_{21}|$) between them. The frequency range for which $S_{11} <$ -10 dB is selected. A THRU calibration is performed in this position which calibrates the S_{21} data to 0 dB for every frequency point in the band. In order to suppress spurious reflections from the nearby objects, the time domain gating facility of the analyzer is used. The gate span is selected according to the largest dimension of the radiator. The antenna positioner is now set to home which automatically sets the current position as 0^0. The software now invokes the radiation pattern routine and reads the normalized S_{21} data for the specified frequency band, for each angular position of the AUT.

2.3.2   In the time domain

Antennas intended for UWB systems need to possess superior pulse handling capabilities. Analysis of the transient response of the antenna is performed by direct time domain measurements or by a frequency domain measurement followed by Fourier Transformation. Measurements in the time domain is presented in [Jongh R. K., 1997; Shlivinski A., 1997]. Frequency domain measurements take advantage of the high dynamic range and the standardized calibration of the vector network analyzer and is equally accurate to the direct time domain measurements [Sorgel W., 2003, 2005].

In the latter method, the antenna is considered as a linear time invariant system described by its transfer function (gain and phase) and the associated impulse response [Zwierzchowski S., 2003; Mohammadian A. H., 2003]. Transfer functions and impulse responses modeling UWB antennas are spatial vectors as the antenna characteristics depend on the signal propagation direction [Sorgel W., 2003, 2005]. Figure 2.3(a) presents the classical approach, to characterize an ideal UWB channel, i.e., a radio link made up of two antennas in free space and under the approximation of far–field and line-of-sight propagation. The emission model takes into account the Tx antenna and the channel jointly, while in reception only the Rx antenna is considered.

The model by [Duroc & Tedjini, 2007] in which the transmitting, receiving antennas are characterized by eliminating channel effects is adapted for the present study. This is shown in Figure 2.3(b).

2.3.3   Transient Reception

The time domain relation between the received voltage pulse $\overrightarrow{U}_{Rx}(\omega, r, \theta, \varphi)$ and the incident electric field pulse $\overrightarrow{E}_{rad}(\omega, r, \theta, \varphi)$ is [Sorgel W., 2005],

$$\frac{\overrightarrow{U}_{Rx}(\omega, r, \theta, \varphi)}{\sqrt{z_c}} = \overrightarrow{h}_{Rx}(\omega, \theta, \varphi) \frac{\overrightarrow{E}_{rad}(\omega, r, \theta, \varphi)}{\sqrt{z_0}} \qquad (2.6)$$

In the time domain, the corresponding relation is,

$$\frac{\overrightarrow{u}_{Rx}(t, r, \theta, \varphi)}{\sqrt{z_c}} = \overrightarrow{h}_{Rx}(t, \theta, \varphi) \otimes \frac{\overrightarrow{e}_{rad}(t, r, \theta, \varphi)}{\sqrt{z_0}} \qquad (2.7)$$

z_c and z_0 are respectively the characteristic impedance of the antenna port
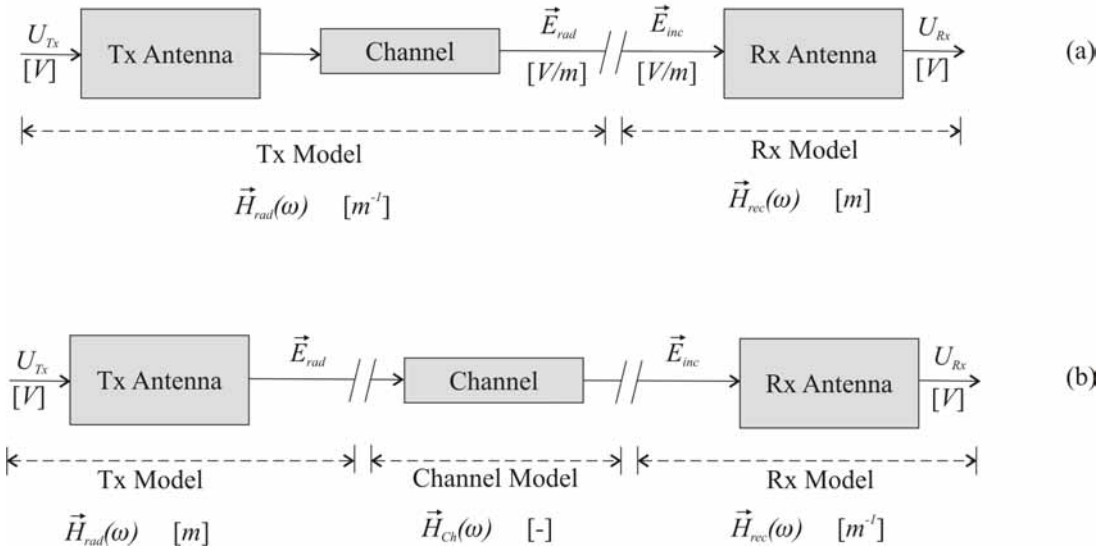
Figure 2.3: UWB channel model (a) classical (b) contemporary.

and that of free–space and $\otimes$ indicates convolution operation. Both the transfer function $\overrightarrow{h}_{Rx}(\omega, \theta, \varphi)$ and the impulse response $\overrightarrow{h}_{Rx}(t, \theta, \varphi)$ of the antenna are in general a function of the direction of arrival of the incident field pulse.

An ideal receiving antenna will have a Dirac–delta impulse response (independent of arrival angle) with the effect that the received voltage pulse will always have the same shape as the incident field pulse on the antenna. In the frequency domain this will relate to an antenna transfer function with a constant amplitude response and a linear phase response (or constant group delay). In the real world the received field pulse will always be band limited, and for practical purposes, the required receiving antenna transfer function is one with a constant amplitude response and linear phase response within the operating band.

2.3.4 Transient Radiation

The frequency domain relation between the transmitted electric field pulse and the incident voltage pulse is,

$$\frac{\overrightarrow{E}_{rad}(\omega, r, \theta, \varphi)}{\sqrt{z_0}} = \overrightarrow{h}_{Tx}(\omega, \theta, \varphi) \frac{e^{-j\omega r/c}}{r} \frac{U_{Tx}(\omega, r, \theta, \varphi)}{\sqrt{z_c}} \qquad (2.8)$$

and,

$$\overrightarrow{h}_{Tx}(\omega, \theta, \varphi) = \frac{j\omega}{2\pi c} \, \overrightarrow{h}_{Rx}(\omega, \theta, \varphi) \tag{2.9}$$

The time domain relation between the transmitted electric field pulse $\overrightarrow{e}_{rad}(t, r, \theta, \varphi)$ and the incident voltage pulse $\overrightarrow{u}_{Tx}(t, r, \theta, \varphi)$ at the transmitting antenna is,

$$\frac{\overrightarrow{e}_{rad}(t, r, \theta, \varphi)}{\sqrt{z_0}} = \frac{1}{r} \, \partial(t - \frac{r}{c}) \otimes \left[\frac{1}{2\pi c} \frac{\partial}{\partial t} \overrightarrow{h}_{Rx}(t, \theta, \varphi) \right] \otimes \frac{u_{Tx}(t, r, \theta, \varphi)}{\sqrt{z_c}} \tag{2.10}$$

where,

$$\overrightarrow{h}_{Tx}(t, \theta, \varphi) = \frac{1}{2\pi c} \frac{\partial}{\partial t} \overrightarrow{h}_{Rx}(t, \theta, \varphi) \tag{2.11}$$

The convolution with the Dirac-delta function in 2.10 represents the time retardation due to the finite speed of light, which is denoted by c. From 2.11 one can observe that the transmit impulse response $\overrightarrow{h}_{Tx}(t, \theta, \varphi)$ is directly proportional to the time derivative of the receive impulse response $\overrightarrow{h}_{Rx}(t, \theta, \varphi)$. The consequence of this is that an ideal antenna (with $\overrightarrow{h}_{Rx}(t, \theta, \varphi) = \partial(t)$) will radiate an electric field pulse that is proportional to the first–order time derivative of the input voltage pulse.

2.3.5   Model of Transient Transmission

From 2.6 and 2.8, it is possible to determine the full input-to-output characteristics, in both frequency and time domians.

$$\begin{aligned}
\frac{\overrightarrow{U}_{Rx}(\omega, r, \theta, \varphi)}{U_{Tx}(\omega, r, \theta, \varphi)} &= \overrightarrow{A}_{Tx,Rx} \frac{e^{-j\omega r/c}}{r} \, \overrightarrow{h}_{Rx}(\omega, \theta, \varphi) \\
&= \sqrt{\frac{2\omega}{c}} \, \overrightarrow{A}_{Tx,Rx} \frac{c \, e^{-j\omega r/c}}{2r\omega} \sqrt{\frac{2\omega}{c}} \, \overrightarrow{h}_{Rx}(\omega, \theta, \varphi) \quad (2.12)
\end{aligned}$$

where,

$$\overrightarrow{A}_{Tx,Rx} = \frac{j\omega}{2\pi c} \, \overrightarrow{h}_{Rx}(\omega, \theta, \varphi)$$

$$S_{21}(\omega) = \frac{\overrightarrow{U}_{Rx}(\omega, r, \theta, \varphi)}{U_{Tx}(\omega, r, \theta, \varphi)} = \overrightarrow{H}_{Tx}(\omega, \theta, \varphi) \, H_{Ch}(\omega) \, \overrightarrow{H}_{Rx}(\omega, \theta, \varphi) \tag{2.14}$$

where,

$$\overrightarrow{H}_{Tx}(\omega, \theta, \varphi) = \sqrt{\frac{2\omega}{c}} \; \overrightarrow{A}_{Tx,Rx} \tag{2.15}$$

$$H_{Ch}(\omega) = \frac{c \; e^{-j\omega r/c}}{2r\omega} \tag{2.16}$$

$$\overrightarrow{H}_{Rx}(\omega, \theta, \varphi) = \sqrt{\frac{2\omega}{c}} \; \overrightarrow{h}_{Rx}(\omega, \theta, \varphi) \tag{2.17}$$

In the time domain, 2.12 reads,

$$\frac{\overrightarrow{u}_{Rx}(t, r, \theta, \varphi)}{u_{Tx}(t, r, \theta, \varphi)} = \overrightarrow{h}_{Tx}(t, \theta, \varphi) \otimes h_{Ch}(t) \otimes \overrightarrow{h}_{Rx}(t, \theta, \varphi) \tag{2.18}$$

2.3.6 Implementation in CST

For the time domain characterization of the antenna discussed in this thesis, fourth derivative of the Gaussian pulse is chosen as the input pulse whose mathematical form is given in Equation 2.19. This pulse is shown in Figure 2.4(a).

$$s_i(t) = A \cdot \left[3 - 6 \left(\frac{4\pi}{T^2} \right) (t - \tau)^2 + \left(\frac{4\pi}{T^2} \right)^2 (t - \tau)^4 \right] e^{-2\pi \left(\frac{t-\tau}{T} \right)^2} \quad \left(\frac{V}{m} \right) \tag{2.19}$$

This pulse conforms to the FCC spectral mask as shown in Figure 2.4(b) when A = 0.333 and T = 0.175 nS.

For the antennas discussed in this thesis, the input voltage $u_{Tx}(t)$ $(= s_i(t))$ is specified in CST Microwave Studio and the radiated pulse $\overrightarrow{e}_{rad}(t, r, \theta, \varphi)$ is calculated on a sphere of radius 25cm. Fourier transforms of these two quantities are then calculated and 2.8 is utilized to calculate the transfer function $\overrightarrow{h}_{Rx}(\omega, \theta, \varphi)$. The impulse response $\overrightarrow{h}_{Rx}(t, \theta, \varphi)$ can be calculated using an IFFT.

2.3.7 Practical Approach

In practice, from a simple measurement of the scattering parameter S_{21} in the frequency domain, transfer functions of both the transmitting and receiving antennas can be deduced. Using two identical horn antennas oriented for bore
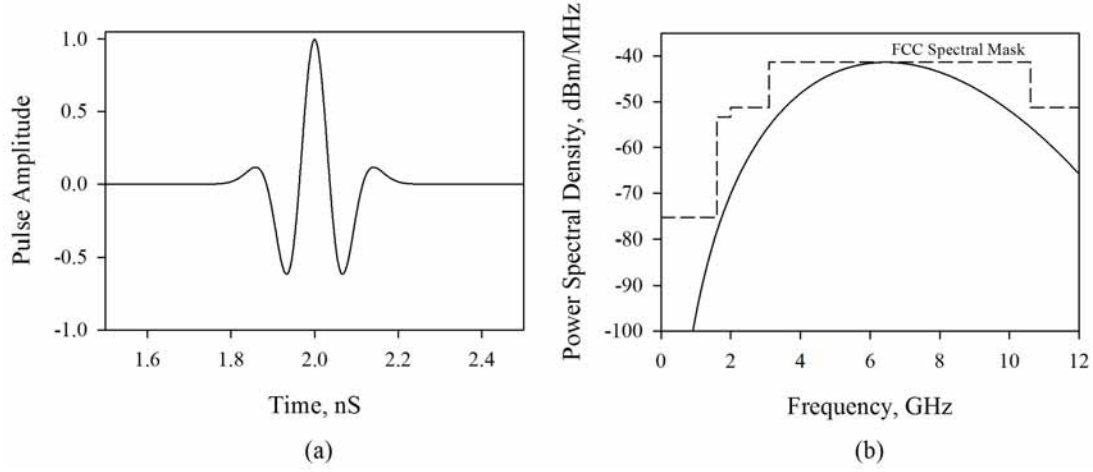
Figure 2.4: (a) Input pulse (b) Power Spectral density.

sight transmission and reception, and considering Equation 2.12, the corresponding transfer functions are found out from

$$H_{Tx}(\omega, \theta, \varphi) = \sqrt{\frac{j}{2\pi} \left(\frac{\omega}{c}\right)^2 \frac{S_{21}(\omega, \theta, \varphi)}{H_{Ch}(\omega, \theta, \varphi)}} \qquad (m^{-1}) \qquad (2.20)$$

$$H_{Rx}(\omega, \theta, \varphi) = \sqrt{\frac{2\pi}{j} \left(\frac{c}{\omega}\right)^2 \frac{S_{21}(\omega, \theta, \varphi)}{H_{Ch}(\omega, \theta, \varphi)}} \qquad (m) \qquad (2.21)$$

where the free space transfer function is,

$$H_{Ch}(\omega) = \frac{c}{2d\omega} exp\left(\frac{-j\omega d}{c}\right) \qquad (2.22)$$

Once the reference antenna (Tx Antenna) is characterized, transfer function of the AUT is found for multiple orientations using,

$$H_{AUT}(\omega, \theta, \varphi) = \frac{S_{21}(\omega, \theta, \varphi)}{H_{Tx}(\omega)H_{Ch}(\omega)} \qquad (2.23)$$

2.3.8   Data Processing, Windowing

S_{21} is measured with frequency resolution 15.25 MHz and Equations 2.20–2.23 are used to compute the corresponding transfer functions. The data is complemented

by zero padding for 0–2 GHz and 12–62.47 GHz. The pass band now consists of 4096 points. The conjugate of this signal is taken and is reflected to the negative frequencies to get a spectrum which is symmetric around DC. The resulting doubled–sided spectrum corresponds to a real signal which is then transformed to the time domain using IFFT.

Results of the measurements using two identical wide band horns are shown in Figure 2.5. In Figure 2.5(a), the measured antenna transfer functions are shown. Figure 2.5(b) and shows the real and imaginary parts of the transfer functions after conjugate reflection in the frequency domain. Transmitting and receiving antenna impulse responses are shown in Figures 2.5(c) which indicate that $\overrightarrow{h}_{Tx}(t)$ is the derivative of $\overrightarrow{h}_{Rx}(t)$.

2.3.9 Time Domain Parameters

Antenna effects on the transmitted/ received signals are investigated in the time domain by analyzing the envelope of the analytic response for co–polarization. The real valued antenna's transient response is,

$$h_n(t) = \Re \overrightarrow{h}_n(t) \tag{2.24}$$

According to 2.6, the peak output voltage from an incident wave form depends on the peak value $p(\theta, \varphi)$ of the antenna's transient response:

$$p(\theta, \varphi) = max \ t \ |\overrightarrow{h}_n(t, \theta, \varphi)| \tag{2.25}$$

A measure for the linear distortion of the antenna is the envelope width, which is defined as the full width at half maximum (FWHM) of the magnitude of the transient response envelope.

$$FWHM_{0.5}(\theta, \varphi) = t_2|_{p/2} - t_1|_{p/2, \ t_1 < t_2} \tag{2.26}$$

The duration of the ringing is defined as the time until the envelope has fallen from the peak value below a fraction α of the main peak.

$$RINGING_\alpha = t_2|_{\alpha \cdot p} - t_1|_{p, \ t_1 < t_2} \tag{2.27}$$

The lower bound for α is chosen according to the noise floor of the measurement. In order to compare the ringing of antennas with different gains under the
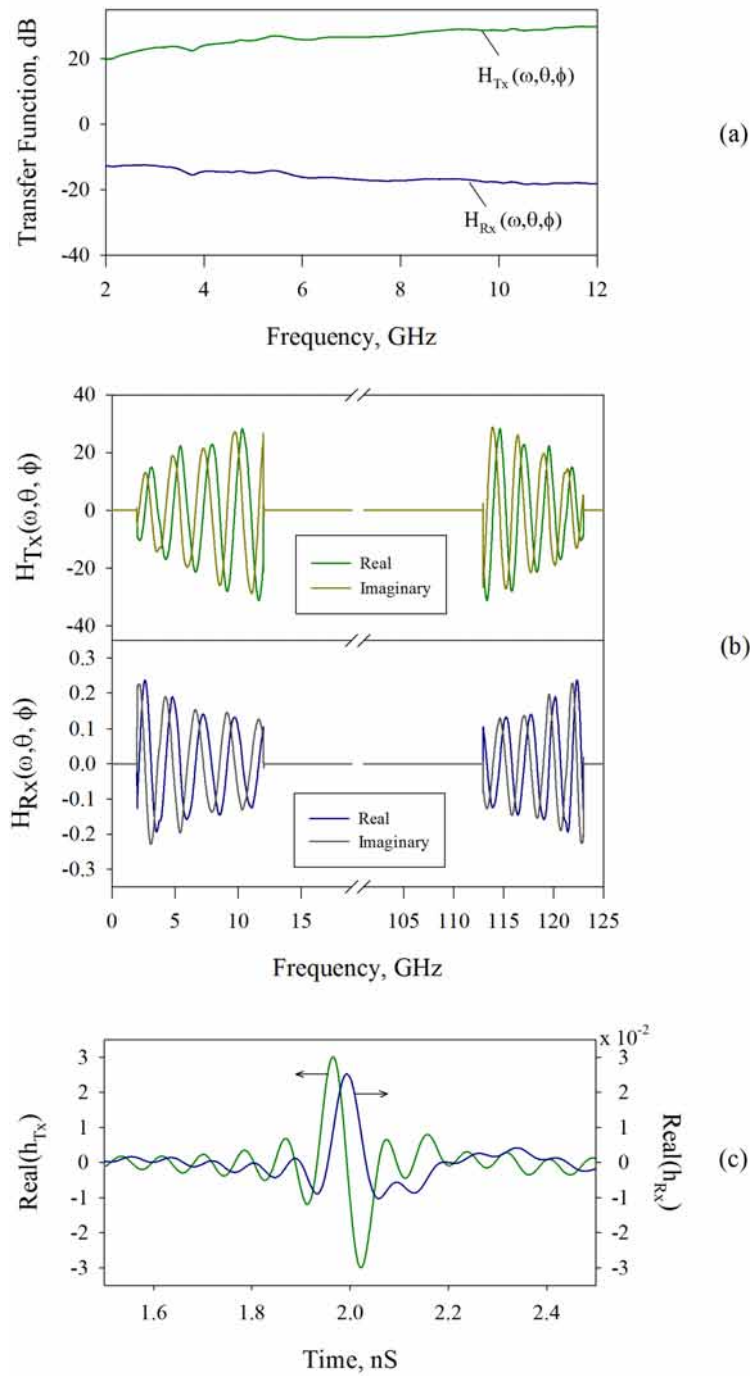
Figure 2.5: (a) Transmitting and receiving transfer functions of identical wide band horn antennas (b) Transmitting and receiving transfer functions after conjugate reflection (c) Impulse response of the transmitting antenna and receiving antenna.

constraint of constant noise floor, the fraction α is chosen to be $\alpha = 0.22$ (–13 dB).

2.3.10 Pulse Distortion Analysis

The analytic response $\overrightarrow{h}_n(t, \theta, \varphi)$ can be convoluted with the input pulse $s_i(t)$ to obtain effects of the antenna on the received signals as a waveform distortion.

$$s_o(t) = \overrightarrow{h}_n(t, \theta, \varphi) \otimes s_i(t) \tag{2.28}$$

For UWB systems, receivers are in general based on the pulse energy detection or correlation with the template waveform. Therefore, the pulse distortions can be examined by calculating fidelity factor which is defined as [Nikolay Telzhensky, 2006],

$$F = max \ \frac{\int_{-\infty}^{+\infty} s_i(t) \cdot s_o(t - \tau) \ dt}{\sqrt{\int_{-\infty}^{+\infty} |s_i(t)^2| \ dt \cdot \int_{-\infty}^{+\infty} |s_o(t)^2| \ dt}} \tag{2.29}$$

where τ is the delay which is varied to maximize the numerator. The fidelity parameter is the maximum of the cross–correlation function and compares only shapes of both waveforms, not amplitudes. This measurement is performed for different spatial orientations of the test antenna.

2.4 conclusion

In this chapter, the methodology adopted for the design and characterization of the antennas in the present work is outlined. Pre–fabrication studies including a parametric analysis is performed in CST Microwave Studio. Measurements in the frequency domain include return loss, radiation pattern and Gain. Time domain studies are performed after measurement in the frequency domain followed by Fourier Transformation. Following chapters are build on techniques outlined in this Chapter.

References

BALANIS, C. A. 1996. *Antenna Theory: Analysis and Design*. C. A. Balanis, New York, NY, USA. 19

DUROC, Y., GHIOTTO A. VUONG T. P., & TEDJINI, S. 2007. Uwb antennas: Systems with transfer function and impulse response. *IEEE Transaction on Antennas and Propagation*, **55**(5), 1449–1451. 24

IEEE. 1979. *IEEE standard test procedures for antennas (IEEE Std 149–1979)).* New York: IEEE. 22

JONGH R. K., M. HAJIAN, L. P. LIGTHART. 1997. Antenna time–domain measurement techniques. *IEEE Antennas and Propagation Magazine*, **39**(5), 7–12. 24

MOHAMMADIAN A. H., A. RAJKOTIA, S. S. SOLIMAN. 2003 (November). Characterization of UWB transmit–receive antenna system. *Pages 157–161 of: IEEE Conf. Ultra Wideband Systems and Technology.* 24

NIKOLAY TELZHENSKY, YEHUDA LEVIATAN. 2006. Novel method of UWB antenna optimization for specified input signal forms by means of genetic algorithm. *IEEE Transaction on Antennas and Propagation*, **54**(8), 2216–2225. 31

SCHANTZ, HANS GREGORY. 2002 (May). Radiation efficiency of uwb antennas. *In: Proceedings of the 2002 ieee uwbst conference.* 22

SHLIVINSKI A., E. HEYMAN, R. KASTNER. 1997. Antenna characterization in the time domain. *IEEE Transactions on Antennas and Propagation*, **45**(7), 1140–1149. 24

SORGEL W., W. WEISBECK. 2005. Influence of the antennas on the ultra–wideband transmission. *EURASIP Journal on Applied Signal Processing*, **3**, 296–305. 24

SORGEL W., S. KNORZER, W. WIESBECK. 2003 (September). Measurement and evaluation of ultra wideband antennas for communications. *Pages 377–380 of: International ITG Conference on Antennas – INICA2003.* 19, 24

ZWIERZCHOWSKI S., P. JAZAYERI. 2003. Derivation and determination of the antenna transfer function for use in ultra–wideband communications analysis. *Wireless Proceedings*, July. 24

Chapter 3

The Square Monopole Antenna

Monopole antennas are used in communication systems at a wide range of frequencies. Electrical properties of these antennas are dependent upon the geometry of both the monopole element and the ground plane. The monopole element is either electrically short with length much less than a quarter-wavelength or near-resonant with length approximately a quarter-wavelength. This element can be thin with length-to-radius ratio much greater than 10^4 or thick with length-to-radius ratio of $10^1 - 10^4$. In addition, the ground-plane dimensions may vary from a fraction of a wavelength to many wavelengths [Weiner, 2003]. Traditionally, a monopole geometry consists of a vertical cylindrical element at the center of a perfectly conducting, infinitely thin, circular ground plane in free space. Electrical characteristics of such antennas are primarily a function of only three parameters; the element length, element radius, and the ground-plane radius, when each is normalized to the excitation wavelength. Radiation pattern of such antennas are uniform in the azimuthal direction.

UWB monopole antennas fall in to volumetric and non–volumetric categories based on their structures. Non–volumetric UWB antennas are microstrip planar structures evolved from the volumetric structures, with different matching techniques to improve the bandwidth ratio without loss of the radiation pattern properties.

3.1   Volumetric UWB Antennas

Volumetric UWB antennas date from the days of spark gap systems. In 1898, Oliver Lodge disclosed spherical dipoles, square plate dipoles, bi–conical dipoles and bow–tie dipoles [Lodge, 1898] and introduced the concept of a monopole antenna with earth as the ground. A renewed interest in the wide band antennas led to the rediscovery of biconical and conical monopoles by Carter in 1939 [Carter, 1939a]. Carter improved upon Lodge's original design by incorporating a broadband transition between a feed line and radiating elements [Carter, 1939b]. The complete analysis of these antennas can be found in [Stutzman, n.d.].

Another remarkable invention is the classic "volcano smoke antenna developed by Kraus in 1945, a detailed report of which can be found in [Lee Paulsen, 2003]. This antenna topology offers exceptional bandwidth and azimuthal omni–directionality.

Sleeve monopole configurations [Stutzman, n.d.] excited using a coaxial transmission line exhibit broad band radiation behavior. The sleeve exterior acts as a radiating element while its interior acts as the outer conductor of the feed coaxial transmission line.

Stohr proposed the use of ellipsoidal monopoles and dipoles [Stohr, 1968] which was re–discovered in [Narayan Prasad Agarwall, 1998]. This paper presents the extensive analysis carried out on square, rectangular and hexagonal disc monopole antennas in addition to the elliptical design.

Square/ rectangular monopole antennas are inherently bandwidth limited and in order to improve the bandwidth, various techniques were proposed. In [Lee E., 1999], it was demonstrated that when a shorting pin is added to a planar monopole antenna, an additional mode is excited below the fundamental mode. By optimizing the dimensions 50% size reduction is obtained when compared to an equivalent planar monopole without a shorting pin. In [Anob P. V., 2001], two techniques are presented; offset feeding and the use of orthogonal square monopoles on a circular base to obtain wide band response and omnidirectional radiation.

The use of beveling technique [Ammann, 2001] and that of a shorting pin [Ammann, 2003] can improve the overall impedance bandwidth of square monople antennas. In [Antonino-Daviu E., 2003] the use of double feeding and in [Kin-

Lu Wong, 2005b], a trident shaped feeding is proposed to improve the impedance bandwidth of such antennas.

Effect of finite ground plane on the impedance bandwidth of planar monopole antenna was studied in [Saou-Wen Su, 2004]. Their study shows that the first resonance is greatly affected by the ground plane and that there exists an optimal diameter of the circular ground plane for achieving a maximum impedance bandwidth. Large ground–plane effects on the radiation pattern and antenna gain are also studied in this paper, especially for the lower frequencies in the antennas impedance bandwidth.

In [Kin-Lu Wong, 2004b], a metal-plate monopole of inverted-L shape with a matching tuning portion is mounted at the top edge of the supporting metal frame to create an antenna with ultra wide bandwidth. Impedance bandwidth of this antenna is from 1.89 –10.14 GHz. A modified version of this antenna is proposed in [Kin-Lu Wong, 2004a], with bandwidth from 1.890 – 6.450 GHz to integrate with laptops as it covers the UMTS (1.920 – 2.170 GHz) and WLAN (5.150–5.350/ 5.725–5.875 GHz) bands.

To improve the impedance bandwidth, wide slots are embedded in the rectangular monopole in [Valderas D., 2005]. The slots created additional resonances and the achieved bandwidth ratio is 1 : 3.75.

In [Saou-Wen Su, 2005a], a 'U' shaped slot is incorporated to a square planar antenna with beveling to realize band notch to forbid interference with the IEEE 802.11a and HIPERLAN/2 systems. An annular slot inside the same monopole effectively notched out the 5.15–5.35 and 5.15–5.825 GHz bands with a VSWR > 14 as demonstrated in [Jianming Qiu, 2005]. In [Kin-Lu Wong, 2005a] an arc shaped slot is incorporated in to a circular disc monopole antenna to achieve the band–notch. The length of the arc controls the frequency that is being notched.

To design a rectangular monopole antenna with improved bandwidth, a 'U' shaped metal plate monopole in implemented in [Saou-Wen Su, 2005b].

In [Xuan Hui Wu, 2005], the characteristics of four planar dipoles are studied. Pulses radiated in different directions are presented in this paper for both single-band and multi-band schemes in UWB applications.

In [Chen, 2005] the design of broad band bi-arm rolled monopole antenna, constructed by wrapping a planar monopole is presented and its transfer response have been analyzed.

The coupled sectorial loop antenna in [Nader Behdad, 2005] achieves ultra-wide bandwidth through a magnetic coupling of two adjacent sectorial loops. The antenna exhibits 8.5:1 frequency range with a VSWR lower than 2.2. Dimension of this antenna is smaller than 0.37 λ_0 at the lowest frequency of operation and has consistent radiation pattern throughout the band.

The monopole in [Ka-Leung Lau, 2005] is formed by connecting four trapezoidal plates orthogonally. A circular patch which is shorted to the circular ground plane by four shorting wires is placed at the top of the monopole. The antenna posses –10 dB bandwidth of 138 % which is about 49 times that of the corresponding monopole wire-patch antenna.

In [Valderas D., 2006] a design process for improving the bandwidth of beveled planar monopole antennas has been proposed by studying movements over the Smith chart. The involved monopole variables were the height, the width, the bevel angle of the lower edge, the feeding length, and the capacitance with the ground plane. These parameters are conveniently combined to implement a UWB antenna with a frequency-independent bandwidth greater than 1 : 37 for VSWR < 2. The radiation patterns are nearly constant and omnidirectional at the representative frequencies.

The antenna optimization proposed in [Nikolay Telzhensky, 2006] makes use of the genetic algorithm and is based on the time domain characteristics of the antenna. Optimization procedure presented in this paper aims at finding an antenna with low VSWR and low-dispersion to ensure high correlation between the time-domain transmitting antenna input signal and the receiving antenna output signal. This procedure has been applied to a simplified version of the volcano smoke antenna proposed by Kraus, and can be extended to any other type of UWB antenna.

In [George Thomas K., 2006], the authors proposed a new ultra wide band, sleeved transmission line-fed rectangular planar disc monopole antenna with a small ground plane. Objective of the authors was to design a monopole antenna with improved radiation performance than existing ones. The antenna offers an ultra broadband performance in the frequency band 0.5 – 9.0 GHz with a VSWR of less than 2.5 : 1.

Certain UWB applications such as a wireless dongle require antennas constricted in space and an antenna design suitable for such applications were

proposed in [Saou-Wen Su, 2007]. This compact antenna comprises a L–shaped rectangular monopole element and a matching section and is relatively easy to fabricate. In [Jaewoong Shin, 2007] yet another design can be found suitable for UWB dongle applications. In [Saou-Wen (Stephen) Su, 2007] the antenna is mounted at the top portion of the PCB and one end of the radiating arm is short-circuited to the system ground plane. With the proposed antenna structure, wide operating bandwidth of larger than 7.6 GHz is obtained that easily cover the 3.1–10.6 GHz band.

In [Irene Ang, 2007] design of a double layer, probe–proximity coupled, stacked diamond–shaped microstrip patch antenna is proposed with ultra wide bandwidth. The authors have shown that broadband characteristic can be achieved by exciting all the higher order modes in the microstrip patch antenna simultaneously by shorting the ringing tail through simple capacitor coupling. The proposed antenna has an impedance bandwidth of 101.8 % for VSWR < 2.

A compact wide band folded–shorted antenna is presented in [Giuseppe Ruvio, 2007] that employs different impedance bandwidth enhancing techniques together to cover the UWB spectrum. The microstrip feed of the antenna is printed on FR4 and a folded thin metallic sheet is connected to the printed element and shorted across the full length of the ground plane. This grounding significantly enhances the impedance bandwidth and helps to mitigate the effect of the asymmetry due to the offset feed arrangement.

An omnidirectional monopole antenna shaped by symmetrically wrapping a PEC sheet that has two trapezoidal cuts at the bottom corners is proposed in [Xuan Hui Wu, 2008]. It has an extremely wide impedance bandwidth of 132 % while keeping an omnidirectional and wide band radiation over the 3.1–10.6 GHz band. Finite ground plane of this antenna introduces ripples in the gain versus frequency response which can be estimated by a simple expression with the knowledge of ground plane size. Furthermore, the ripples can be removed by resistively loading the edge of the ground plane.

3.2 Non-Volumetric UWB Antennas

As already mentioned, non-volumetric UWB antennas are microstrip planar structures evolved form the volumetric structures. In [Schantz H. G., 2001],

the diamond and in [Lu G., 2003], the rounded diamond antennas have been shown to have wide-band properties suitable for ultra wide–band applications. In [Guofeng Lu, 2004], theoretical analysis, simulations and experiments are all conducted to further characterize these two antennas in terms of radiation pattern, gain versus frequency and impedance properties.

UWB on–body propagation channel measurements were performed in [Alomainy A., 2005] to study the deterministic channel characteristics. A printed horn shaped self–complementary antenna and a planar inverted cone antenna were investigated for their effects on the channel behavior. Results show that the hybrid use of different types of UWB antennas can effectively improve channel behavior in body-centric wireless networks.

In [Low Z. N., 2005], a monopole antenna is proposed where the authors used three techniques to realize compactness and wide bandwidth; dual slots on the rectangular patch, a tapered connection between the rectangular patch and the feed line and a partial ground plane flushed with feed line. This antenna shows stable characteristics over the entire UWB frequency band.

The correspondence [Chen Ying, 2005] presented a planar antenna in low-temperature co–fired ceramic technology for a single–package solution of UWB radio. The antenna has an elliptical radiator fed through a microstrip line. The radiator and the microstrip line share the same ground plane with the other UWB radio circuitry. The prototype antenna has achieved bandwidth of ∼110% from 3–10.6 GHz with broad patterns, and relatively constant group delay.

The printed circular disc monopole antenna fed by microstrip line is investigated [Jianxin Liang, 2005]. Impedance band width of this antenna is from 2.78 – 9.78 GHz and the first resonance has been well accounted numerically. The antenna has been characterized in the frequency and time domains.

In [Joeri R. Verbiest, 2005], a new antenna topology is presented based on the printed tapered monopole antenna. A slot is added in the tapered radiating element and in the ground plane, to yield wide band behavior and good matching. The matching performance and the pulse distortion of the antenna in the presence of human tissue are also studied.

In [Yu-Jiun Ren, 2006], an annular ring is electromagnetically coupled to realize UWB. Ground plane of the microstrip line is removed beneath the annular ring and the –10 dB impedance bandwidth of the antenna is from 2.8 to 12.3

GHz. Radiation patterns are stable within the operating bandwidth with an average antenna efficiency of 81%.

In [Yildirim, 2006], a microstip fed, small, low profile, branched monopole antenna is presented with ultra wide bandwidth. By adjusting the branch length and/or adding another branch, the design can be adapted for WLAN, Bluetooth and UWB applications. However, asymmetry in the geometry of the antenna has affected the radiation pattern, which is slightly modified from omnidirectional.

A double-sided rounded bow-tie antenna with ultra wide bandwidth is proposed in [Tutku Karacolak, 2006]. The authors have shown that antennas with rounded patches provide wider bandwidth with higher co-polarization and lower cross-polarization levels for the UWB range compared to their flat-end counterparts.

In [Shi-Wei Qu, 2006] an ultra wide–band a monopole antenna with rounded corners is proposed. By introducing a coplanar waveguide resonant cell, the proposed antenna could notch the WLAN bands for a VSWR > 10. This compact antenna operates from 2.67 to over 12 GHz, and shows omnidirectional radiation pattern.

The proposed antenna design in [Peyrot-Solis M. A., 2006] uses the beveling technique for both the radiator and the ground plane so as to provide necessary feed gap between them to achieve wide impedance bandwidth.

In [Young Jun Cho, 2006], a staircase shape is incorporated in the monopole element and the ground plane is redesigned to realize a UWB antenna with a compact configuration of 25x26 mm^2. Measured bandwidth of the antenna is from 2.9–14.5 GHz and a detailed characterization in the frequency and time domains have been presented.

In [Michitaka Ameya, 2006], design of planar broadband antennas consisting of self-complementary radiating elements and a tapered microstrip line is proposed. Detailed FDTD analysis of these antennas are also presented in this paper.

In [Kuramoto, 2006], design of a planar radiator that does not require a large ground is presented. The design consists of large and small elliptical elements in parallel arrangement. To reduce mutual coupling between these elements and to improve impedance bandwidth, an elliptical slot is designed in the large elliptical element.

In [Shun-Yun Lin, 2006], a pentagon shaped monopole is proposed with ultra wide bandwidth. By embedding an inverted V-shaped slot along the boundary of

this antenna, controllable notch has been demonstrated.

Design of textile antennas for UWB wireless body area network (WBAN) applications is presented in [Maciej Klemm, 2006]. The proposed coplanar waveguide fed printed monopole and UWB annular slot antennas offer direct integration into clothing due to a very small thickness (0.5 mm) and flexibility. The antennas cover the 3.1–10.6 band and the transfer functions are comparable to the PCB realization. The authors have successfully transmitted very short pulses using textile antennas.

Design of the printed-circuit antenna in [Rambabu K., 2006] uses a stepped-patch in combination with multiple resonating elements to realize a bandwidth of more than 150%. The authors have performed a phase center analysis which shows very small variations over the entire available bandwidth.

In [Sachin Gupta, 2006], microstrip and CPW based configurations of planar inverted conical antennas are presented and compared for UWB systems. Design of these antennas follows a third order polynomial equation and hence can be designed easily.

A variation of the defected microstrip structure technique is employed to enlarge the bandwidth of a planar ultra wide-band monopole in [Peyrot-Solis M. A., 2007]. By introducing a defect in the microstrip feed line, the lower bandwidth limit is lowered without affecting the antenna gain and radiation pattern. The bevel technique in the ground plane near to the feeding point is used to increase the highest bandwidth limit. The 50 x 50 mm^2 planar omnidirectional antenna has a voltage standing wave ratio 2 from 2.1 to 12.3 GHz.

In [Ntsanderh C. Azenui, 2007], a compact crescent-shape microstrip antenna is proposed, evolved from the elliptical patch antenna by carving a circular hole inside symmetrically. The circular aperture introduces an additional antenna in-band resonance and provides wider bandwidth with more design flexibility. Radiation properties of this antenna is similar to the full elliptical antenna, with 40% reduction in area (60% of the ellipse area). The characteristic current modes on the crescent antenna are identified and design equation are derived for the lowest frequency of operation of this antenna.

In [Francis Jacob K., 2007], different branches are top loaded on a planar strip monopole and dimensions of the branches are optimized for UWB performance. The antenna shows 10 dB return loss from 3.1 – 9.6 GHz and monopole- like

radiation. The proposed antenna of dimension 65x35 mm^2 can fit into the present day mobile hand sets of typical dimension 100 x 45 mm^2.

The broadband microstrip-fed printed antenna proposed in [Eldek, 2007] for phased antenna array systems consists of two parallel-modified dipoles of different lengths. The regular dipole shape is modified to a quasi-rhombus shape by adding two triangular patches. A modified array configuration is proposed to further enhance the antenna radiation characteristics and usable bandwidth. The proposed antenna provides end fire radiation patterns with high gain, high front-to-back ratio, low cross-polarization level, wide beam width, and wide scanning angles in a wide bandwidth of 103 %.

In [Jin-Ping Zhang, 2007], a microstrip fed semi-elliptical dipole antenna is proposed and designed to cover the 3.1 – 10.6 GHz UWB. Radiation patterns are similar to those of a conventional dipole antenna with dimension only about one third of the wavelength instead of half wavelength at the lower frequency. With simple and proper modification of the patches, a frequency-notched antenna is also designed.

In [Zhi Ning Chen, 2007], a small printed antenna is described with reduced ground-plane effect. The radiator and ground plane of the antenna are etched on a printed circuit board with an overall size of 25 x 25 mm^2. A notch is cut from the radiator and a strip is asymmetrically attached to the radiator. The antenna achieves a broad operating bandwidth of 2.9–11.6 GHz for a 10-dB return loss. Effect of the ground-plane on the impedance bandwidth is greatly reduced by the notch in the radiator because the electric currents on the ground plane are significantly suppressed at the lower edge operating frequencies. The antenna features three-dimensional omni-directional radiation with high radiation efficiency of 79–95% across the UWB bandwidth.

In [Yi-Min Lu, 2007], ultra wide band antenna is designed using a double-printed circular disc. Reasonable theoretical analysis of the antenna has been carried out in this paper.

A simple design of a printed circular monopole antenna with band-notch characteristic is presented in [Chih-Yu Huang, 2007]. Frequency notch in this antenna is created by cutting a pie-shaped slot on the circular radiating patch.

A parametric study of the printed elliptical monopole antennas is presented in [Anob P. V., 2001]. Based on this, design equations are derived for these antennas

which are validated by measurements.

A planar shorted dipole antenna capable of generating a 9:1 bandwidth (820–7340 MHz) is presented in [Wei-Yu Li, 2007]. The radiating element consists of two C- shaped radiating arms occupying a compact area of 0.30λ x 0.47λ, where λ is the wavelength of the desired lower edge of the band of operation. In addition to the use of C-shaped radiating arms, which reduces the total length of the proposed antenna when compared to the case of using straight radiating arms, the short circuiting of the two radiating arms further effectively decreases the lower frequency with a fixed antenna size.

In [Tzyh-Ghuang Ma, 2007], to achieve band-rejection at the WLAN bands, strips of the fork shaped monopole are folded back to result in a pair of coupled lines on the radiator. Based on the band-notched resonance, an equivalent circuit model is proposed for the antenna and the calculated antenna input admittance has been shown to agrees with the full-wave simulation data. Using the normalized antenna transfer function, the radiation characteristics are investigated thoroughly. The transmission responses of a transceiving antenna system and their corresponding transient analysis are also discussed in this paper.

The lower edge curve of a monopole antenna is an important parameter in determining the impedance bandwidth. In [Ching Wei Ling, 2007], a new edge curve characterized by the binomial function is proposed. The effect on the impedance bandwidth with different order of the binomial function and the gap between the antenna and ground plane has been investigated in this paper.

Impacts of the 3.1–10.6 GHz on-human-body UWB channel on the impulse radio wireless body area network system has been studied in [Yue Ping Zhang, 2007]. A performance evaluation method is presented in this paper for the realistic UWB-WBAN systems, which observes the waveform distortion along the signal path. Measurement and characterization of the 3.1–10.6 GHz on-human-body UWB channel are devised to generate the radiographs of path loss and delay spread for the first time in this paper. The study shows that the human body effect is more significant than environment effect when the propagation channel contains no line-of-sight path. Various candidate pulse shapes and modulation schemes for UWB WBAN are studied and their performances with the measured WBAN channel are evaluated and compared.

In [Ching-Hsing Luo, 2007], a dual band-notched CPW fed monopole antenna

is proposed where a ring in the feeding structure is used to increase the impedance bandwidth. Two quarter-wavelength tuning stubs inserted into the feeding ring and radiating ring, respectively, creates two band-notches at 5.15 and 5.75 GHz across the UWB from 2.6 – 12 GHz. The novel design is quiet compact and suitable for creating UWB antenna with dual narrow frequency notches.

In [Keyvan Bahadori, 2007], an elliptic-card ultra wide band planar antenna is proposed. The design consists of an elliptic radiating element and a rectangular ground plane. The feeding mechanism comprises of a microstrip line on the other side of the substrate and connecting the line to the elliptic element by a via. The structure of the antenna is miniaturized by optimizing its elliptic profile and the required ground plane size is only 22x 40 mm^2. Housing effects on the antenna performance are also studied in this paper.

In [Yi Ding, 2007], a very compact elliptical monopole antenna with a size of 35x20 mm^2 is designed with ultra wide bandwidth. Wide impedance match is by two matching slits at the lower section of the elliptical patch. In addition, using a slot and embedded resonant cell, the authors have demonstrated band notch at 5.5 GHz.

The CPW fed band-notched antenna proposed in [Sang-Ho Lee, 2007] uses tilt steps of two different sizes for improving band width and two folded strip lines for band notch.

The antenna proposed in [Chong Yu Hong, 2007] consists of a radiation patch that has an arc-shaped edge and a partially modified ground plane. The ground design comprises of two bevel slots on the upper edge and two semicircle slots at the bottom edge of the ground plane to improve the input impedance bandwidth and the high frequency radiation performance. By embedding a pair of T-shaped stubs inside an elliptical slot cut in the radiation patch, a notch at 5.5 GHz is obtained.

In [Reza Zaker, 2008], a novel modified microstrip-fed ultra wide-band planar monopole antenna with variable frequency band-notch characteristic is presented. By inserting two slots in the ground plane on both sides of the microstrip feed line, wide impedance bandwidth is produced. A modified H-shaped conductor-backed plane with variable dimensions is used in order to generate the frequency band-stop performance and control band-notch frequency and bandwidth. The designed antenna has a small size of 22x22 mm^2 and operates over the frequency

band between 3.1 and 14 GHz for VSWR < 2 while showing the band rejection performance in the 5.1 to 5.9 GHz frequency band.

The antenna design proposed in this chapter is a planar square monopole with redesigned ground plane to operate in the ultra wide band. As already mentioned, typical design practice to achieve UWB with a square/ rectangular patch is by beveling, parasitic strips or by employing multiple feeding, which may add to the design complexity. The proposed design is novel by introducing cuts in the ground plane that follow specific design guidelines. From a parametric study, design equations are obtained to facilitate designing the antenna on laminates of any permittivity. A band notch scheme is also proposed to limit radiation in the WLAN band. Studies conducted on the frequency domain radiation characteristics of the prototype antenna is also presented in this chapter.

3.3   Antenna Geometry, Design and Optimization

3.3.1   Geometry

Geometry of the square monopole antenna is shown in Figure 3.1 and the corresponding parameters in Table 3.1. This antenna shows a single resonance as in Figure 3.2 in accordance with a quarter wave variation in h. Figure 3.2(a) shows the effect of the ground plane in this resonance and Figure 3.2(b) that of the gap between the ground plane and the square patch. It is clear that these parameters affect only the matching of the antenna.

To design this antenna for ultra wide bandwidth, the design procedure outlined in Figure 3.3 is followed. As shown in Figure 3.3(a), the ground plane with length l is divided in to 9 equal sections having width w and few sections in the ground plane are removed. This antenna can be designed with a microstrip feed either as in Figure 3.3(b) or Figure 3.3(c). The return loss plots of these antennas are shown in Figure 3.5 and the resonances are indicated in Table 3.1. Antennas-b,c,d with modified ground plane have wide impedance bandwidth and among them, Ant.-b exhibits a superior performance in terms of the overall bandwidth. It has been seen, however, that by adjusting $l,\ d$ and w, impedance bandwidths of Antenna-c and d can be improved. A variation study performed with w is shown in Figure 3.4. As w is increased, the second and third resonances merge and improve the –10dB bandwidth. Since the resonances shift to the lower side of the
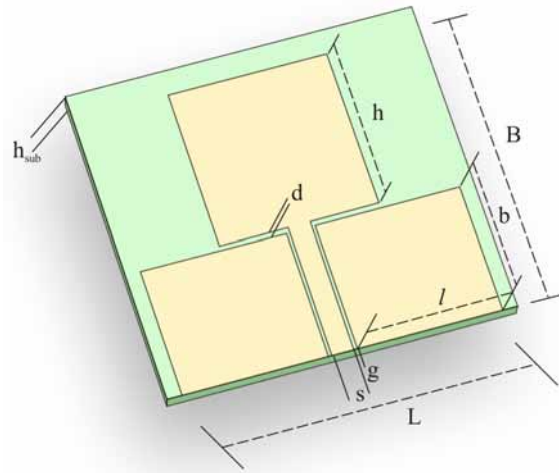
Figure 3.1: The square monopole antenna (Ant.-a).
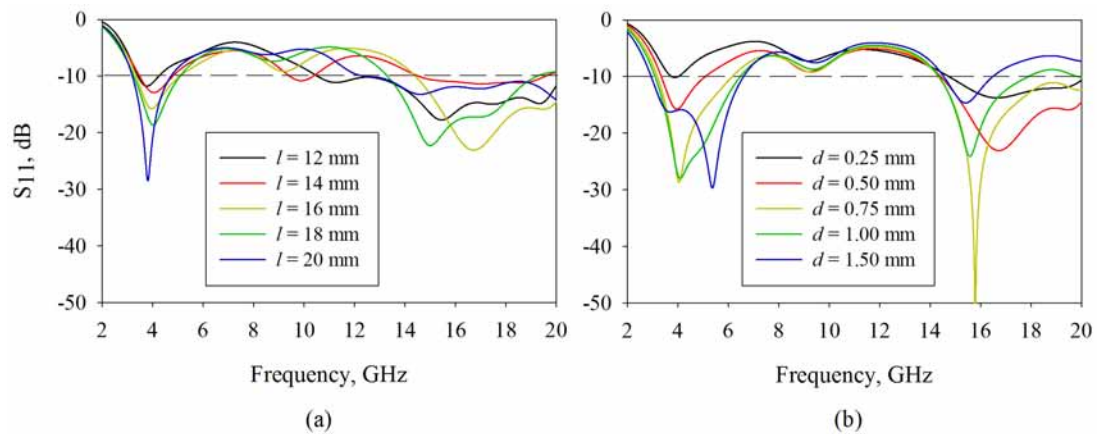
Figure 3.2: Effect of (a) ground plane on the resonance, d = 0.5 (b) gap between the ground plane and the square patch, l = 16 (c) Effect of the variation of w on the return loss (in *mm*)

spectrum with increase in w, it should be fixed at an optimum value that give maximum bandwidth.

For the work presented in this thesis, Antenna-b is selected.

3.3.2   Design

To study the radiation mechanism of this antenna, the surface current distribution is analyzed at the three resonances; 3.8 GHz, 7.9 GHz and 13.4 GHz. Inspecting

Table 3.1: Geometric parameters of the antennas (in mm) in Figure 3.1 and Figure 3.3 on substrate with $\varepsilon_r = 4.4$, $tan(\delta) = 0.02$, $h_{sub} = 1.6$ mm

	s	g	l	b	d	h	w	LxB	f_1, f_2, f_3 (GHz)
Antenna-a	2.3	0.48	14.57	13	0.5	16	–	32x29.6	3.8
Antenna-b	2.3	0.48	14.57	13	0.5	16	1.4	32x29.6	3.77, 7.94, 13.4
Antenna-c	3	–	16	13	0.5	16	1.4	32x29.6	3.65, 6.78, 10.17
Antenna-d	3	–	16	13	0.5	16	1.4	32x29.6	3.60, 7.36, 9.8
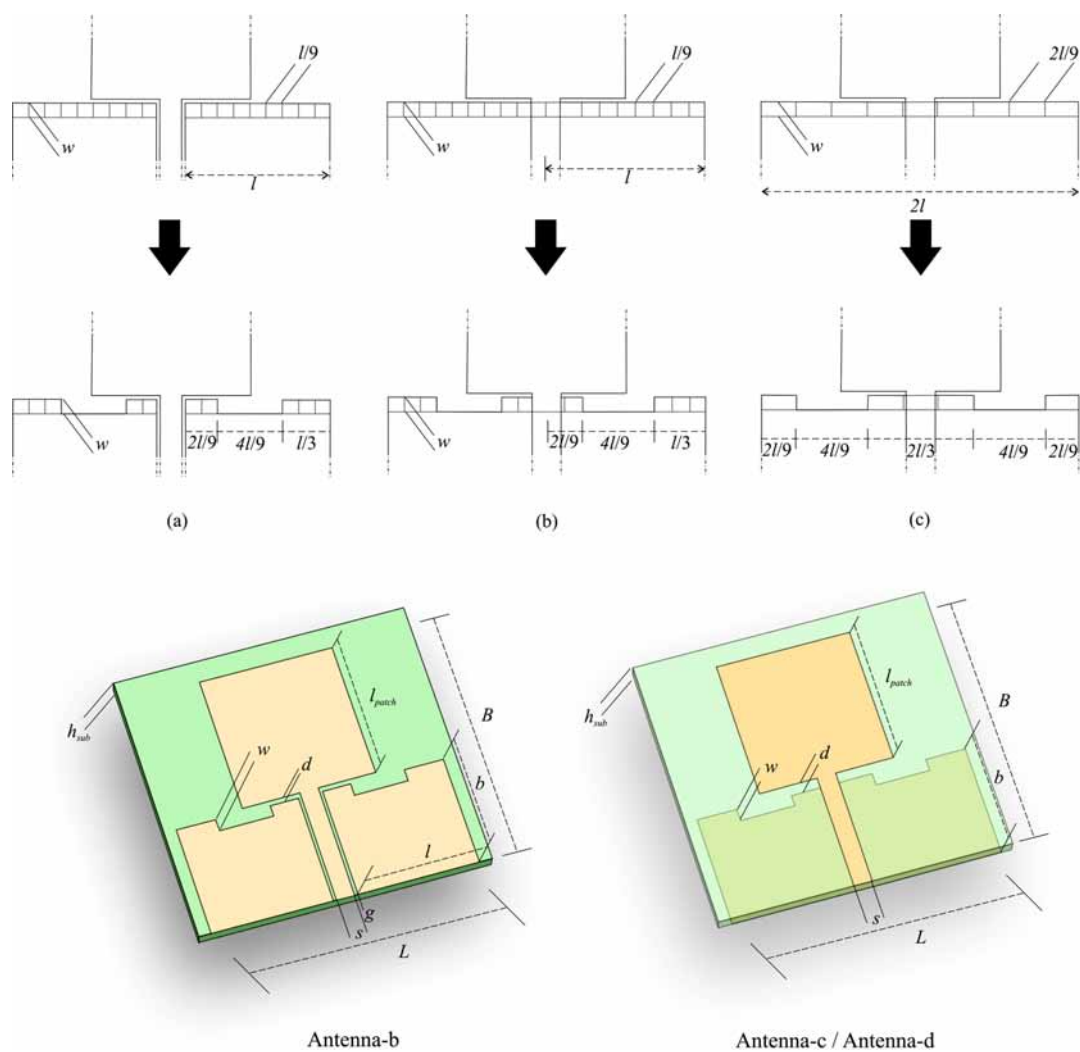
Figure 3.3: Design of UWB square monopole antennas (a) Antenna-b (b) Antenna-c (c) Antenna-d.

Fig. 3.6(a), the first resonance can be accounted as,

$$l_1 \approx \frac{\lambda_{g,1}}{4} \tag{3.1}$$
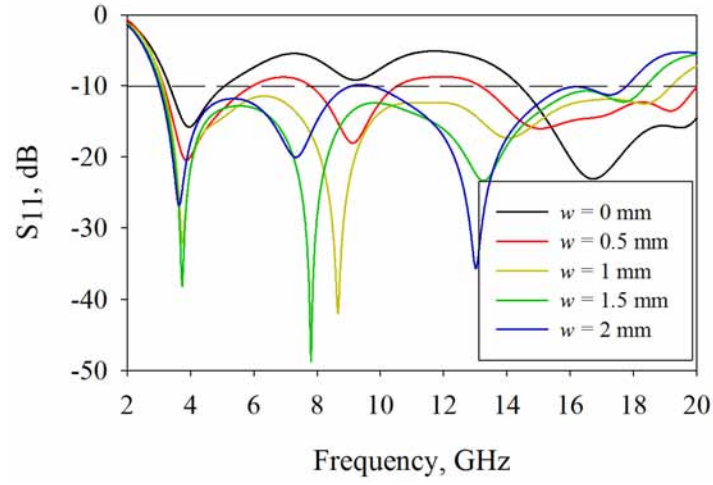
Figure 3.4: Effect of the variation of w on the return loss
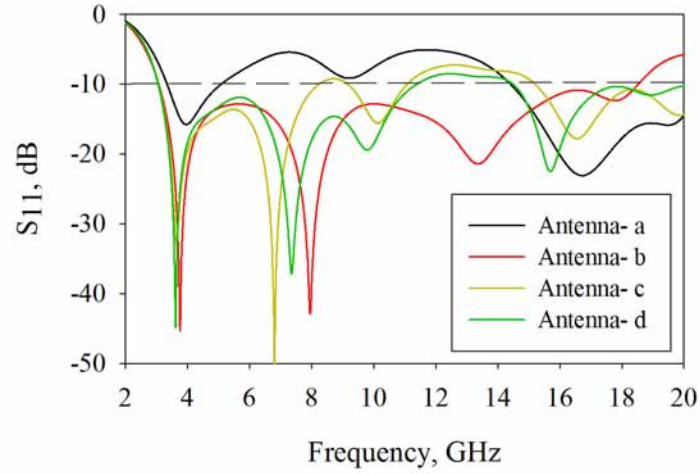
Figure 3.5: Return loss of the antennas in Table 3.1

Similarly, from Fig. 3.6(b) and Fig. 3.6(c), the second and third resonances as,

$$l_2 \approx \frac{\lambda_{g,2}}{4} \tag{3.2}$$

and

$$l_3 \approx \frac{\lambda_{g,3}}{4} \tag{3.3}$$

Here, $\lambda_{g,i}$ is the wavelength in the dielectric which is computed from the free
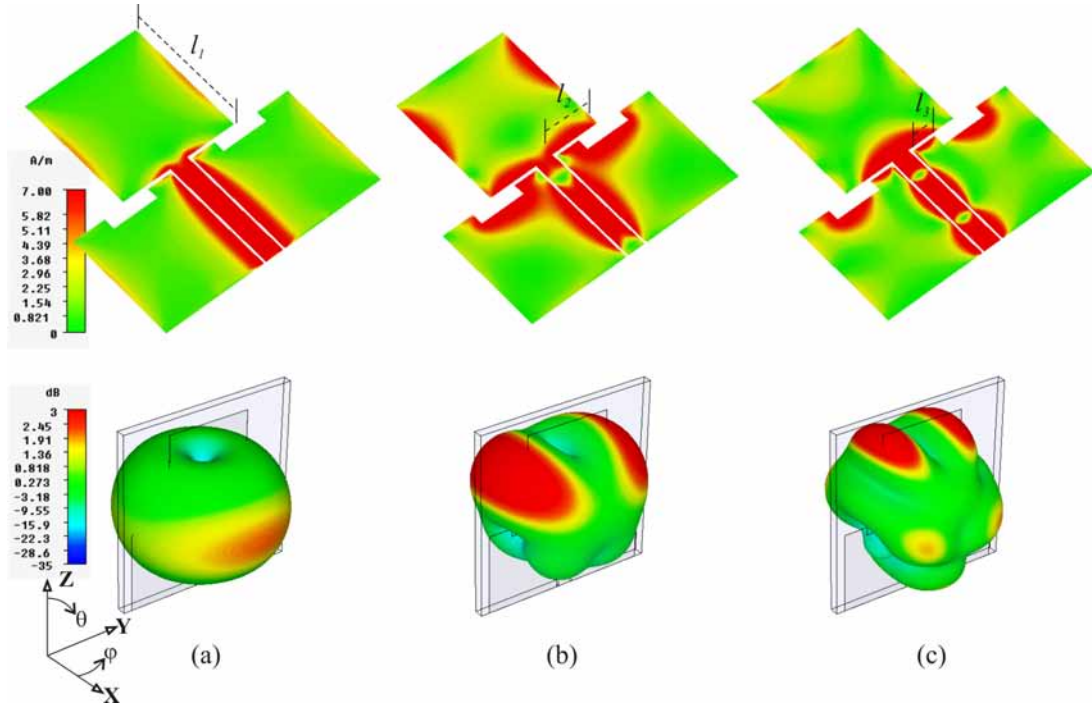
Figure 3.6: Surface current distribution on the antenna at (a) 3.8 GHz (b) 7.9 GHz (c) 13.4 GHz

space wavelength $\lambda_{0,i}$ as,

$$\lambda_{g,i} = \frac{\lambda_{0,i}}{\sqrt{\varepsilon_{re}}}, i = 1, 2, 3 \tag{3.4}$$

where ε_{re} is the effective permittivity of the substrate which is computed from,

$$\varepsilon_{re} = \sqrt[2]{\varepsilon_r \cdot \varepsilon_{air}} \tag{3.5}$$

3.3.3   Optimization

Based on the observations aforementioned, a design procedure for the UWB square monopole antenna is framed as below. The three resonances are fixed at 3.8, 7.9 and 13.4 GHz.

1. Design a 50 Ω CPW / Microstrip line on a substrate with permittivity ε_r and thickness h_{sub}.

Table 3.2: Antenna description

	Antenna-1	Antenna-2	Antenna-3	Antenna-4	Antenna-5
Laminate	Rogers 5880	Taconic RF-30	FR4 Epoxy	Rogers RO3006	Rogers 6010LM
h_{sub}	1.57	1.52	1.6	1.28	0.635
ε_r	2.2	3	4.4	6.15	10.2
$tan(\delta)$	0.001	0.0013	0.02	0.001	0.001
s (mm)	2.3	2.3	2.3	2.3	2.3
g (mm)	0.12	0.18	0.28	0.34	0.6
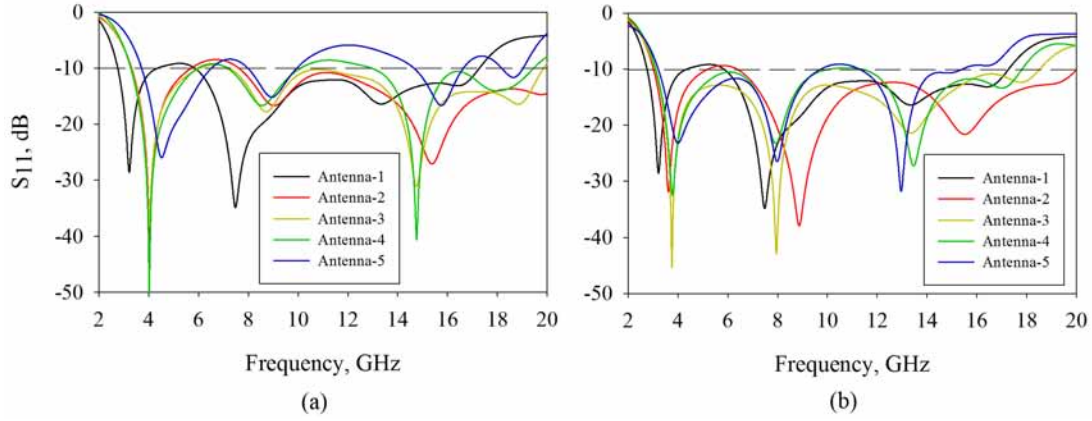
Figure 3.7: Return loss of the antennas (a) with computed geometric parameters (b) with optimized geometric parameters

2. Design the square patch to have the first resonance at 3.8 GHz using Eqn. 3.1. The length of the ground plane is
   $l \approx \lambda_{g,1}/4$, for Antenna-b and c and
   $l \approx \lambda_{g,1}/4 + s + g$, for Antenna-d.

3. Incorporate the pockets in the ground plane by following the guideline in Fig. 3.3. Adjust w to merge the second and third resonances.

4. Perform minor adjustments in l, d and w for the three resonances to be at 3.8. 7.9 and 13.4 GHz.

This design guideline is one of the many approaches that can be tried to design this antenna. Using the parameters so computed, the antenna was studied

Table 3.3: Computed and optimized geometric parameters for the square monopole antenna

Parameter (mm)	Antenna-1		Antenna-2		Antenna-3		Antenna-4		Antenna-5	
	Computed	Optimized	Computed	Optimized	Computed	Optimized	Computed	Optimized	Computed	Optimized
l	16.42	16.42	15.19	16.17	13.8	14.01	12.7	14.01	11.19	14
b	15	15	13	13	13	13	13	13	12	12
d	0.3	0.3	0.5	0.5	0.5	0.5	0.6	0.6	0.75	0.75
h	16.42	16.42	15.19	16.4	13.8	16	12.7	14.4	11.19	14
w	1.3	1.3	13	13	1.4	1.4	1.5	1.5	1.6	1.6
LxW	35.6 x 31.82	38 x 32.4	33.24 x 28.69	35 x 29.8	26 x 27.3	29.5 x 32	26.3 x 28.38	31 x 29.5	24.8 x 23.94	30.4 x 26.75
f_1, f_2, f_3 (GHz)	3.2, 7.5, 13.3	3.2, 7.5, 13.3	4, 9, 16	3.6, 8.8, 15.4	4, 8.67, 14.7	3.75, 8, 13.4	4, 8.65, 14.7	3.79, 8, 13.5	4.48, 8.9, 15.7	3.85, 7.89, 13

on substrates with different permittivity, described in Table 3.2. Figure 3.7(a) shows the return losses of the antennas with the computed geometric parameters given in Table 3.3. Resonances of these antennas show slight deviation from the designed values but the bandwidth is almost similar for all the antennas except for Antenna-5. Due to the shift in the resonance towards the higher side, the lower edge of the band has also been shifted and hence the designs needed to be optimized to cover the 3.1– 10.6 UWB. The optimized design parameters are tabulated in Table 3.3 and the return loss is shown in Fig. 3.7(b). The slight disparity in the computed and optimized design parameters can be attributed to the ambiguity in the exact value of ε_{re}.

3.4 Band Notch Design

In the proposed antenna, to avoid interference with electronic systems operating in the IEEE802.11a and HIPERLAN/2 bands, a band reject mechanism is incorporated by symmetrically cutting two narrow slot resonators perpendicular the lower edge of the square patch (Fig. 3.8). The slot parameters can control the centre frequency, width of the rejection band as well as the peak VSWR of the rejection band. The centre frequency of the band to be rejected is determined by length l_s as shown in Fig. 4.5(a). While designing the resonator, l_s is fixed first. Then, the width of the rejection band and its VSWR is tuned by d_s and t_s. Fig. 4.5(b) and (c) show the effect of these parameters on the rejected band.

Simulation studies on substrates with different permittivity have shown that for a given notch frequency, length of the slit is given by

$$l_s = \lambda_{g,5.5}/4 \tag{3.6}$$

where $\lambda_{g,5.5} = \lambda/\sqrt{\varepsilon_{re}}$ and $\varepsilon_{re} = (\varepsilon_e + 1)/2$

Referring to Fig. 3.8(b), at 5.5 GHz, current is concentrated around the slits and oppositely directed on either sides of the slot. The slots function as shorted transmission lines having an electrical length of approximately $\lambda_g/4$ at 5.5 GHz, giving a high input impedance [Visser, 2005; Pozar, 1998]. The CST simulated value of this impedance is 22+j160 Ω.

The optimized design parameters for getting ultra wide band performance with a rejection band centered at 5.5 GHz is: l_s, d_s, t_s = 7.8 *mm*, 6.8 *mm*, 0.15
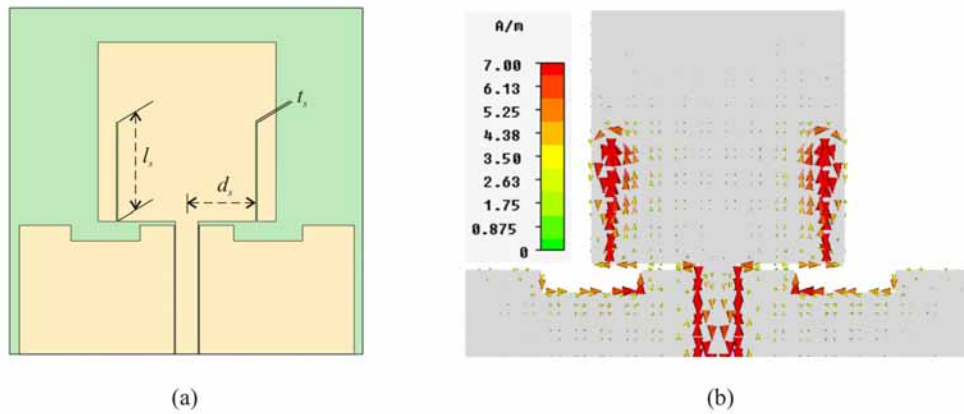
Figure 3.8: UWB Square monopole antenna with slot resonator for band notch (a) design parameters (b) current distribution along the periphery of the slot at 5.5 GHz
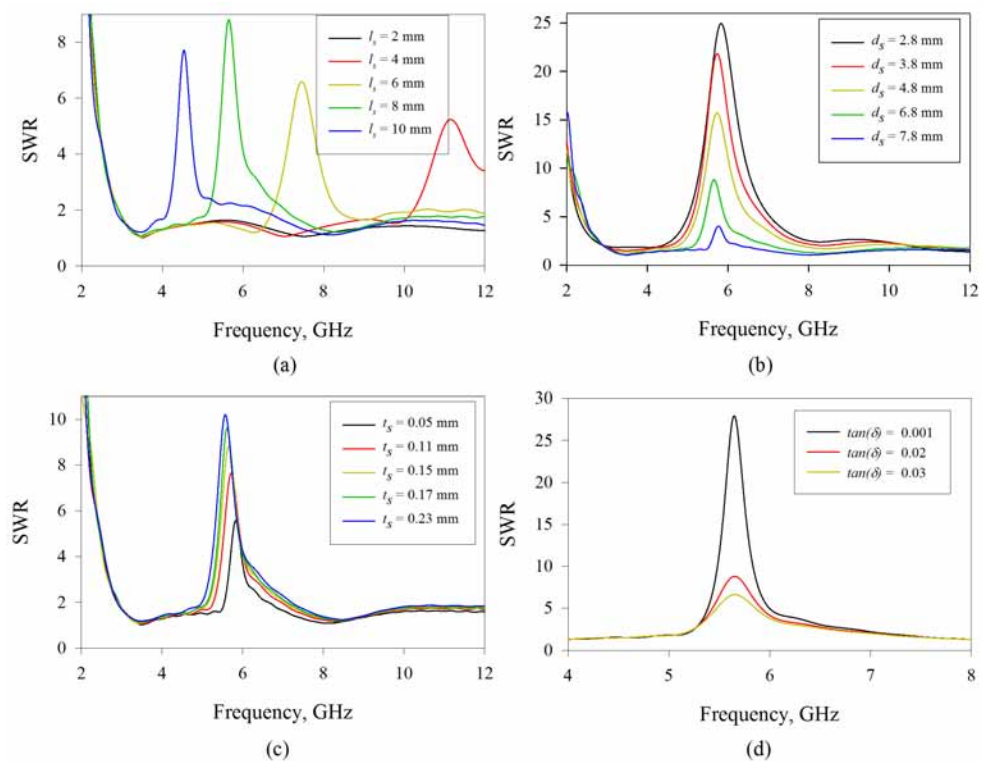
Figure 3.9: VSWR vs. Frequency of the band notch UWB antenna for different (a) slot lengths while $t_s = 0.15mm$ and $d_s = 6.8mm$ (b) slot position while $t_s = 0.15mm$ and $l_s = 7.8mm$ (c) slot width while $l_s = 7.8mm$ and $d_s = 6.8mm$.

mm. Simulation studies have also shown that sharp notch edges and high VSWR (>15) can be obtained if low loss substrates are used.

3.5 Experiment Results

Measured return loss of the UWB square monopole antenna shown in Fig. 3.10(a). The plots are in agreement at the lower frequencies and the slight variation at the higher side could be due to the SMA connector, which, has not been accounted in the simulation. As shown in Fig. 3.10(b), measured and simulated VSWR plots of the band notched UWB antenna also has good agreement and is high (> 3) in the 5.2 - 6 GHz sub band.

Radiation patterns of the antenna at different frequencies are shown in Fig. 3.11 for co and cross polarizations. Each pattern is normalized with respect to the peak value of the corresponding plane. It is found that the patterns are omnidirectional in the H-plane (x-y plane). Across the 3.1-10.6 GHz UWB, the patterns are stable and at higher frequencies, they are slightly distorted.

Radiation pattern of the antenna at the notched frequency is shown in Fig. 3.12. Pattern at 5.5 GHz has been normalized w.r.t that at 3.75 GHz for comparison. Measured gain and radiation efficiency of the square monopole antenna without the band notch resonator and with band notch resonator is shown in Figure 3.13(a) and (b) respectively. Antenna polarization is found to be along the z direction. Measured gain remains constant throughout the band and the average value is found to be 3.75 dBi in the 3.1-10.6 GHz band as shown in Figure 3.13(a). As shown in Figure 3.13(b), there is large decrease in gain when there is a band rejection mechanism as low as -9dB compared to the rest of the band. Measured radiation efficiencies are also reasonably good and is in agrement with simulation.
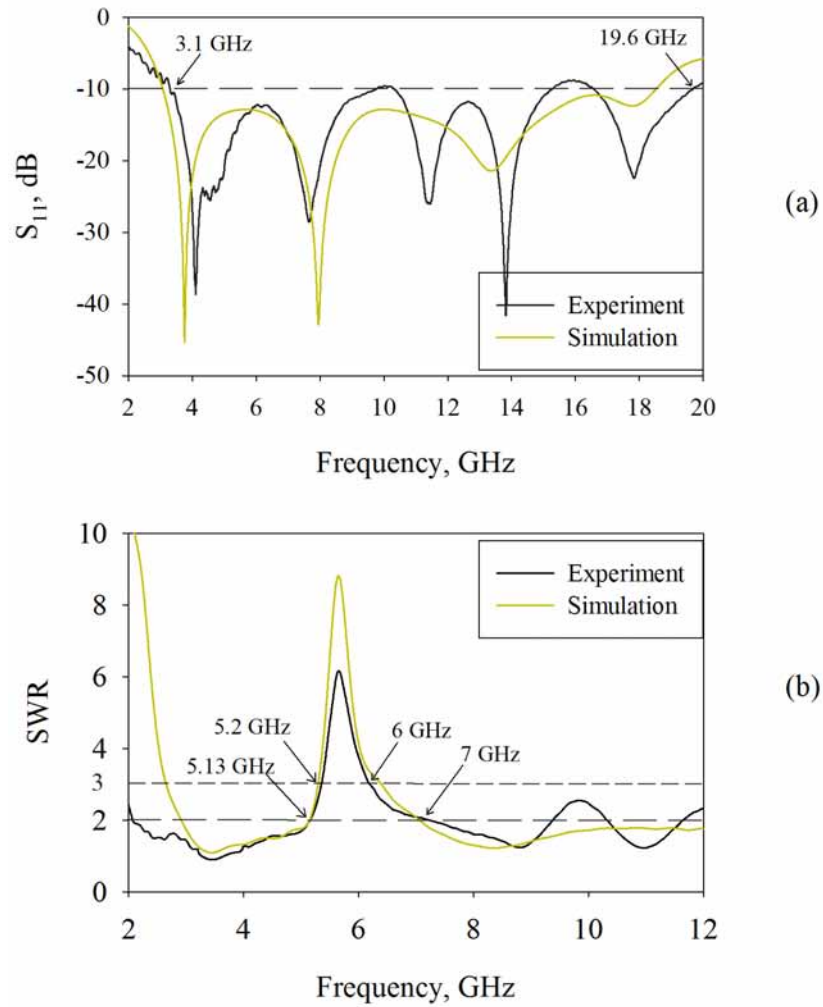
Figure 3.10: Measured and simulated (a) S_{11} of the UWB square monopole antenna (b) VSWR of the band notch antenna
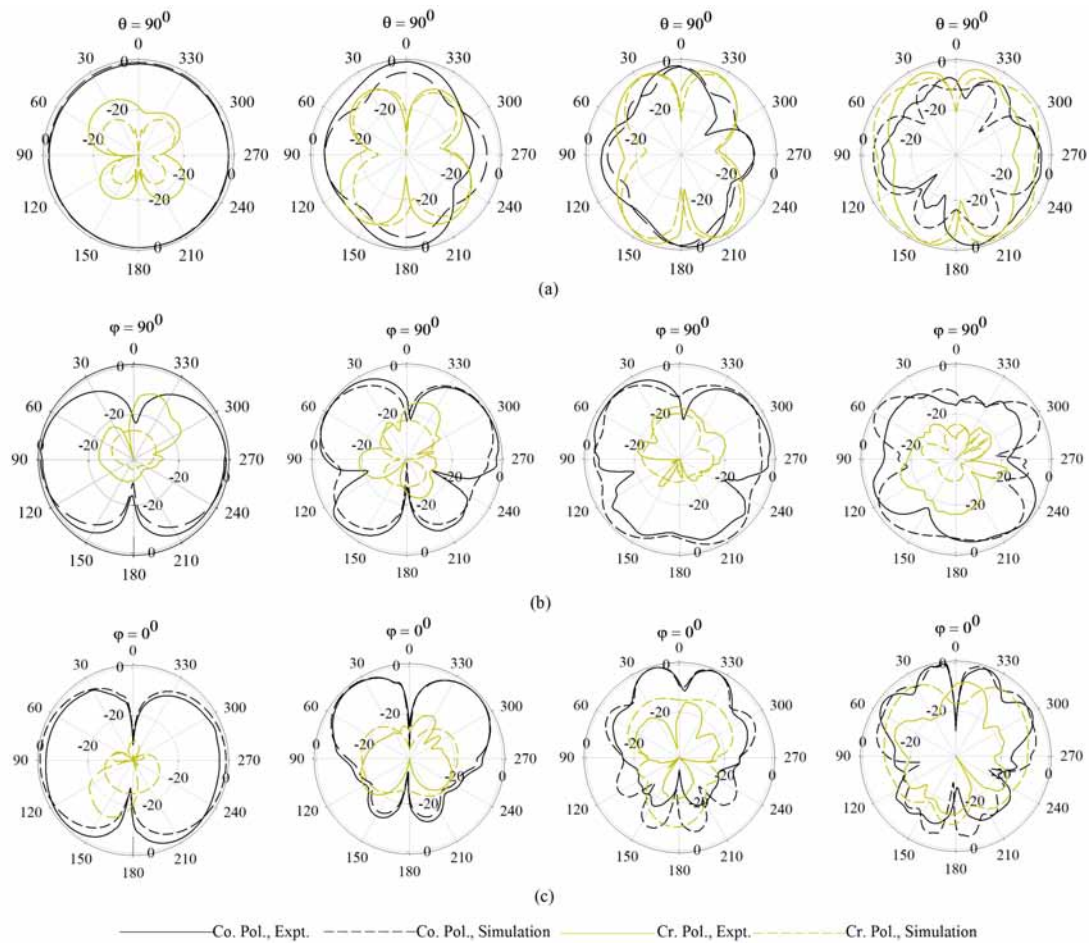
Figure 3.11: Radiation patterns of the UWB square monopole in the (a) x-y plane: 3.75, 8, 13 GHz, 17 GHz (b) y-z plane: 3.75, 8, 13 GHz, 17 GHz (c) x-z plane: 3.75, 8, 13, 17 GHz
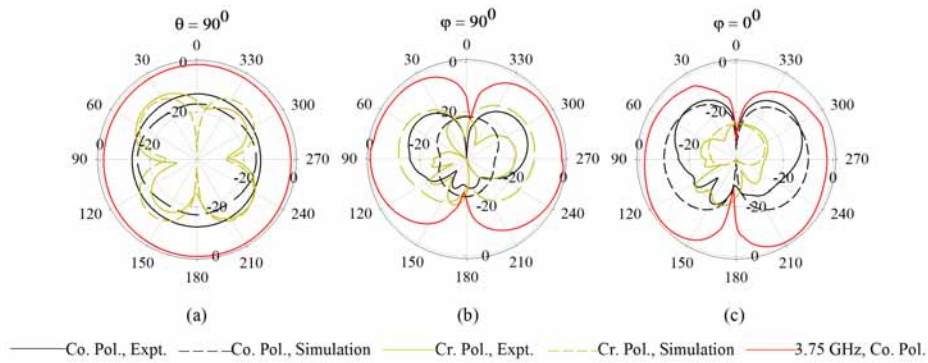
Figure 3.12: Radiation patterns of the band notch antenna at 5.5 GHz (a) x-y plane (b) y-z plane (c) x-z plane
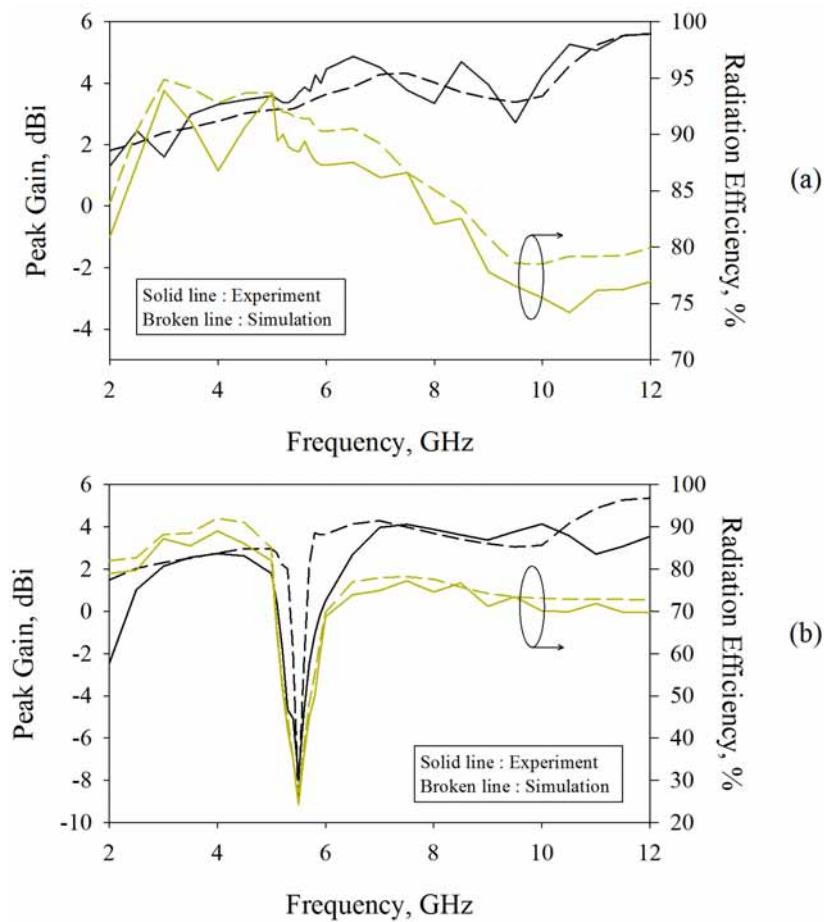
Figure 3.13: Measured and simulated peak gains and radiation efficiency of the square monopole antenna (a) without slot resonator (b) with slot resonator

3.6 Conclusion

A Square Monopole Antenna with ultra wide bandwidth is designed and characterized in this chapter. UWB is achieved by a novel ground modification technique, which minimize pernicious reflections within the antenna structure. This antenna can be designed on any commercially available microwave laminate since universal design guidelines are available. Impedance bandwidth of the antenna is from 3.1–19.6 GHz with stable radiation patterns and gain in the 3.1–10.6 operational band. A band notch technique is also proposed to limit interference with WLAN systems, which is tunable.

References

ALOMAINY A., PARINI C. G., HALL P. S. 2005. Comparison between two different antennas for uwb on–body propagation measurements. *IEEE Transaction on Antennas and Propagation*, **4**, 31–34. 38

AMMANN, MAX J. 2001. Control of the impedance bandwidth of wideband planar monopole antennas using a beveling technique. *Microwave and Optical Technology Letters*, **30**(4), 229–232. 34

AMMANN, MAX J. 2003. A wide–band shorted planar monopole with bevel. *IEEE Transaction on Antennas and Propagation*, **51**(4), 901–903. 34

ANOB P. V., RAY K. P., GIREESH KUMAR. 2001 (July). Wideband orthogonal square monopole antennas with semi-circular base. *In: IEEE Antennas and Propagation Society International Symposium.* 34, 41

ANTONINO-DAVIU E., M. CABEDO-FABRES, M. FERRANDO-BATALLER-A. VALERO-NOGUEIRA. 2003. Wideband double–fed planar monopole antennas. *IEE Electronics Letters*, **39**(November), 1635–1636. 34

CARTER, P. S. 1939a. *Short wane antenna.* US Patent 2, 175, 252. 34

CARTER, P. S. 1939b. *Wide band short wave antenna and transmission system.* US Patent 2, 181, 870. 34

CHEN, ZHI NING. 2005. Novel bi–arm rolled monopole for UWB applications. *Microwave and Optical Technology Letters*, **44**(4), 294–295. 35

CHEN YING, Y. P. ZHANG. 2005. A planar antenna in ltcc for single–package ultrawide–band radio. *IEEE Transaction on Antennas and Propagation*, **53**(9), 3089–3093. 38

Chih-Yu Huang, Wei-Chun Hsia. 2007. Planar ultra wide band antenna with a frequency notch characterestic. *Microwave and Optical Technology Letters*, **49**(2), 316–320. 41

Ching-Hsing Luo, Chien-Ming Lee, Wen-Shan Chen-Chih-Ho Tu Ying-Zong Juang. 2007. Dual band notched ultra wideband monopole antenna with an annula cpw feeding structure. *Microwave and Optical Technology Letters*, **49**(10), 2376–2379. 42

Ching Wei Ling, Wen Hsin Lo, Ran Hong Yan-Shyh Jong Chung. 2007. Planar binomial curved monopole antennas for ultrawideband communication. *IEEE Transaction on Antennas and Propagation*, **55**(9), 2622–2624. 42

Chong Yu Hong, Ching Wei Ling, I-Young Tarn-Shyh Jong Chung. 2007. Design of a planar ultrawideband antenna with a new band-notch structure. *IEEE Transaction on Antennas and Propagation*, **55**(12), 3391–3397. 43

Eldek, Abdelnasser A. 2007. Ultrawideband double rhombus antenna with stable radiation patterns for phased array applications. *IEEE Transaction on Antennas and Propagation*, **55**(1), 84–91. 41

Francis Jacob K., Suma M. N., Rohith K. Raj-Manoj Joseph Mohanan P. 2007. Planar branched monopole antenna for UWB applications. *Microwave and Optical Technology Letters*, **49**(1), 45–47. 40

George Thomas K., Lenin N., Sivaramakrishnan R. 2006. Ultrawideband planar disc monopole. *IEEE Transaction on Antennas and Propagation*, **54**(4), 1339–1341. 36

Giuseppe Ruvio, Max J. Ammann. 2007. A novel wideband semi-planar miniaturized antenna. *IEEE Transaction on Antennas and Propagation*, **55**(10), 2679–2685. 37

Guofeng Lu, Stefan von der Mark, Ilya Korisch Larry J. Greenstein Predrag Spasojevic. 2004. Diamond and rounded diamond antennas for ultrawide–band communications. *IEEE Antennas and Wireless Propagation Letters*, **3**, 249–252. 38

Irene Ang, Ooi B. L. 2007. An ultra wide-band stacked microstrip patch antenna. *Microwave and Optical Technology Letters*, **49**(7), 1659–1665. 37

Jaewoong Shin, Seokjin Hong, Jaehoon Choi. 2007. A compact internal UWB antenna for wireless USB dongle application. *Microwave and Optical Technology Letters*, **50**(6), 1643–1646. 37

Jianming Qiu, Zhengwei Du, Jianhua Lu Ke Gong. 2005. A band-notched uwb antenna. *Microwave and Optical Technology Letters*, **45**(2), 152–154. 35

Jianxin Liang, Choo C. Chiau, Xiaodong Chen Clive G. Parini. 2005. Study of a printed circular disc monopole antenna for uwb systems. *IEEE Transaction on Antennas and Propagation*, **53**(11), 3500–3504. 38

JIN-PING ZHANG, YUN-SHENG XU, WEI-DONG WANG. 2007. Microstrip-fed semi-elliptical dipole antennas for ultrawideband communications. *IEEE Transaction on Antennas and Propagation*, **56**(1), 241–244. 41

JOERI R. VERBIEST, GUY A. E. VANDENBOSCH. 2005. A novel small–size printed tapered monopole antenna for UWB WBAN. *IEEE Antennas and Wireless Propagation Letters*, **5**, 377–379. 38

KA-LEUNG LAU, PEI LI, KWAI-MAN LUK. 2005. A monopolar patch antenna with very wide impedance bandwidth. *IEEE Transaction on Antennas and Propagation*, **2**(53), 655–661. 36

KEYVAN BAHADORI, YAHYA RAHMAT-SAMII. 2007. A miniaturized elliptic-card UWB antenna with WLAN band rejection for wireless communications. *IEEE Transaction on Antennas and Propagation*, **55**(11), 3326–3332. 43

KIN-LU WONG, YUN-WEN CHI, CHIH-MING SU FA-SHIAN CHANG. 2005a. Band–notched ultra-wideband circular–disc monople antenna with an arc–shaped slot. *Microwave and Optical Technology Letters*, **45**(3), 188–191. 35

KIN-LU WONG, LIANG-CHE CHOU, HONG-TWU CHEN. 2004a. Ultra–wide band metal plate monopole antenna for laptop application. *Microwave and Optical Technology Letters*, **43**(5), 384–386. 35

KIN-LU WONG, TING-CHIH TSENG, PEY-LING TENG. 2004b. Low profile ultra-wide band antenna for mobile phone applications. *Microwave and Optical Technology Letters*, **43**(1), 7–9. 35

KIN-LU WONG, CHIH-HSIEN WU, SAOU-WEN (STEPHEN) SU. 2005b. Ultrawide-band square planar metal-plate monopole antenna with a trident-shaped feeding strip. *IEEE Transaction on Antennas and Propagation*, **53**(4), 1262–1268. 34

KURAMOTO, AKIO. 2006. Flat–type uwb antenna consisting of two kinds of elliptical elements located in parallel. *Electronics and Communications in Japan*, **89**(12), 54–61. 39

LEE E., HALL P. S., GARDNER P. 1999. Compact wideband planar monopole antenna. *IEE Electronics Letters*, **35**(25), 2157–2158. 34

LEE PAULSEN, JAMES B. WEST, W. F. PERGER JOHN KRAUS. 2003 (June). Recent investigations on the Volcano Smoke Antenna. *Pages 845–848 of: IEEE Antennas and Propagation Society International Symposium*, vol. 3. 34

LODGE, OLIVER. 1898. *Electric Telegraphy*. US Patent 609, 154. 34

LOW Z. N., CHEONG J. H., LAW C. L. 2005. Low–cost PCB antenna for UWB applications. *IEEE Antennas and Wireless Propagation Letters*, **4**, 237–239. 38

Lu G., Spasojevic P., Greenstein L. 2003 (August). Antenna and pulse designs for meeting UWB spectrum density requirements. *In: IEEE Conf. Ultra Wideband Systems and Technologies*, vol. 4. 38

Maciej Klemm, Gerard Troester. 2006. Textile UWB antennas for Wireless Body Area Networks. *IEEE Transaction on Antennas and Propagation*, **54**(11), 3192–3197. 40

Michitaka Ameya, Manabu Yamamoto, Toshio Nojima Kiyohiko Ito. 2006. Broadband printed dipole antenna employing self–complementary radiating element and microstrip line feed. *Electronics and Communications in Japan*, **82**(12), 62–74. 39

Nader Behdad, Kamal Sarabandi. 2005. A compact antenna for ultrawide–band applications. *IEEE Transaction on Antennas and Propagation*, **53**(7), 2185–2192. 36

Narayan Prasad Agarwall, Girish Kumar, Ray K. P. 1998. Wide–band planar monopole antennas. *IEEE Transactions on Antennas and Propagation*, **46**(2), 294–295. 34

Nikolay Telzhensky, Yehuda Leviatan. 2006. Novel method of UWB antenna optimization for specified input signal forms by means of genetic algorithm. *IEEE Transaction on Antennas and Propagation*, **54**(8), 2216–2225. 36

Ntsanderh C. Azenui, Yang H. Y. D. 2007. A printed crescent patch antenna for ultrawideband applications. *IEEE Antennas and Wireless Propagation Letters*, **6**, 113–116. 40

Peyrot-Solis M. A., Galvan-Tejada G. M., Jardon-Aguilar H. 2006. A novel planar UWB monopole antenna formed on a printed circuit board. *Microwave and Optical Technology Letters*, **48**(5), 933–935. 39

Peyrot-Solis M. A., Tirado-Mendez J. A., Jardon-Aguilar H. 2007. Design of multiband UWB planarized monopole using DMS technique. *IEEE Antennas and Wireless Propagation Letters*, **6**, 77–79. 40

Pozar, David M. 1998. *Microwave Engineering*. John Wiley & Sons Inc., New York. 51

Rambabu K., Thiart H. A., Bornemann J. Yu S. Y. 2006. Ultrawideband printed-circuit antenna. *IEEE Transactions on Antennas and Propagation*, **54**(12), 3908–3911. 40

Reza Zaker, Changiz Ghobadi, Javad Nourinia. 2008. Novel modified UWB planar monopole antenna with variable frequency band–notch function. *IEEE Antennas and Wireless Propagation Letters*, **7**, 112–114. 43

Sachin Gupta, Ramesh M., Kalghatgi A. T. 2006. Ultra wide band embedded planar inverted conical antenna. *Microwave and Optical Technology Letters*, **48**(12), 1698–1701. 40

Sang-Ho Lee, Jung-Woo Baik, Young-Sik Kim. 2007. A coplanar waveguide fed monopole ultra wide band antenna having band–notched frequency function by two folded strip line. *Microwave and Optical Technology Letters*, **49**(11), 2747–2750. 43

Saou-Wen (Stephen) Su, Jui-Hung Chou, Kin-Lu Wong. 2007. Internal ultrawideband monopole antenna for wireless USB dongle applications. *IEEE Transactions on Antennas and Propagation*, **55**(4), 2216–2225. 37

Saou-Wen Su, Kin-Lu Wong, Chia-Lun Tang. 2005a. Band–notched ultra-wideband planar–monopole antenna. *Microwave and Optical Technology Letters*, **44**(3), 217–219. 35

Saou-Wen Su, Kin-Lu Wong. 2005b. Broadband omnidirectional U–shaped metal–plate monopole antenna. *IEEE Transactions on Antennas and Propagation*, **53**(2), 365–369. 35

Saou-Wen Su, Kin-Lu Wong, Yuan-Tung Cheng Wen-Shyang Chen. 2004. Finite ground plane effects on the ultra–wide band planar monopole antenna. *Microwave and Optical Technology Letters*, **43**(6), 535–537. 35

Saou-Wen Su, Austin Chen, Yung-Tao Liu. 2007. Wide band omnidirectional L–shaped monopole antenna for a wireless USB dongle. *Microwave and Optical Technology Letters*, **49**(3), 625–628. 37

Schantz H. G., Fullerton L. 2001 (August). The diamond dipole: A gaussian impulse antenna. *Pages 100–103 of: IEEE Antennas and Propagation Soc. Int. Symp.*, vol. 4. 37

Shi-Wei Qu, Jia-Lin Li, Quan Xue. 2006. A band-notched ultrawideband printed monopole antenna. *IEEE Antennas and Wireless Propagation Letters*, **5**, 495–498. 39

Shun-Yun Lin, Kuang-Chih Huang. 2006. Printed pentagon monople antenna with a band–notched function. *Microwave and Optical Technology Letters*, **48**(10), 2016–2018. 39

Stohr, W. 1968. *Broadband ellipsoidal dipole antenna*. US Patent 3, 364, 491. 34

Stutzman, Warren L. John Wiley & Sons Inc. 34

Tutku Karacolak, Erdem Topsakal. 2006. A double–sided rounded bow–tie antenna (DSRBA) for UWB communication. *IEEE Antennas and Wireless Propagation Letters*, **5**, 446–449. 39

Tzyh-Ghuang Ma, Sung-Jung Wu. 2007. Ultrawideband band-notched folded strip monopole antenna. *IEEE Transaction on Antennas and Propagation*, **55**(9), 2473–2478. 42

Valderas D., Cendoya I., Berenguer R. Sancho I. 2006. A method to optimize the bandwidth of UWB planar monopole antennas. *Microwave and Optical Technology Letters*, **48**(1), 155–159. 36

VALDERAS D., MELENDEZ J., SANCHO I. 2005. Some design criteria for UWB planar monopole antennas: Application to a slotted rectangular monopole. *Microwave and Optical Technology Letters*, **46**(1), 6–11. 35

VISSER, HUBREGT J. 2005. *Array and phased array antenna basics.* New York: John Wiley & Sons Inc. 51

WEI-YU LI, KIN-LU WONG, SAOU-WEN SU. 2007. Ultra wide band planar dipole antenn with two C–shaped arms for wireless communications. *Microwave and Optical Technology Letters*, **49**(5), 1132–1135. 42

WEINER, MELVIN M. 2003. *Monopole Antennas.* Marcel Dekker Inc., New York. 33

XUAN HUI WU, AHMED A. KISHK. 2008. Study of an ultrawideband omnidirectional rolled monopole antenna with trapezoidal cuts. *IEEE Transactions on Antennas and Propagation*, **56**(1), 1449–1451. 37

XUAN HUI WU, ZHI NING CHEN. 2005. Comparison of planar dipoles in UWB applications. *IEEE Transactions on Antennas and Propagation*, **6**(53), 1973–1983. 35

YI DING, GUANG-MING WANG, JIAN-GANG LIANG. 2007. Compact band notched ultra wide band antenna. *Microwave and Optical Technology Letters*, **49**(11), 311–313. 43

YI-MIN LU, XUE-XIA YANG, GUO-XIN ZHENG. 2007. Analysis on a novel ultra wide bandwidth antenna of double printed circular disc. *Microwave and Optical Technology Letters*, **49**(2), 311–313. 41

YILDIRIM, BAHADIR S. 2006. Low-profile and planar antenna suitable for wlan/bluetooth and uwb applications. *IEEE Transaction on Antennas and Propagation*, **5**, 438–441. 39

YOUNG JUN CHO, KI HAK KIM, DONG HYUK CHOI SEUNG SIK LEE SEONG-OOK PARK. 2006. A miniature UWB planar monopole antenna with 5–Ghz band-rejection filter and the time-domain characteristics. *IEEE Transactions on Antennas and Propagation*, **54**(5), 1453–1460. 39

YU-JIUN REN, KAI CHANG. 2006. An annual ring antenna for UWB communications. *IEEE Antennas and Wireless Propagation Letters*, **5**, 274–276. 38

YUE PING ZHANG, QIANG LI. 2007. Performance of UWB impulse radio with planar monopoles over on human body propagation channel for wireless body area networks. *IEEE Transactions on Antennas and Propagation*, **55**(10), 2907–2914. 42

ZHI NING CHEN, TERENCE S. P. SEE, XIANMING QING. 2007. Small printed ultrawideband antenna with reduced ground plane effect. *IEEE Transactions on Antennas and Propagation*, **55**(2), 383–388. 41

Chapter 4

The Semi Elliptic Slot Antenna

A slot antenna comprises of a slot of appropriate shape on a thin flat sheet of metal and the slot radiate on both sides of the sheet when excited by a voltage source. The electric field distribution in the slot can be obtained from the relationship between the slot and complementary wire antennas, as established by Booker [Booker, 1946]. The electric field distribution (magnetic current) in the slot is identical to the electric current distribution on a complementary wire. The electric field everywhere is normal to the surface of the slot antenna except in the region of the slot. The radiation of the currents in the sheet can be deduced directly from the distribution of the electric field in the slot. Consequently, the radiated field of an elementary magnetic dipole within the slot boundaries should include the contribution of the electric current flowing on a metal surface.

To broadband microstrip patch antennas, aperture coupling method is deployed where coupling between a near resonant slot and the patch broaden the bandwidth to about 30 percent or higher. Another preferred location for the slot is the patch surface itself. A U-shaped slotted patch was experimentally investigated in [Huynh T., 1995] and an impedance bandwidth of 27% from 1.565–2.065 GHz, was obtained. Several researchers have attempted similar approaches with microstrip patch antennas, a detailed account of which has been compiled in [Wong, 2002] and [Godara, 2002].

Another technique is to excite a narrow rectangular slot with a simple microstrip feed line as in [Yoshimura, 1972] and [Pozar, 1986]. In [Yoshimura, 1972], the feed point is shifted from the center of the slot and is short circuited through the dielectric substrate with the slot side, which is located further from the

feed input. A similar technique of feed point shifting close to the slot end was used in [Pozar, 1986]. In both cases, the offset of the feed point lead to perfect impedance matching in a narrow frequency band and the impedance bandwidth is approximately 20%.

As the width of the slot increases, radiation resistance of the slot also increases and this leads to impedance mismatch between the slot and microstrip feed line. This in turn reduces the impedance bandwidth of the antenna [Kahrizi M., 1993]. In [Shum S. M., 1995] the possibility of increasing the bandwidth of the wide rectangular slot antenna by terminating the open end of the feed line within the width of the slot has been shown even though substantial bandwidth improvement could not be achieved.

In [Myung Ki Kim, 2000], a wide rectangular aperture is excited by a T-shaped microstrip tuning stub to realize a wide bandwidth from 1.5–3.2 GHz, approximately 58% which is considerably wider than the narrow rectangular slot antenna. In [Wen-Shan Chen, 2000], it is shown that a modification of the shape of the slot can also result in broadband operation. The authors used a semi-circular slot and a protruding square shape to realize a bandwidth of 46%, which is about three times that of a corresponding printed wide rectangular slot antenna.

In [Jia-Yi Sze, 2001], a wide aperture is excited by a fork like tuning stub to realize wide band width. A 1 : 1.5 VSWR band width of 1 GHz is achieved at operating frequencies around 2 GHz, which is nearly ten times that of a conventional microstrip-line-fed printed wide-slot antenna.

In [Jang, 2001], the wide aperture is excited by an inverted T-shaped microstrip tuning stub. Reported bandwidth of the antenna is from 1.877–5.638 GHz which is approximately 114% (VSWR $\leq$ 2).

In [Lei Zhu, 2003], a novel broadband microstrip-fed slot antenna with double rejection zeros is proposed and developed by constructing simultaneously a wide-slot radiator and a quarter-wavelength microstrip line resonator. Experimental results exhibit that significant increase in the bandwidth of the proposed antenna, up to 32.0% as compared to 9.0% of its traditional counterpart.

In the wide square aperture, conducting strips are incorporated on each corners diagonally in [Jyh-Ying, 2003] to improve the bandwidth greater than 60%, about two times that of a simple CPW-fed wide slot antenna. The broad band circularly

polarized antenna proposed in [Jia-Yi Sze, 2003] followed a similar approach. In this design, broadband circular polarization operation is achieved by protruding a T-shaped metallic strip from the ground plane toward the slot center and feeding the square slot antenna using a 50–Ω CPW with a protruded signal strip at 90^0 to the T-shaped strip. The 3–dB and 1–dB axial-ratio bandwidths are as large as 18% and 13% respectively.

The designs in [Xianming Qing, 2003; Chair R., 2004] incorporated a microstrip feed line with a fork-shaped tuning stub to excite a rectangular slot on the ground plane to achieve ultra wide band width. The complete study of this antenna in the frequency and time domains is carried out in [Gino Sorbello, 2005]. The same antenna has been studied in [Marchais C., 2006] giving emphasis to the direct time domain measurement.

The broad band design in [Wen-Shan Chen, 2004] used a triangular slot and a small rectangular slot protruded from this to create a new resonant mode in the vicinity of the fundamental resonant mode of the triangular slot. A good impedance matching of both the fundamental and the new mode lead to an enhanced bandwidth of 84% for the proposed antenna.

In [Liu Y. F., 2004], the feed-slot combination and the feed gap width are studied for ultra wide band behavior of the antenna. For the study, an antenna with an arc-shape slot and a square-patch feed and an antenna that has a triangular-shape slot and an equilateral triangular-patch feed are used. Widths and lengths for both feeds are about one third of the slot size and their lengths are close to but less than the quarter wavelength measured at the lower frequency edge. The lengths are shorter than a printed monopole at the same frequency, because the slot edge acts as a capacitive load to the monopole. With these antennas, almost 100% bandwidth could be achieved.

Further research interests in the above design has resulted in [Shi-Wei Qu, 2006] where rounded corners are used to improve the bandwidth to 158%. A relatively simple version of the above antennas was proposed in [T. A. Denidni, 2006] wherein the authors used circular slot and a circular tuning stub to realize an antenna with as much as 110% bandwidth. A band notch is realized in this antenna using a pie-cut in the tuning stub [Chin-Ju Pan, 2006]. In [Mohamed A. Habib, 2006], the authors explored the use of stubs other than the circular one to excite the circular slot. Their findings reveal that slots and stubs of

similar geometry can result in the widest possible bandwidth of all the possible combinations. Details of a similar study can be found in [Fabrizio Consoli, 2006] which include a detailed time domain analysis.

In [Evangelos S. Angelopoulos, 2006a], the authors have studied the use of ellipses of various ellipticity ratios for the ground as well as the tuning stub. Their studies propose the use of an elliptical design if PCB space is the concern and a circular design for wider bandwidth. The antennas proposed in this paper are able to cover the FCC UWB with good radiation characteristics. The authors have also shown that a modified design of this antenna will suit the KU-band satellite communication application and designed a wide band 1x8 array in [Evangelos S. Angelopoulos, 2006b]. The paper [Jiechen Ding, 2007] explored the possibility of using split ring resonators of various dimensions to result in multiple band notch in the circular slot antenna.

The UWB antenna designs using fork–like stubs require relatively large apertures and contain many parameters for the complex geometry. The design proposed in [Yi-Cheng Lin, 2006] used a rectangular stub to constrict the slot aperture to an area of 13x23 mm^2. The authors have discussed the correlation between the mode-based field distributions and radiation patterns. Further, three advanced band notch designs are also proposed in this paper. In [Wen-jun Lui, 2007], a modified version of this design has been studied for UWB applications. The authors have proposed the use of a square ring resonator inside the rectangular stub to achieve a sharp band notch and has investigated the time domain performance of the antenna also in this paper. An offset fed square slot antenna with a rectangular stub can also result in UWB as demonstrated in [Horng-Dean Chen, 2006]. In [Aliakbar Dastranj, 2008], an E–shaped slot is excited using a microstrip feed having E–shaped stub to achieve a percentage bandwidth of 120.

In [Jiao J. J., 2007], a wide square slot is excited using a 50Ω feed line without terminating the end with a stub. An additional rectangular slot beneath the microstrip line connected to the wide square slot so as to form a T-shaped aperture, aid in the wideband operation of the antenna. By this approach, overall size of the antenna could be reduced by 26% compared to the wide slot antenna and the bandwidth is about 121%. The antenna design in [Jia-Yi Sze, 2008], where a wide square slot is excited using a 50Ω feed line without terminating

the end with a stub, uses a hat shaped back-patch to result in UWB. A rejected frequency band within this band is produced by embedding a pair of U-shaped slot lines in the back-patch.

In [Tharaka Dissanayake, 2008], two wide band antennas are reported to operate in the upper half of the direct sequence spread spectrum UWB. One L–slot antenna has a planar ground plane and the other modified L–slot antenna has a ground plane consisting of a planar section and two sidewalls. The highlight of this paper is the detailed performance analysis from impedance matching to pattern stability. Wide band radiation characteristics and the pattern stability of these antennas are investigated with the help of pattern stability factor (PSF).

In [Aidin Mehdipour, 2008], the authors evolved a UWB slot antenna from the basic design of an elliptical dipole antenna. A circuit model of the antenna has been used to analyze the input impedance of the antenna. The paper is complete with detailed parametric and time domain analysis of the antenna.

The LTCC based slot antenna in [Ooi B. L., 2008] adopted the waveguide technology, instead of the aperture technology, to improve wide band matching. The multi–layer antenna is excited by a microstrip line feed with a V–shaped tuning stub. To create an electric wall, two rectangular slots at different layers are connected together by vias. Wider bandwidth is obtained by placing diagonal strips along the four corners of the rectangle slots. This design offers a percentage bandwidth of 133 and cover the 3.2–10.6 UWB.

The compact UWB slot antenna in [Jorge R. Costa, 2009] is based on a combination of two crossed exponentially tapered slots and a star-shaped slot to produce a stable radiation pattern with very stable polarization over the 3.1–10.6 GHz FCC assigned band. The antenna diameter is only 35 mm (0.3 λ_0 at 3.1 GHz) and can be easily re-designed for MIMO systems with very low mutual coupling. This antenna is especially attractive since it combines the UWB concept with diversity and MIMO strategies to enhance link capacity and improve range, which is constrained by the FCC power emission mask for UWB.

In [Chen & Lin, 2009] a monopole-slot hybrid antenna is proposed for UWB applications. Even though antenna is compact, the radiation patterns have been affected at higher frequencies due to the asymmetry associated with its design.

The design details of a wide aperture slot antenna with geometry optimized for wireless dongle applications can be found in [Deepti Das Krishna, 2009]. Dongle

antennas are required to be constrained to an area of 23x70 mm^2 along with omnidirectional radiation and ground independence. Compact geometry of the present antenna is due to multiple matching techniques employed and it has also shown that the effect of ground plane on the radiation characteristics are minimal.

For applications that require unidirectional radiation in addition to wide impedance bandwidth, cavity backed slot antennas were proposed as in [Quan Li, 2002a,b]. An optimized rectangular cavity at the back of these antennas creates an additional resonance to enhance the bandwidth. In [Quan Li, 2002a], design of a single slot with 22% bandwidth and in [Quan Li, 2002b], a cavity backed slot array with 43% bandwidth and improved gain is proposed. Even though the percentage bandwidth is only 24%, the antenna derived from [Quan Li, 2002b] and reported in [Weihua Gao, 2007] offers high gain compared to its predecessor. In [Boyu Zheng, 2005], the authors investigated the effect of a finite ground plane on microstrip-fed cavity-backed slot antennas by the uniform geometrical theory of diffraction. It is demonstrated that the finite ground plane has a small effect on a slot antennas radiation performance, indicating their superiority for use in mobile terminals compared to microstrip patch antennas.

In this chapter, design of a semi-elliptic slot antenna with wide impedance band width of ~150% is presented. The ground plane and patch is shaped as semi-ellipse to minimize any pernicious reflections inside the structure. Resonances in the antenna are due to different modes excited in the slot geometry which can be accounted mathematically, that facilitate it's design on any microwave laminate. A band notch mechanism suitable for the present design is also proposed and the antennas are characterized in the frequency domain.

4.1   Antenna Geometry, Design and Optimization

4.1.1   Geometry

Fig. 4.1 shows the geometry of the proposed semi-elliptic slot antenna. The ground plane of the antenna is shaped as a semi-ellipse near the patch with a_1 and b_1 as major and minor radii. The patch is also semi-elliptic with major and minor radii a_2 and b_2 respectively. The patch is displaced from the ground plane by a distance d. The ground plane extends beyond the patch to form an 'L' shaped section of length $l_1 + l_2$.
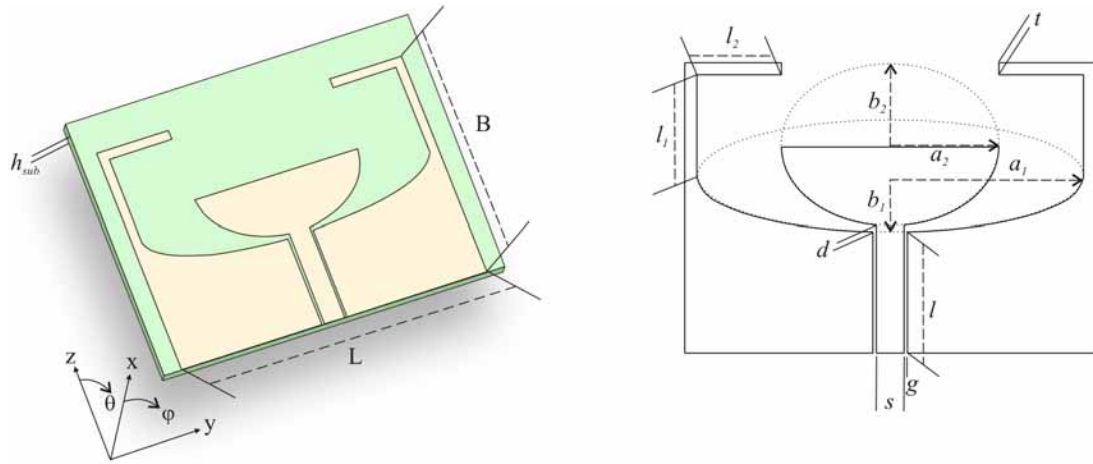
Figure 4.1: Geometry of the semi-elliptic slot antenna
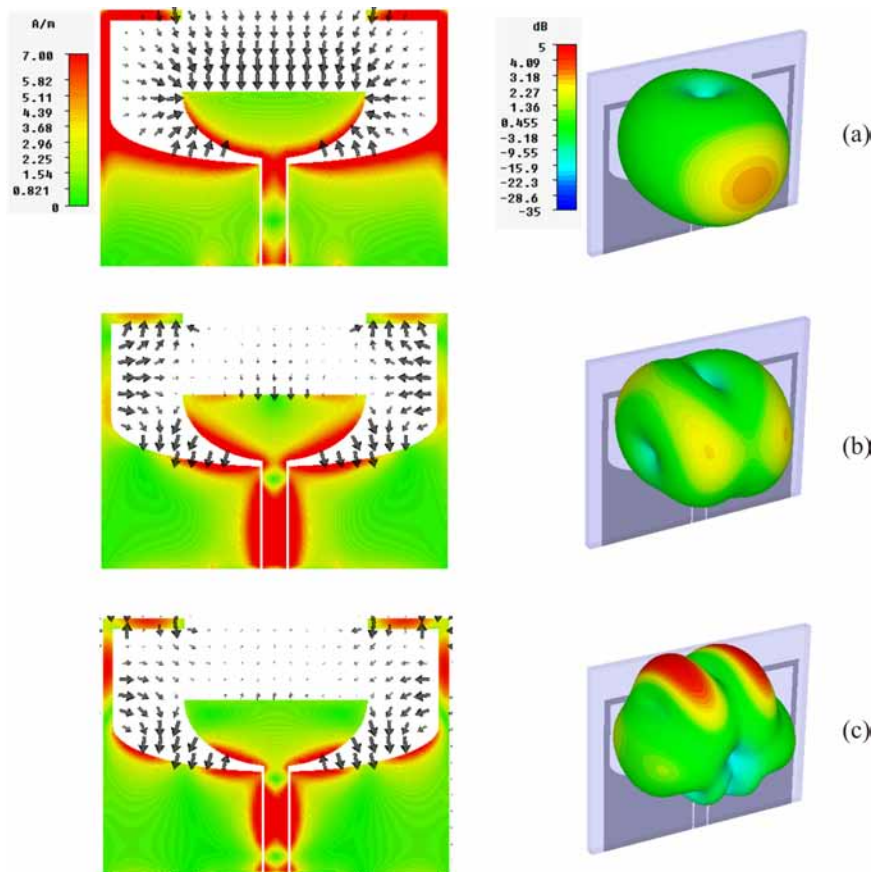
Figure 4.2: Surface current distribution (Intensity) and aperture electric field (vector) at (a) 3.2 GHz (b) 8.5 GHz (c) 12 GHz.

Table 4.1: Computed and optimized geometric parameters of Semi–Elliptic Slot Antennas (also see Table 3.2)

Parameter (mm)	Antenna–1 (Rogers 5880)		Antenna–2 (FR4 Epoxy)		Antenna–3 (Rogers RO3006)		Antenna–4 (Rogers 6010LM)	
	Computed	Optimized	Computed	Optimized	Computed	Optimized	Computed	Optimized
a_1	17.43	19.36	14.1	16	12.94	14.72	12.28	13.76
b_1	4.9	5.45	3.96	4.48	3.64	4.11	3.45	3.83
a_2	10.39	11.52	8.18	9	7.37	8.28	6.85	7.69
b_2	7.43	8.27	5.84	6.44	5.26	5.92	4.89	5.49
l	10	10	10	10	10	10	10	10
l_1	10.55	11.73	8.31	9.5	7.49	8.74	6.95	8.29
l_2	8.3	9.25	6.53	7	5.88	6.71	5.46	6.23
d	0.26	0.26	0.44	0.48	0.45	0.67	0.87	0.87
t	1	1	1	1	1	1	1	1
LxB (mm^2)	36.95 x 26	40.65 x 30	30.13 x 23	34 x 25	28 x 22.15	31.42 x 23.85	22.85 x 21.42	29.24 x 23
f_1, f_2 (GHz)	3.4, 9.46	3.18,8.6	3.5,9.23	3.2, 8.57	3.8, 9.5	3.3, 8.4	3.85,10	3.3, 8.5

4.1.2 Design

As shown in the intensity distribution in Fig. 4.2(a), the curved path OA is approximately half a wave long at the first resonance. i.e.,

$$\frac{p_1}{4} + l_1 + l_2 - g - \frac{s}{2} \approx \frac{\lambda_{g,1}}{2} \tag{4.1}$$

where p_1 is the perimeter of the ellipse in the ground plane given by,

$$p_1 \approx 2\pi \sqrt{\frac{a_1{}^2 + b_1{}^2}{2}} \tag{4.2}$$

The path $O^/A^/$ in the antenna as shown in Fig. 4.2(b) is responsible for the second resonance. From the field distribution in Figure 4.2(b), it can be arrived that,

$$\frac{p_2}{2} \approx \frac{\lambda_{g,2}}{2} \tag{4.3}$$

where p_2 is the perimeter of the ellipse with a_2 and b_2 as the major and minor radii. Here, $\lambda_{g,i}$ is the wavelength in the dielectric which is computed from the free space wavelength $\lambda_{0,i}$ as,

$$\lambda_{g,i} = \frac{\lambda_{0,i}}{\sqrt{\varepsilon_{re}}}, i = 1, 2 \tag{4.4}$$

and ε_{re} is the effective permittivity of the substrate. In designing the antenna proposed in this paper, the first resonance is designed to fall in the lower UWB (3.1 - 5.1 GHz) and the second resonance in the upper UWB (5.825 - 10.6 GHz). From the vector distribution of the aperture field shown in Figure 4.2, it can be seen that the modes excited resemble the fundamental modes of typical aperture antennas [Yi-Cheng Lin, 2006], namely TE_{01} and TE_{11} at the first and the second resonances. The lower and upper resonances are fixed at 3.2 and 8.5 GHz respectively and a smooth transition between them is obtained by adjusting the spacing d. Extensive simulation studies indicate that the optimum ellipticity values $(a_1 : b_1)$ and $(a_2 : b_2)$ are at 3.55 and 1.4 respectively. It is observed that the parameter t does not contribute to the resonances or the bandwidth of the antenna. Hence in the proposed design, a thin strip of width 1 mm is employed.
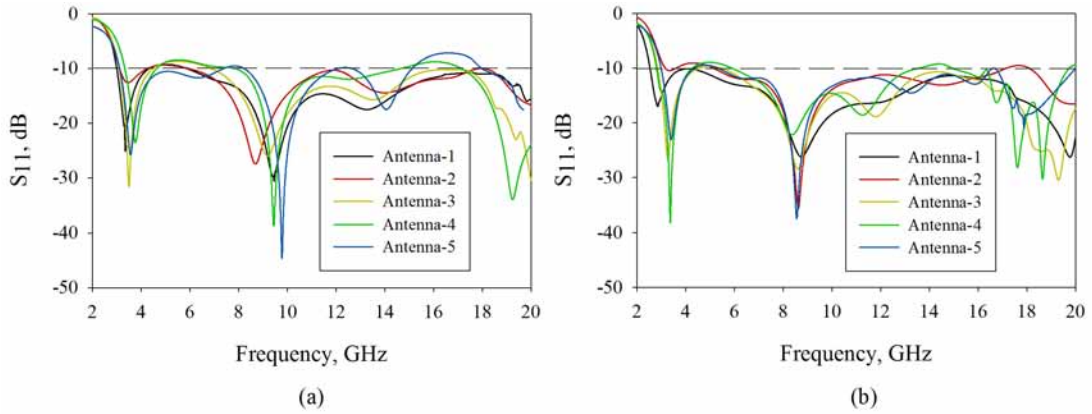
Figure 4.3: Return loss of antennas with (a) computed geometric parameters (b) optimized geometric parameters.

4.1.3   Optimization

Based on the observations aforementioned, a design procedure for the semi-elliptic antenna can be framed as explained in this section.

1. Design a 50 CPW line on a substrate with permittivity ε_r and thickness h. Calculate ε_{re} using the s and g values of the CPW line.

2. Design the ground to create the first resonance (f_1) using $l_1 = \lambda_{g,1}/6$
   $l_2 = \lambda_{g,1}/9$
   and then compute b_1 and a_1 using,
   $b_1 = 0.12(\lambda_{g,1} + s + 2g) - 0.24(l_1 + l_2)$
   $a_1 = 3.55b_1$

3. Design the patch at the second resonance (f_2) using
   $b_2 = 0.26\lambda_{g,2}$
   $a_2 = 1.4b_1$

Using the parameters so computed, the antenna was studied on substrates with different permittivity, described in Table 3.2. Figure 4.3(a) shows the return losses of the antennas with the computed geometric parameters given in Table 4.1. Resonances of these antennas show slight deviation from the designed values but there is impedance match throughout the band. The reason for this is that the effective permittivity computed for the CPW line does not hold for the radiating

part of the antenna where the CPW line can be considered as flared. This value of ε_{re} is lower than that computed. Hence, the parameters are optimized using CST to have resonances at 3.2GHz and 8.5GHz. The S_{11} plots of these antennas are shown in Figure 4.3(b).

4.2 Band notch Design

To this design, a 'T' section is appended, as in Figure 4.4(a) that results in the required band notch. The parameters for this section are l_s and t_s and w_s as indicated whose variation studies are given in Figure 4.5.

To design the slot resonator for band notch, the equation to be followed is

$$l_s + t_s = \lambda_{g,5.5}/4 \tag{4.5}$$

where $\lambda_{g,5.5}$ is the guide wavelength computed at 5.5 GHz as in 3.6. The optimum values for these parameters are, $l_s = 6.45$mm, $t_s = 0.9$mm and $w_s = 0.4$mm.

4.3 Experiment results

A prototype of the antenna was fabricated on a substrate of $\varepsilon_r = 4.4$ and $h = 1.6$ mm with the optimized parameters in Table 4.1. Return loss measurements indicate a wide band width from 2.85 - 20 GHz, in agreement with the simulation as shown in Figure 4.6(a). The slight deviation from the simulation at higher frequencies could be due to the SMA connector which is not accounted in the simulation. Since the antenna is for use in the 3.1- 10.6 GHz band, this can be ignored. VSWR measurement of the band notch antenna is shown in Figure Radiation patterns of the antenna in the X-Y, X-Z and Y-Z planes for three different frequencies are shown in Figure 4.7. The patterns are stable throughout the band and resembles that of a monopole; omnidirectional in the H-plane (X-Y) and bidirectional in the E-planes (Y-Z and X-Z). Polarization of the antenna is along the Z direction. Measured gain of the antenna is compared with the simulated one in Figure 4.9(a) and (b) which shows reasonable agreement throughout the band. Average value of gain when slot resonator not incorporated
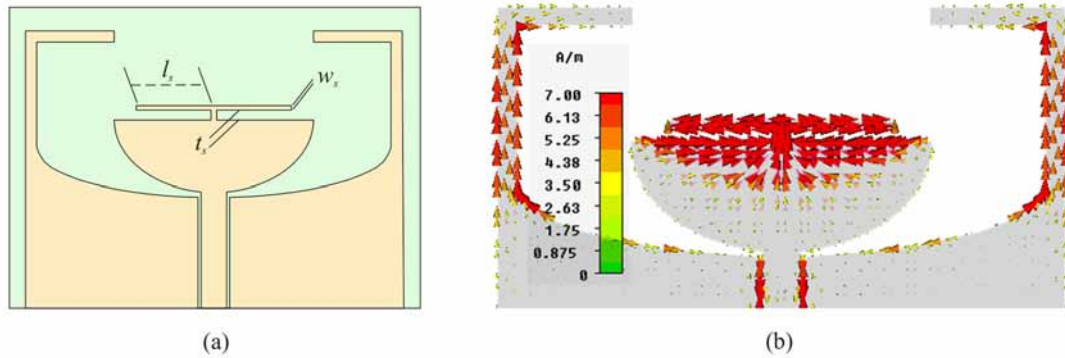
Figure 4.4: Semi elliptic slot antenna with slot resonator for band notch (a) design parameters (b) current distribution along the periphery of the slot
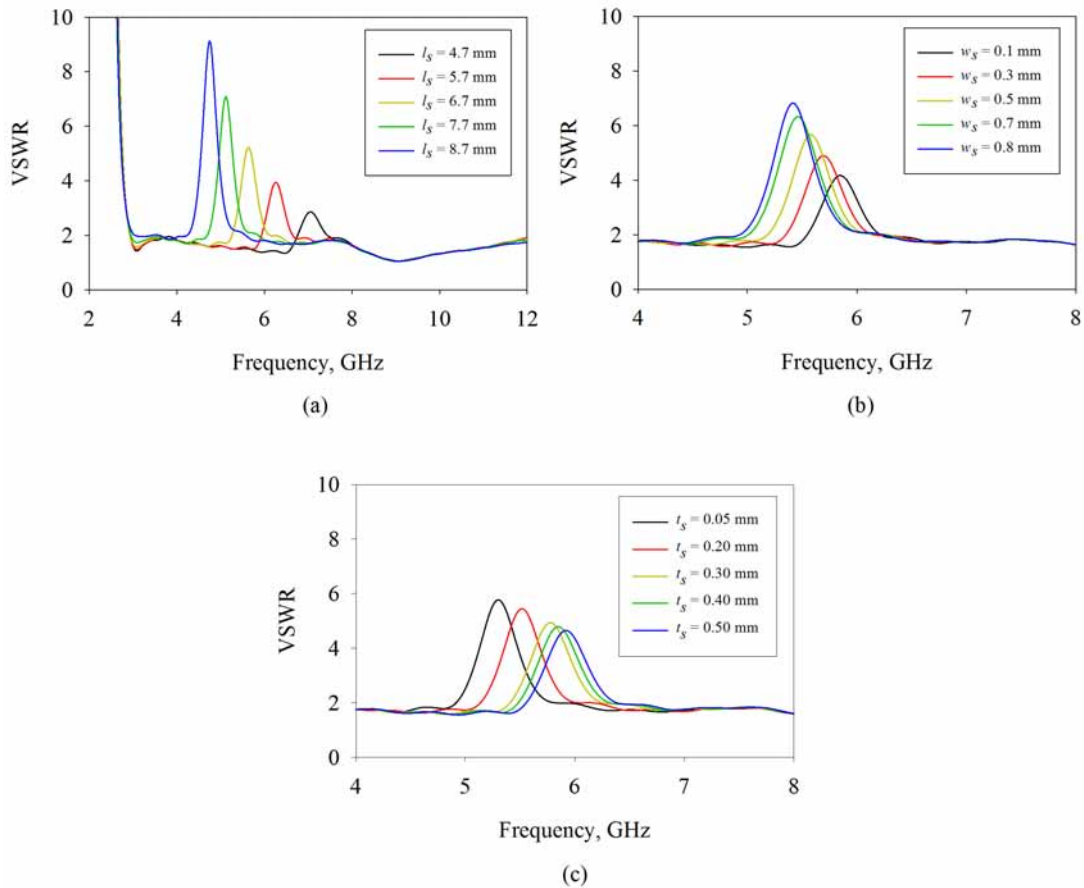
Figure 4.5: VSWR vs. Frequency of the band notch semi elliptic slot antenna for different (a) slot lengths while $t_s = 0.9mm$ and $w_s = 0.4mm$ (b) widths w_s while $t_s = 0.9mm$ and $l_s = 6.45mm$ (c) slot width t_s while $l_s = 6.45mm$ and $w_s = 0.4mm$
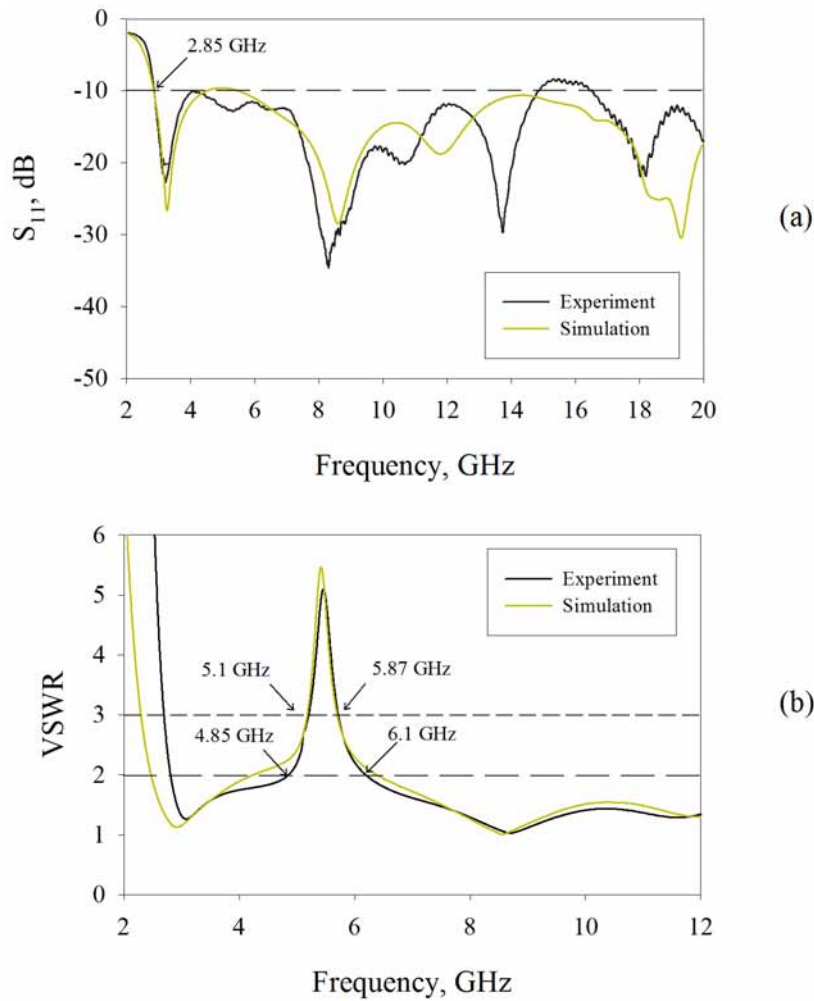
Figure 4.6: Measured and simulated (a) S_{11} of the UWB semi elliptic slot antenna (b) VSWR of the band notch antenna

in the design is found to be 3.64 dBi. The antenna has adequate radiation efficiency as shown in the same figure.

4.4 Conclusion

A compact slot antenna with minimum insidious reflections is proposed for UWB operation. The antenna features wide impedance bandwidth from 2.85–20 GHz and stable radiation patterns and gain across its entire operating band. As the Square Monopole Antenna in Chapter 3, this antenna too can be easily fabricated on any commercially available substrates since a reliable empirical design guideline
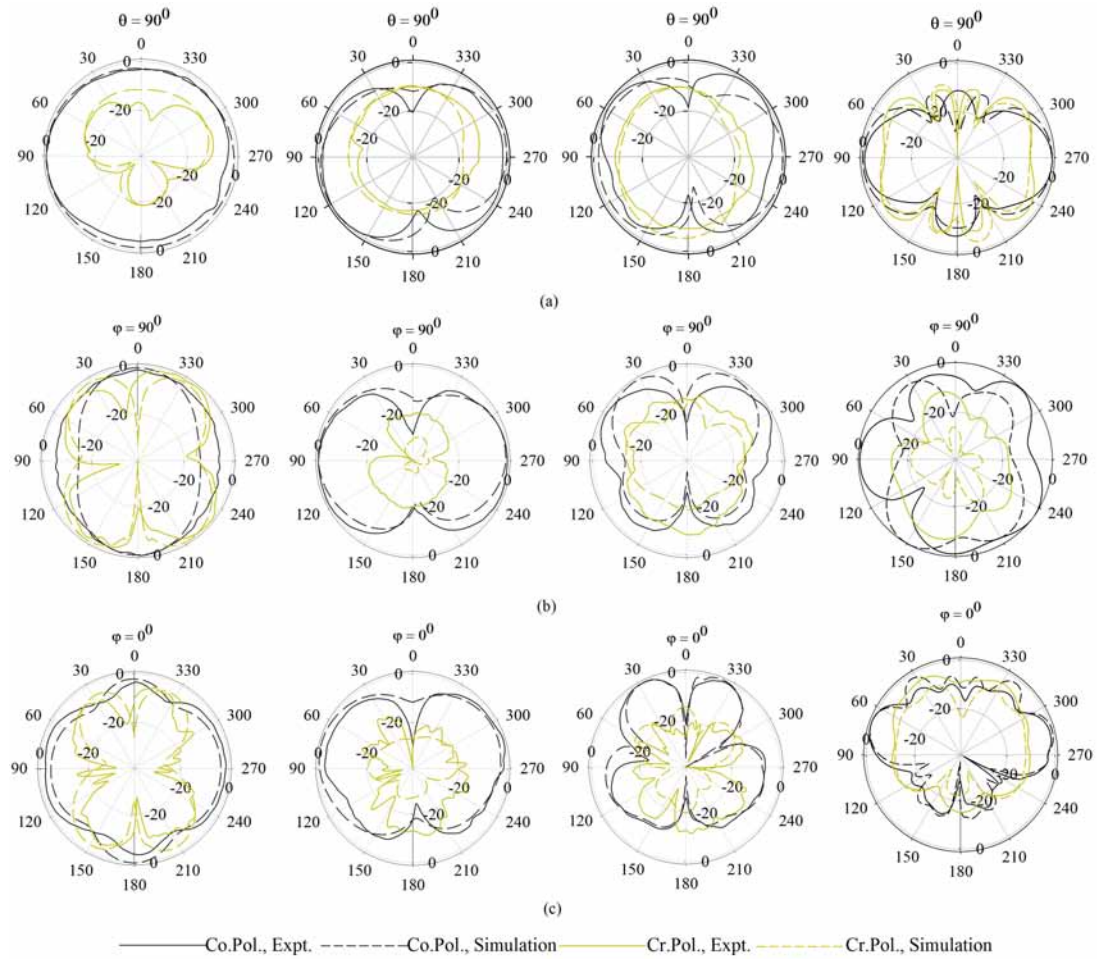
Figure 4.7: Radiation patterns of the UWB semi elliptic slot antenna in the (a) x-y plane: 3.75, 8, 13 GHz, 17 GHz (b) y-z plane: 3.75, 8, 13 GHz, 17 GHz (c) x-z plane: 3.75, 8, 13, 17 GHz
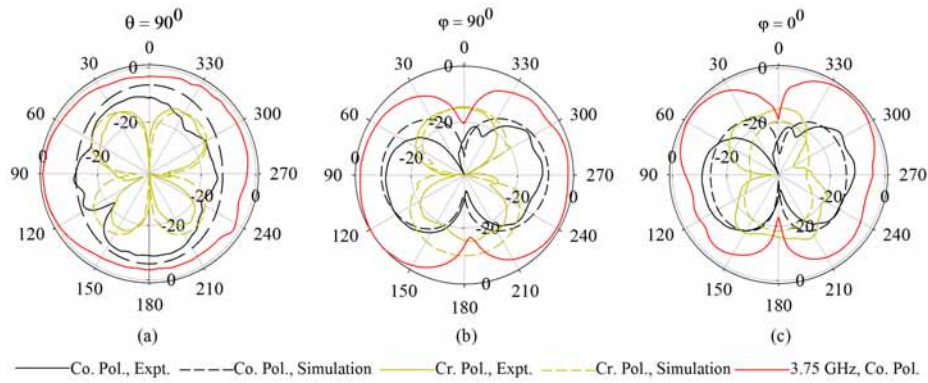
Figure 4.8: Radiation patterns of the semi elliptic slot antenna with band notch at 5.5 GHz (a) x-y plane (b) y-z plane (c) x-z plane
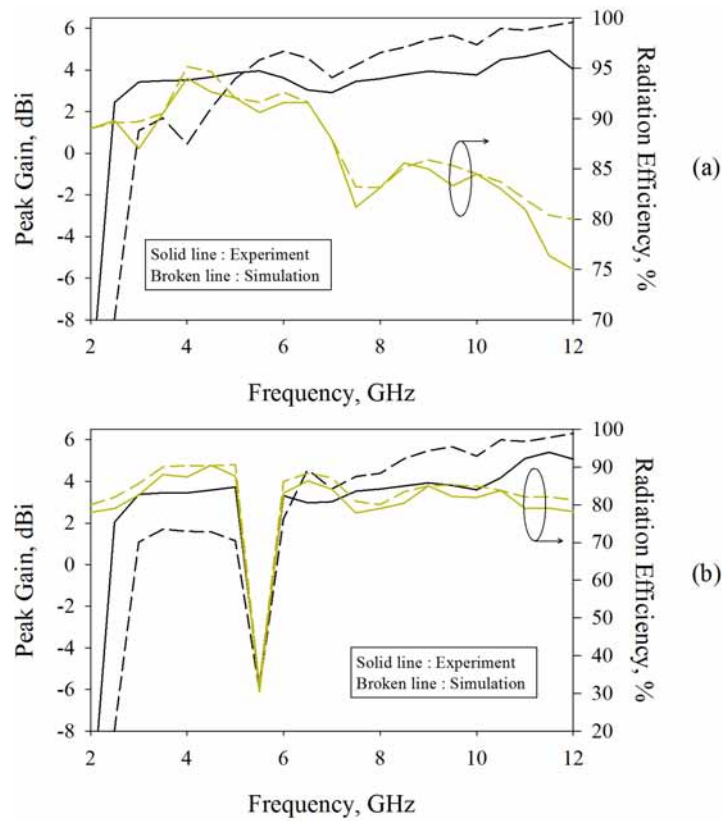
Figure 4.9: Measured and simulated peak gains and radiation efficiency of the semi–elliptic slot antenna (a) without band notch resonator (b) with band notch resonator

is provided. A tunable band notch feature can be integrated in to the antenna to limit radiation in the WLAN band.

References

Aidin Mehdipour, Karim Mohammadpour-Aghdam, Reza Faraji-Dana Mohammad-Reza Kashani-Khatib. 2008. A novel coplanar waveguide-fed slot antenna for ultrawideband applications. *IEEE Transaction on Antennas and Propagation*, **56**(12), 3857–3862. 67

Aliakbar Dastranj, Ali Imani, Mohammad Naser-Moghaddasi. 2008. Printed wide–slot antenna for wideband applications. *IEEE Transaction on Antennas and Propagation*, **56**(10), 3097–3102. 66

Booker, H. G. 1946. Slot aerials and their relation to complementary wire aerials. *Journal of IEE(London), Part III A*, **93**, 620–626. 63

Boyu Zheng, Zhongxiang Shen. 2005. Effect of a finite ground plane on microstrip–fed cavity–backed slot antennas. *IEEE Transaction on Antennas and Propagation*, **53**(2), 862–865. 68

Chair R., Kishk A. A., Lee K. F. 2004. Ultrawide-band coplanar waveguide–fed rectangular slot antenna. *IEEE Antennas and Wireless Propagation Letters*, **3**, 227–229. 65

Chen, Wen-Shan, & Lin, Chi-Huang. 2009. A planar hybrid antenna for UWB application. *Microwave and Optical Technology Letters*, **51**(5), 1243–1246. 67

Chin-Ju Pan, Chungnan Lee, Chih-Yu Huang Hsiao-Cheng Lin. 2006. Band–notched ultra–wideband slot antenna. *Microwave and Optical Technology Letters*, **48**(12), 2444–2446. 65

Deepti Das Krishna, M. Gopikrishna, C. K. Aanandan P. Mohanan K. Vasudevan. 2009. Ultrawideband slot antenna with band–notch characteristics for wireless USB dongle applications. *Microwave and Optical Technology Letters*, **51**(6), 1500–1504. 67

Evangelos S. Angelopoulos, Argiris Z. Anastopoulos, Dimitra I. Kaklamani Antonis A. Alexandridis Fotis Lazarakis Kostas Dangakis. 2006a. Circular and elliptical cpw-fed slot and microstrip-fed antennas for ultrawideband applications. *IEEE Transaction on Antennas and Propagation*, **5**, 294–297. 66

Evangelos S. Angelopoulos, Argyris Z. Anastopoulos, Dimitra I. Kaklamani Antonis A. Alexandridis Fotis Lazarakis Kostas Dangakis. 2006b. A novel wideband microstrip–fed elliptical slot array antenna for ku-band applications. *Microwave and Optical Technology Letters*, **48**(9), 1824–1828. 66

Fabrizio Consoli, Fabio Maimone, Sebastiano Barbarino. 2006. Study of a cpw-fed circular slot antenna for uwb communications. *Microwave and Optical Technology Letters*, **48**(11), 2272–2277. 66

Gino Sorbello, Mario Pavone, Luca Russello1. 2005. Numerical and experimental study of a rectangular slot antenna for UWB communications. *Microwave and Optical Technology Letters*, **46**(4), 315–319. 65

Godara, Lal Chand. 2002. *Handbook of Antennas in Wireless Communications*. Florida: CRC Press. 63

Horng-Dean Chen, Jin-Sen Chen, Jui-Ni Li. 2006. Ultra–wideband square–slot antenna. *Microwave and Optical Technology Letters*, **48**(3), 500–502. 66

Huynh T., Lee K. F. 1995. Single–layer single–patch wideband microstrip antenna. *IEE Electronics Letters*, **31**(August), 1310–1312. 63

Jang, Young-Woong. 2001. Large band–width double T shaped microstrip fed single layer single slot antenna. *Microwave and Optical Technology Letters*, **30**(3), 185–187. 64

Jia-Yi Sze, Kin-Lu Wong, Chieh-Chin Huang. 2003. Coplanar waveguide–fed square slot antenna for broad–band circularly polarized radiation. *IEEE Transaction on Antennas and Propagation*, **51**(8), 2141–2144. 65

Jia-Yi Sze, Jen-Yi Shiu. 2008. Design of band–notched ultrawideband square aperture antenna with a hat–shaped back–patch. *IEEE Transaction on Antennas and Propagation*, **56**(10), 3311–3314. 66

Jia-Yi Sze, Kin-Lu Wong. 2001. Bandwidth enhancement of a microstrip–line-fed printed wide–slot antenna. *IEEE Transaction on Antennas and Propagation*, **49**(7), 194–196. 64

Jiao J. J., G. Zhao, F. S. Zhang H. W. Yuan Y. C. Jiao. 2007. A broadband cpw-fed T–shape slot antenna. *Progress In Electromagnetics Research*, **76**, 237–242. 66

Jiechen Ding, Zhili Lin, Zhinong Ying Sailing He. 2007. A compact ultra-wideband slot antenna with multiple notch frequency bands. *Microwave and Optical Technology Letters*, **49**(12), 3056–3060. 66

Jorge R. Costa, Carla R. Medeiros, Carlos A. Fernandes. 2009. Performance of a crossed exponentially tapered slot antenna for UWB systems. *IEEE Transaction on Antennas and Propagation*, **57**(5), 1345–1351. 67

Jyh-Ying, Jia-Yi Sze, Kin-Lu Wong. 2003. A broad–band CPW–fed strip–loaded square slot antenna. *IEEE Transaction on Antennas and Propagation*, **51**(4), 719–721. 64

Kahrizi M., Sarkar T. K., Maricevic Z. A. 1993. Analysis of a wide radiating slot in the ground plane of a microstrip line. *IEEE Transaction on Antennas and Propagation*, **41**(1), 29–37. 64

Lei Zhu, Rong Fu, Ke-Li Wu. 2003. A novel broadband microstrip–fed wide slot antenna with double rejection zeros. *IEEE Antennas and Wireless Propgation Letters*, **2**, 194–196. 64

Liu Y. F., K. L. Lau, Q. Xue C. H. Chan. 2004. Experimental studies of printed wide-slot antenna for wide–band applications. *IEEE Antennas and Wireless Propagation Letters*, **3**, 273–275. 65

Marchais C., G. Le Ray, A. Sharaiha. 2006. Stripline slot antenna for UWB communications. *IEEE Antennas and Wireless Propagation Letters*, **5**, 319–322. 65

Mohamed A. Habib, Tayeb A. Denidni. 2006. Design of a new wideband microstrip–fed circular slot antenna. *Microwave and Optical Technology Letters*, **48**(5), 919–923. 65

Myung Ki Kim, Kwonil Kim, Young Hoon Suh Ikmo Park. 2000 (June). A T–shaped microstrip-line-fed wide slot antenna. *Pages 1500–1503 of: IEEE Antennas and Propagation Society International Symposium*, vol. 3. 64

Ooi B. L., Irene Ang, X. C. Shan Albert Lu R. Fieck H. D. Hristov. 2008. Wide–slot waveguide antenna on LTCC technology. *Microwave and Optical Technology Letters*, **50**(8), 2181–2184. 67

Pozar, David M. 1986. Reciprocity method of analysis for printed slot antenna and slot–coupled microstrip antennas. *IEEE Transactions on Antennas and Propagation*, **AP–34**(12), 1439–1466. 63, 64

Quan Li, Zhongxiang Shen, Xiaoyong Shan. 2002a. A new microstripfed cavity–backed annular slot antenna. *Pages 68–71 of: IEEE Antennas and Propagation Society International Symposium*, vol. 3. 68

Quan Li, Zhongxiang Shen. 2002b. Inverted microstrip–fed cavity–backed slot antennas. *IEEE Antennas and Wireless Propgation Letters*, **1**, 98–101. 68

Shi-Wei Qu, Chengli Ruan, Bing-Zhong Wang. 2006. Bandwidth enhancement of wide–slot antenna fed by cpw and microstrip line. *IEEE Antennas and Wireless Propagation Letters*, **5**, 15–17. 65

Shum S. M., Tong K. F., Zhang X. Luk K. M. 1995. FDTD modeling of microstrip–line–fed wide slot antenna. *Microwave and Optical Technology Letters*, **10**(October), 118–120. 64

T. A. Denidni, M. A. Habib. 2006. Broadband printed cpw–fed circular slot antenna. *IEEE Electronics Letters*, **42**(3), 135–136. 65

Tharaka Dissanayake, Karu P. Esselle. 2008. Uwb performance of compact L–shaped wide slot antennas. *IEEE Transactions on Antennas and Propagation*, **56**(4), 1183–1187. 67

Weihua Gao, R. Venkatesan, Cheng Li. 2007 (March). A pulse shape design method for ultra–wideband communications. *Pages 2800–2805 of: Wireless Communications and Networking Conference*. 68

WEN-JUN LUI, CHONG-HU CHENG, HONG-BO ZHU. 2007. Improved frequency notched ultrawideband slot antenna using square ring resonator. *IEEE Transactions on Antennas and Propagation*, **55**(9), 2445–2450. 66

WEN-SHAN CHEN, FU-MAO HSIEH. 2004 (June). Broadband design of the printed triangular slot antenna. *Pages 3733–3736 of: IEEE Antennas and Propagation Society International Symposium*, vol. 4. 65

WEN-SHAN CHEN, CHIEH-CHIN HUANG, KIN-LU WONG. 2000. A novel microstrip–line fed printed semicircular slot antenna for broadband application. *Microwave and Optical Technology Letters*, **26**(4), 237–239. 64

WONG, KIN-LU. 2002. *Compact and broadband microstrip antennas.* John Wiley & Sons Inc., New York. 63

XIANMING QING, MICHAEL YAN WAH CHIA, XUANHUI WU. 2003. Wide–slot antenna for UWB applications. *Pages 834–837 of: IEEE Antennas and Propagation Society International Symposium*, vol. 1. 65

YI-CHENG LIN, KUAN-JUNG HUNG. 2006. Compact Ultra Wide Band Rectangular Aperture Antenna and Band–Notched Designs. *IEEE Transactions on Antennas and Propagtion*, **54**(11), 3075–3080. 66, 71

YOSHIMURA, Y. 1972. A microstrip slot antenna. *IEEE Transactions on Microwave Theory and Techniques*, **20**(August), 760–762. 63

Chapter 5

Step and Linear-Tapered Slot Antennas

In certain class of slot antennas, the transverse electric field constricted between a short ended slot–line is transformed in to free waves at the open end. Typically, a microstrip–to– slot line cross transition is used to excite the antenna. Bandwidth limitation of the cross–junction transition results mainly from the frequency dependance of the slot reactance and microstrip reactance [Gupta K. C., 1996]. A short circuited microstrip line minimize microstrip reactance and an open circuited slot line minimize slot reactance. To achieve this, the use of quarter wavelength microstrip–slot line transition first proposed in [Chamber, 1970] and transitions using stubs where the microstrip and slot-line reactances cancel each other was suggested in [Schiek B., 1976; Chramiec, 1989].

The prominent candidate in these class of antennas are the tapered slot antennas first proposed by Gibson [Gibson, 1979]. TSAs are traveling–wave antennas and their operation is based on a traveling wave propagating along the surface of the antenna taper with a phase velocity less than the speed of light. Under this condition, end–fire radiation results [R. Janaswamy, 1987].

A uni–planar microstrip–to–coplanar strip line transition was introduced in [Rainee N. Simons, 1995] to excite a novel linearly tapered slot antenna. The transition uses a microstrip line of characteristic impedance 50Ω which is coupled to two orthogonal microstrip lines of characteristic impedance 70Ω through a quarter–wave stepped impedance–matching transformer. When integrated with the V–shaped tapered slot antenna wide impedance band with and gain as much

as 10 dBi resulted.

Conventional Vivaldi tapered slot antennas offer wide band performance over one or two octaves. In order to improve the bandwidth, [Gazit, 1988] introduced the antipodal Vivaldi configuration. This wide band antenna has a very high level of cross polarization in the upper part of the frequency band and in [Langley J. D. S., 1993] design of the the balanced antipodal Vivaldi antenna with a low level of cross polarization is proposed. In [E. Guillanton, 1998], a new design of a balanced antipodal Vivaldi antenna with a linear polarization is demonstrated in strip-line technology in order to obtain an ultra-wide band (1.3–20 GHz) with respect to the input impedance and the purity of polarization. In [Knott P., 2001], a novel coaxial line balun is integrated with a tapered slot antenna to achieve wide impedance bandwidth. However, the lower edge of the band starts at a higher frequency compared to the antipodal designs. A further simplified antipodal vivaldi design with good radiation characteristics can be found in [Amin M. Abbosh, 2006] with detailed design methodology. This antenna has been studied further in [Garcya E., 2007] to result in improved bandwidth and radiation by giving it a palm tree design.

The tapered slot antenna proposed in [Matsui, 2004] uses an impedance transformer and a Marchand Balun to excite a simple radiator. In [Yoon I. J., 2005], a broadband microstrip–slotline transition with multi–arm stubs is incorporated in to the tapered slot to realize UWB. In addition, $\lambda/4$ short stubs are introduced symmetrically into the radiating structure to realize 5 GHz band rejection.

In [Tzyh-Ghuang Ma, 2005a], the radiating annular slot is excited by a tapered–slot feeding structure which in turn is excited by a microstrip line with open stub termination. The antenna design in [Tzyh-Ghuang Ma, 2005b] consists of a wide–band tapered–slot feeding structure, curved radiators and a parasitic element. It is a modification of the conventional dual exponential tapered slot antenna and can be viewed as a printed dipole antenna with tapered slot feed. The authors also studied a CPW fed tapered ring slot antenna which consists of a 50Ω coplanar waveguide feeding line, wideband coplanar waveguide–to–slotline transition and a pair of curved radiating slots [Tzyh-Ghuang Ma, 2006]. All these designs are capable of radiating in the 3.1–10.6 GHz UWB and can be easily designed since empirical design guidelines are provided in these papers. In addition, detailed time domain analysis is also provided in these papers to ensure

their suitability in UWB systems.

A conformal tapered slot antenna is proposed in [Symeon Nikolaou, 2006] that does not use any complex matching procedures. The antenna is fed using a SMA connector soldered across the slot–line. The return loss remains below 10 dB and the shape of the radiation pattern remains fairly constant in the whole UWB range even when the antenna is significantly conformed.

A simple antenna design that use electric and magnetic type radiators to result in UWB is proposed in [Do-Hoon Kwon, 2008]. The electric radiator is a tapered slot while a slot in the same plane as the tapered slot act as magnetic radiator and these are simultaneously excited in close proximity via one feed point. The combination of radiated fields from different types of sources result in directive radiation patterns without increasing the antenna size as typically observed in antennas using only one type of sources.

The antenna reported in [Yuan Yao, 2008] is a variation of the Vivaldi antenna fed by microstrip line to slot–line wide band transition. The inner and outer edges of the radiator are both parabola tapered to result in ultra wide bandwidth and end fire radiation.

In certain other types of slot antennas, multiple resonances are created using a modified microstrip feed that excite a narrow slot on a substrate, unlike the mechanism in tapered slot antennas. Using a wide–slot radiator and a quarter–wavelength microstrip line resonator, broad band radiation is achieved in [Lei Zhu, 2003]. Measured bandwidth of the antenna is 32%.

In [Behdad & Sarabandi, 2004], the aperture's electric field distribution is manipulated to create two fictitious short circuits along the slot, hence creating two additional resonances besides the main one. The frequencies of these fictitious resonances are chosen so as to increase the overall bandwidth of the antenna. The reported band width ratio of this antenna is 1.8 : 1.

The antenna proposed in [Satish Kumar Sharma, 2004] is a quarter wavelength monopole slot cut in the finite ground plane edge and fed electromagnetically by a microstrip transmission line. These are further investigated for improved bandwidth and size reduction in [Saeed I. Latif, 2005; Wang Ren, n.d.]. A new design of asymmetric $\lambda/4$ open slot antenna with microstrip–line excitation is proposed in [Chen & Ku, 2006]. The authors further modified the design appending notches in the slot, making the antenna suitable for UWB operation
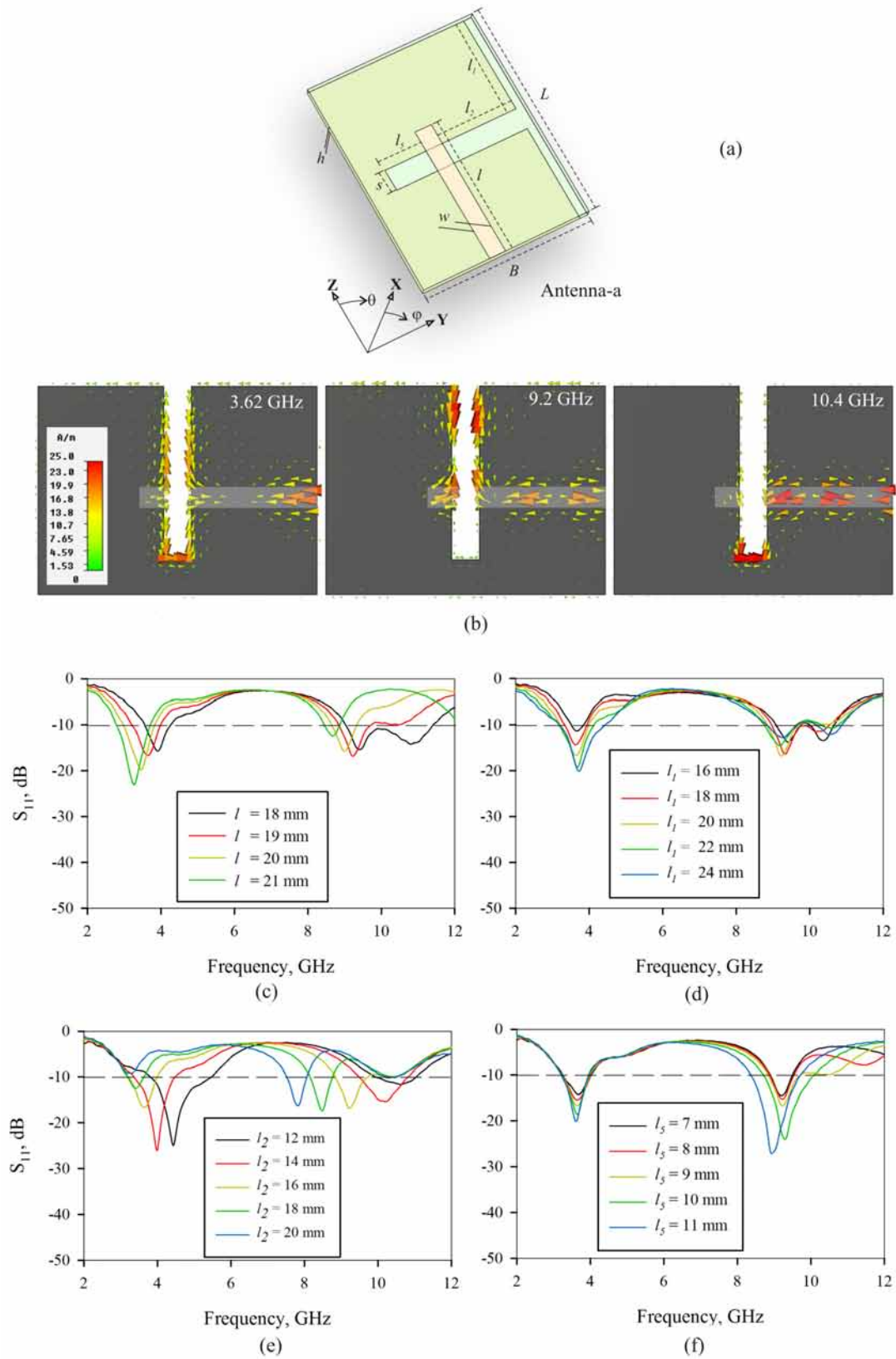
Figure 5.1: Monopole slot antenna (a) geometry (b) surface current distribution (c) variation in l (d) variation in l_1 (e) variation in l_2 (f) variation in l_5

[Wen-Shan Chen, 2008]. In [Sunil Kumar Rajgopal, 2009] instead of a rectangular slot, a pentagonal slot is deployed. A tilted microstrip transmission feed line with a pentagon stub is used to excite this antenna configuration which result in UWB operation.

In the present chapter, two antenna designs which fall in to the above category are proposed with ultra wide band width. The design approach is to generate multiple resonances by modifying the ground plane and match them to result in UWB by a feed modification. The two designs are the Step Slot Antenna and Linear Tapered Slot Antenna.

5.1   Step Slot Antenna: Design

The step slot antenna is evolved from a monopole slot antenna shown in Figure 5.1(a). The monopole slot designed at the bottom of the dielectric substrate is excited using an open end microstrip feed at the top. The configuration Antenna–a in Table 5.1 exhibits three resonances at 3.6 GHz and 9.2 GHz and 10.4 GHz according to the surface current distributions in Figure 5.1(b). Resonance at 3.6 GHz can be attributed to a half wave variation $l_1 + l_2$ while that at 9.2 GHz and 10.4 GHz are approximately due to a half wave variation in l_2 and l_5 respectively. This is further confirmed by the parametric study shown in Figures 5.1(c)–(f). As can be seen in Figure 5.1(c), a variation in length l affects all the three resonances. A variation in l_1 mainly affects the first resonance (Figure 5.1(d)) while the first and second resonances are affected by a variation in l_2 (Figure 5.1(e)). As shown in Figure 5.1(f), the third resonance is determined by length l_5.

It is found that if the ground plane of the antenna is modified as in Antenna–b (Figure 5.2, with geometric parameters in Table 5.1), a resonance can be perturbed at 5.78 GHz. Further, if the feed line is modified as to result Antenna–c, all these resonances can be matched to result UWB.

The first resonance satisfies a half wave variation as shown in Figure 5.3 which can be expressed as,

$$l_1 + l_2 + l_3 + l_4 \approx \lambda_{g,1}/2 \tag{5.1}$$
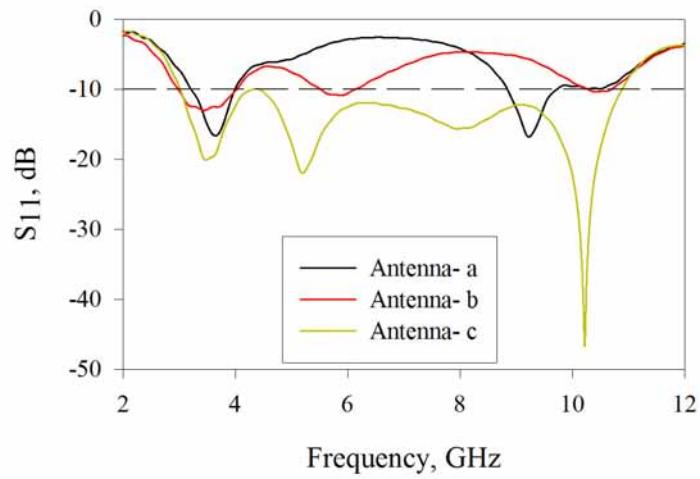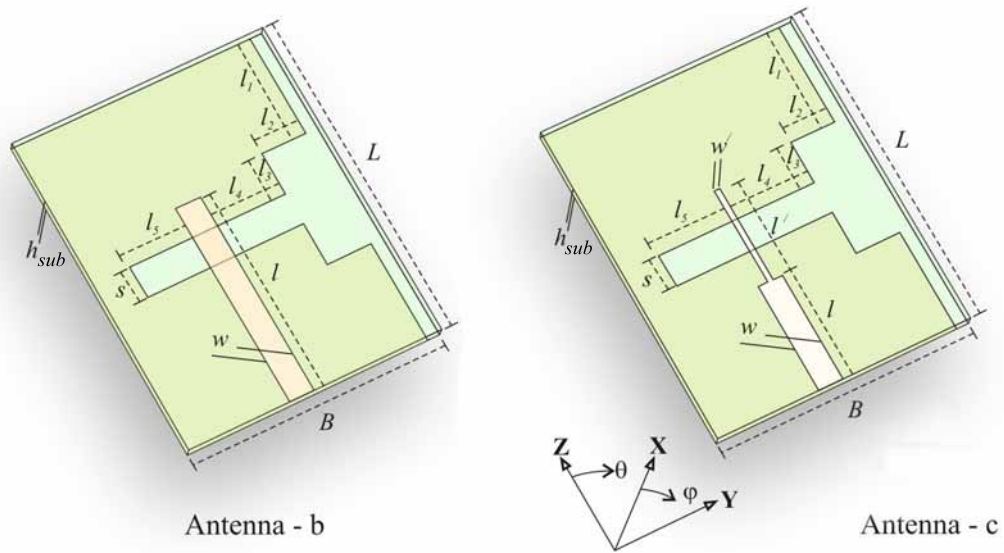
Figure 5.2: Design evolution of the step slot antenna and corresponding S_{11}

Table 5.1: Geometric parameters of the Step Slot antennas (Figures 5.1 and 5.2)

	Antenna–a	Antenna–b	Antenna–c
ε_r	4.4	4.4	4.4
$tan(\delta)$	0.02	0.02	0.02
$h_{sub}(mm)$	1.6	1.6	1.6
$l_1(mm)$	18	12.65	12.65
$l_2(mm)$	14.5	5.5	5.5
$l_3(mm)$	–	5.35	5.35
$l_4(mm)$	–	9	10.15
$l_5(mm)$	7.5	7.5	8.65
$l(mm)$	25.5	25.5	13.5
$l^{/}(mm)$	–	–	12
$w(mm)$	3	3	3
$w^{/}(mm)$	–	–	12
$s(mm)$	4	4	4
$L \text{ x } B\ (mm^2)$	40x31.5	40x31.5	40x31.5

Figure 5.3: Surface current distribution at (a) 3.58 GHz (b) 5.18 GHz (c) 8 GHz and (d) 10.37 GHz.

The second resonance is due to the half wave variation,

$$l_2 + l_3 + l_4 \approx \lambda_{g,2}/2 \tag{5.2}$$
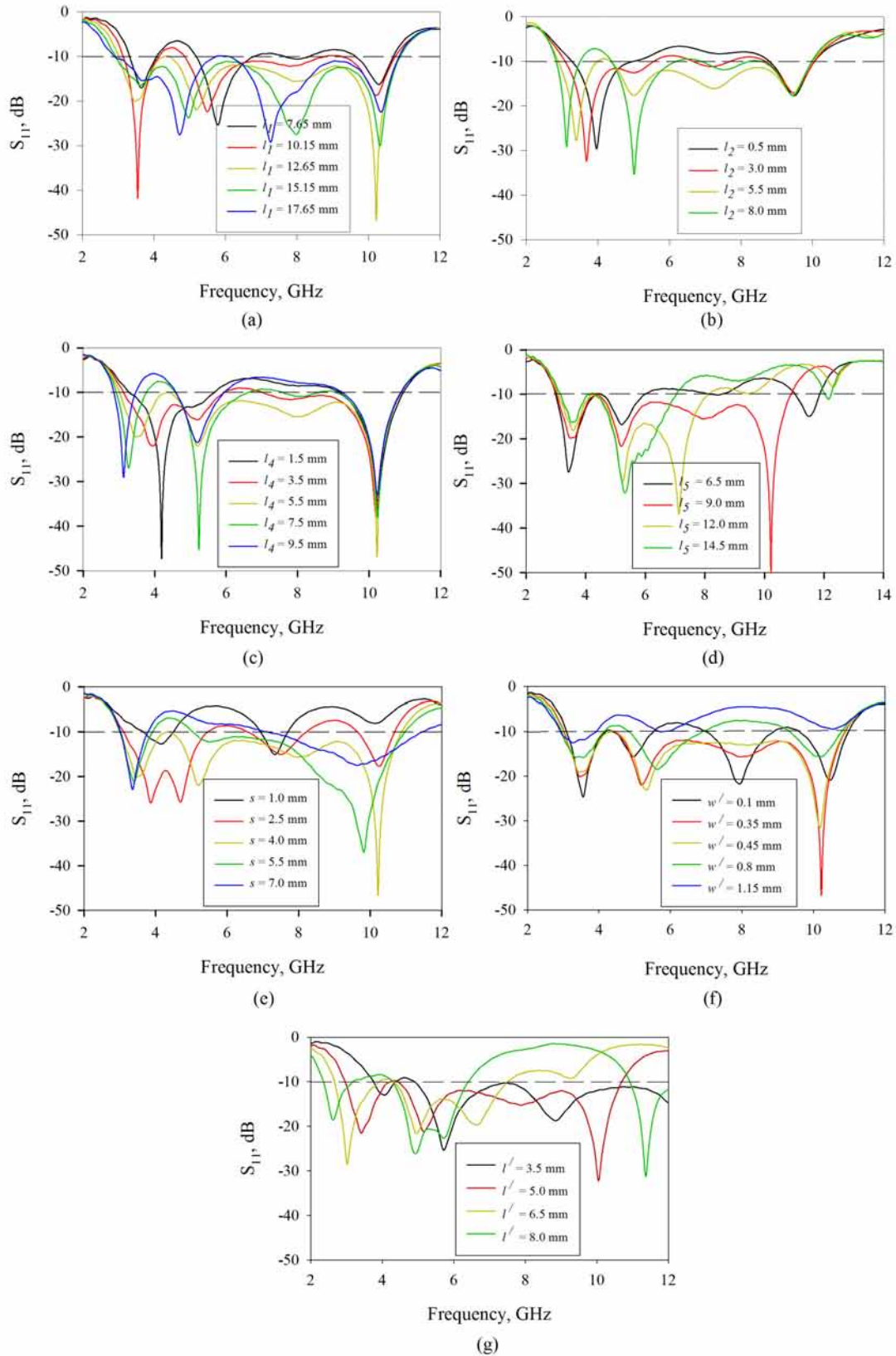
Figure 5.4: Variation in S_{11} with variation in the geometric parameters of Antenna–c

Table 5.2: Computed and optimized geometric parameters of the Step–Slot antennas (also see Table 3.2)

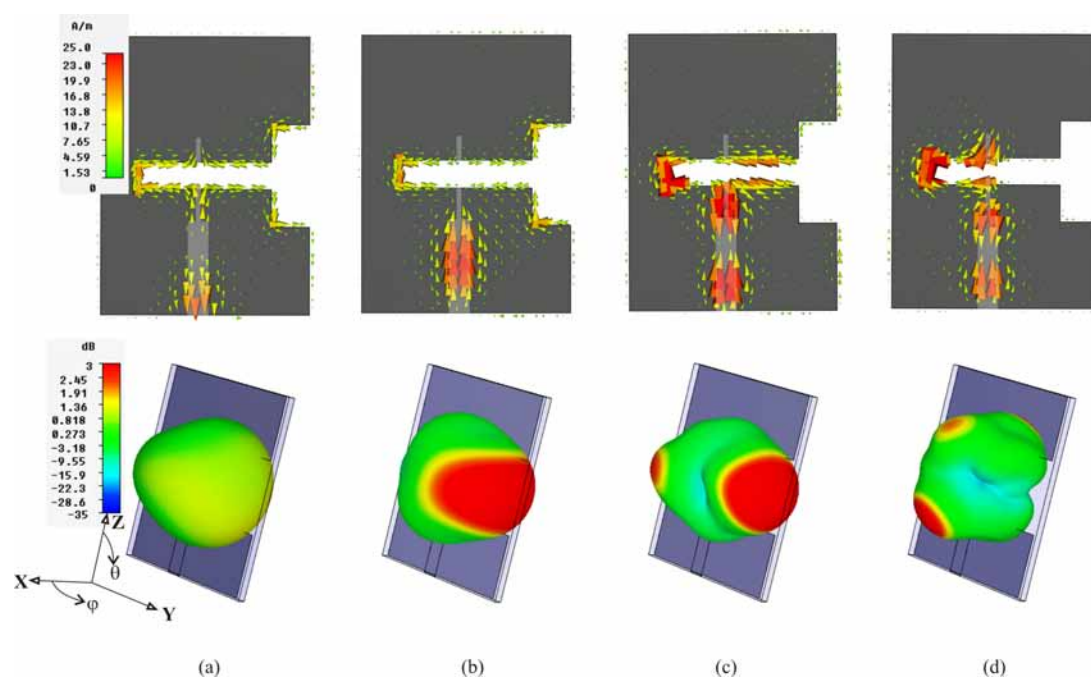| Parameter (mm)	Antenna–1 (Rogers 5880)		Antenna–2 (Taconic RF–30)		Antenna–3 (FR4 Epoxy)		Antenna–4 (Rogers RO3006)	
	Computed	Optimized	Computed	Optimized	Computed	Optimized	Computed	Optimized
l_1	18.65	18.65	15.5	15.6	12.65	12.65	13	13
l_2	5.5	5.5	5.5	5.5	5.5	5.5	5.5	5.5
l_3	5.5	5.5	5.5	5.4	5.5	5.35	5.5	4.8
l_4	14.82	13.5	13.2	12.5	11.41	10.15	9.9	9.9
l_5	11.5	10.8	10.28	10	8.8	8.65	7.7	7.8
l	–	17	–	15.5	–	13.5	–	14.2
$l/$	16.5	17	14.8	14	12.7	12	11	10.7
$w/$	–	2	–	1.2	–	0.7	–	0.4
s	4	4	4	4	4	4	4	4
LxB	52 x 40	52 x 38.5	46 x 36	46 x 36	40 x 33.4	38 x 28	40 x 32	40 x 32
f_1, f_2, f_3, f_4 (GHz)	3.25, 4.52, 7.56, 9.82	3.3, 4.67, 7.65, 10.2	3.25, 4.64, 7.68, 10	3.31, 5, 8, 10.25	3.3, 5, 7.12, 9.5	3.58, 5.18, 8, 10.37	3.5, 5, 7.9, 10	3.5, 5, 8, 10

For the third resonance,

$$l_4 \approx \lambda_{g,3}/2 \tag{5.3}$$

For the fourth resonance,

$$l_5 \approx \lambda_{g,4}/2 \tag{5.4}$$

Here, $\lambda_{g,i} = \lambda_{0,i}/\sqrt{\epsilon_{re}}$ where i = 1, 2, 3, 4; is the free space wavelength computed at the resonance and $\epsilon_{re} = (\epsilon_e + 1)/2$

A variation study of these parameters performed validate these observations as shown in Figure 5.4. As it can be seen in Figure 5.4(a), the parameter l_1 affects the matching of the first resonance and lowers the second resonance as it is increased. However, the first resonance is more affected when the parameter l_2 is varied as shown in Figure 5.4(b). Variation in l_4 is similar to that in l_1 and is shown in Figure 5.4(c). It is seen that as the parameter l_5 is increased, both the third and fourth resonances shift towards the lowers side and in addition, a fifth resonance start to show as in Figure 5.4(d). The slot width s, microstrip width $w^/$ and length $l^/$ can affect the overall impedance matching and are shown in Figures 5.4(e), (f) and (g).

To further validate Equations 5.1–5.4, the antenna (Antenna–c) is designed on laminates with different permittivity, the parameters of which are given in Table 5.2. Impedance bandwidths of these antennas are plotted in Figure 5.5.
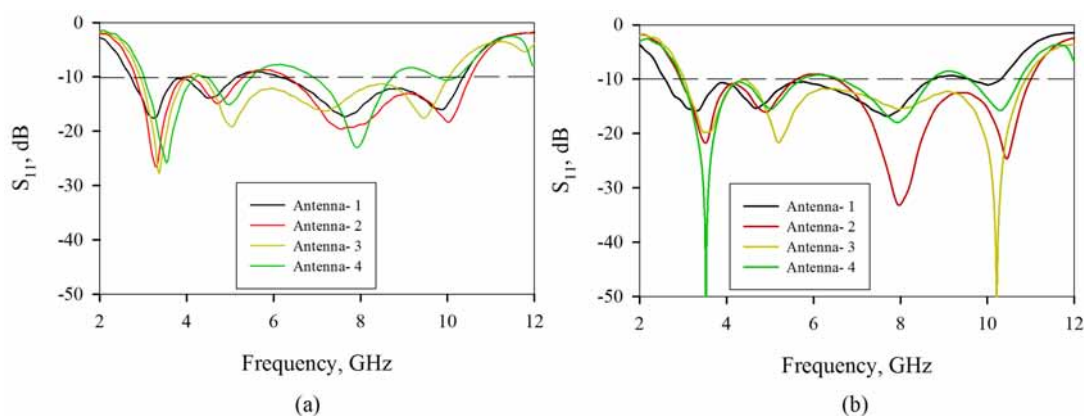
Figure 5.5: Return loss of antennas with (a) computed geometric parameters (b) optimized geometric parameters.

5.2 Experiment results

Figure 5.6 shows the measured and simulated return loss of this antenna. The –10dB bandwidth of the antenna is from 3–11 GHz which covers the band for UWB communication and measurement applications.
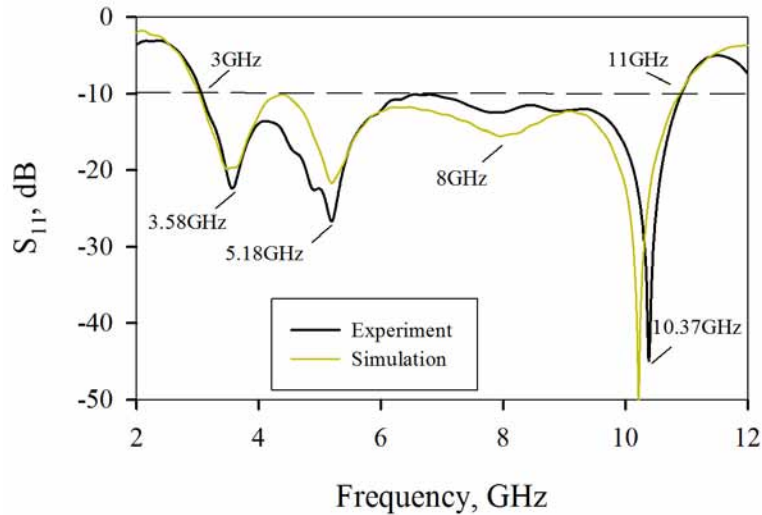
Figure 5.6: Measured and simulated S_{11} of the step slot antenna.

Measured radiation patterns of the antenna in the Y–Z, X–Z and X–Y planes at three different frequencies are shown in Figure 5.7 along with the simulated results. Across all planes, radiation remains approximately omni directional with polarization in the Y– direction. Average value of cross polarization is –20dB except in the X–Z plane, which shows high cross polar radiation throughout the band. The average gain in the 3.1– 10.6 GHz band is observed to be 3.16 dBi. Gain and radiation efficiency measurements show reasonable agreement with simulation as shown in Figure 5.8.
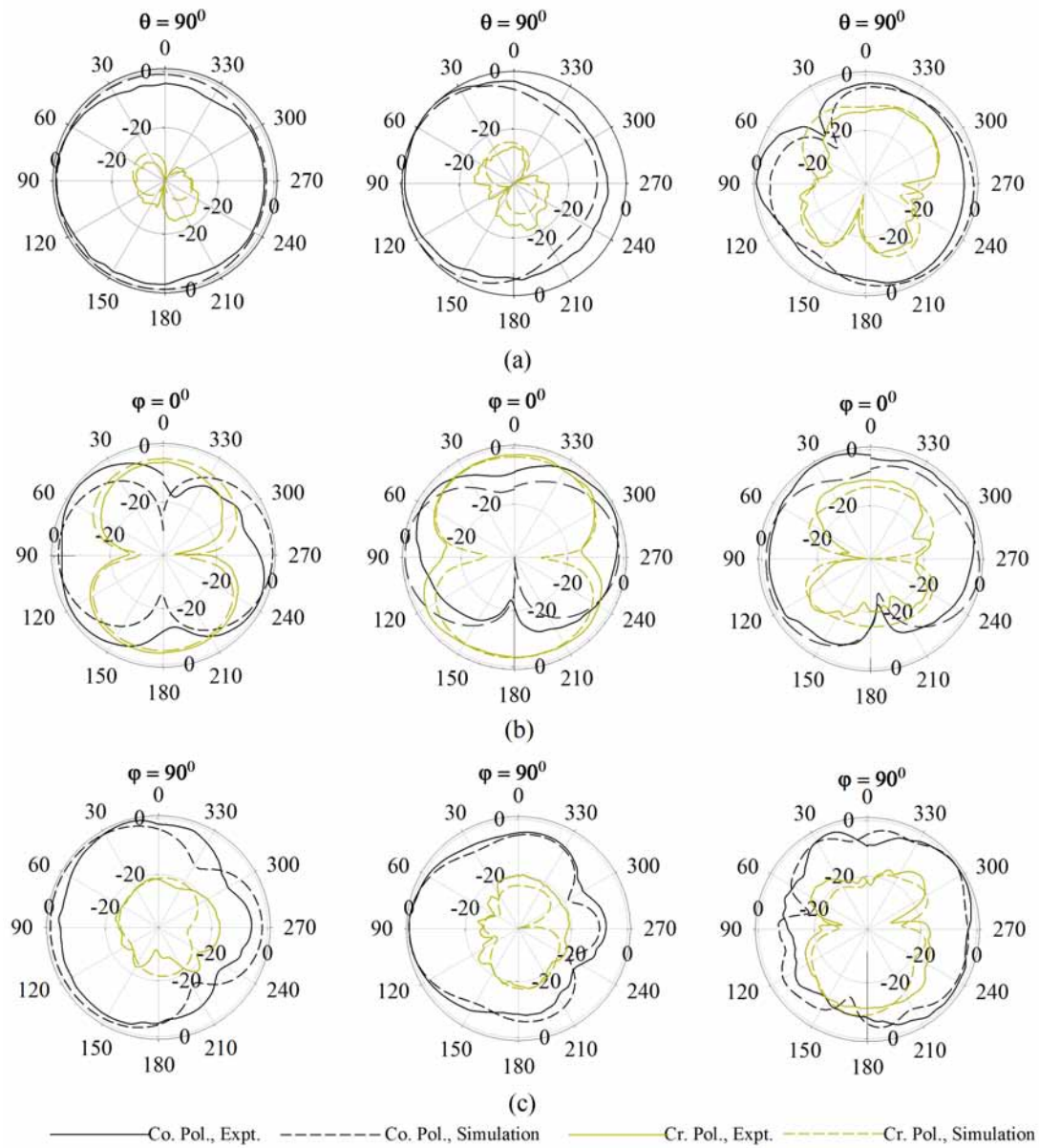
Figure 5.7: Radiation patterns of the step slot antenna in the (a) y-z plane: 3.58, 5.18, 10.37 GHz (b) x-z plane: 3.58, 5.18, 10.37 GHz (c) x-y plane: 3.58, 5.18, 10.37 GHz
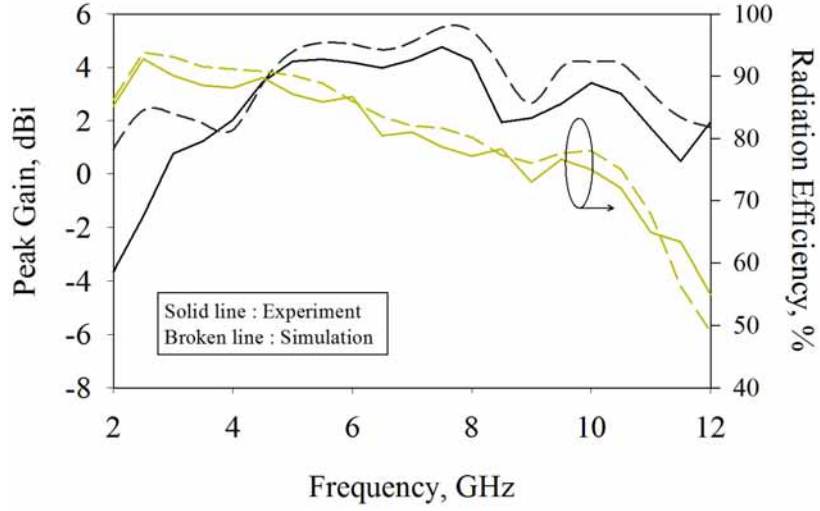
Figure 5.8: Measured and simulated peak gains and radiation efficiency of the step slot antenna

5.3 The Linear–Tapered Slot Antenna: Design

The proposed linear tapered slot antenna is derived form a narrow slot antenna (Antenna–a) shown in Figure 5.9(a), whose geometric parameters are given in Table 5.3. This configuration (Antenna–a) shows three resonances as shown in Figure 5.10. As the open end of the slot is flared to result in parameter g_{s2}, the impedance match within the 3.1–10.6 GHz band improves as shown in this figure. To further improve the impedance bandwidth below –10dB, a rectangular cut is optimized in the microstrip feed (Antenna–c in Figure 5.9).

From the surface current distributions shown in Figure 5.11(a), the first resonance in the antenna can be accounted as,

$$l_{s1} + l_{s2} + l_{s3} + \left(\frac{g_{s2} - g_{s1}}{2}\right) + w \approx \frac{\lambda_{g,1}}{2} \tag{5.5}$$

Refereing to Figure 5.11(a), the second resonance can be accounted as,

$$l_{s1} + l_{s2} + \left(\frac{g_{s2} - g_{s1}}{2}\right) \approx \frac{\lambda_{g,2}}{2} \tag{5.6}$$

and the third resonance as,

$$0.5 \cdot \sqrt{4(l_{s2})^2 + (g_{s2} - g_{s1})^2} + l_{s3} + w \approx \frac{\lambda_{g,3}}{2} \tag{5.7}$$
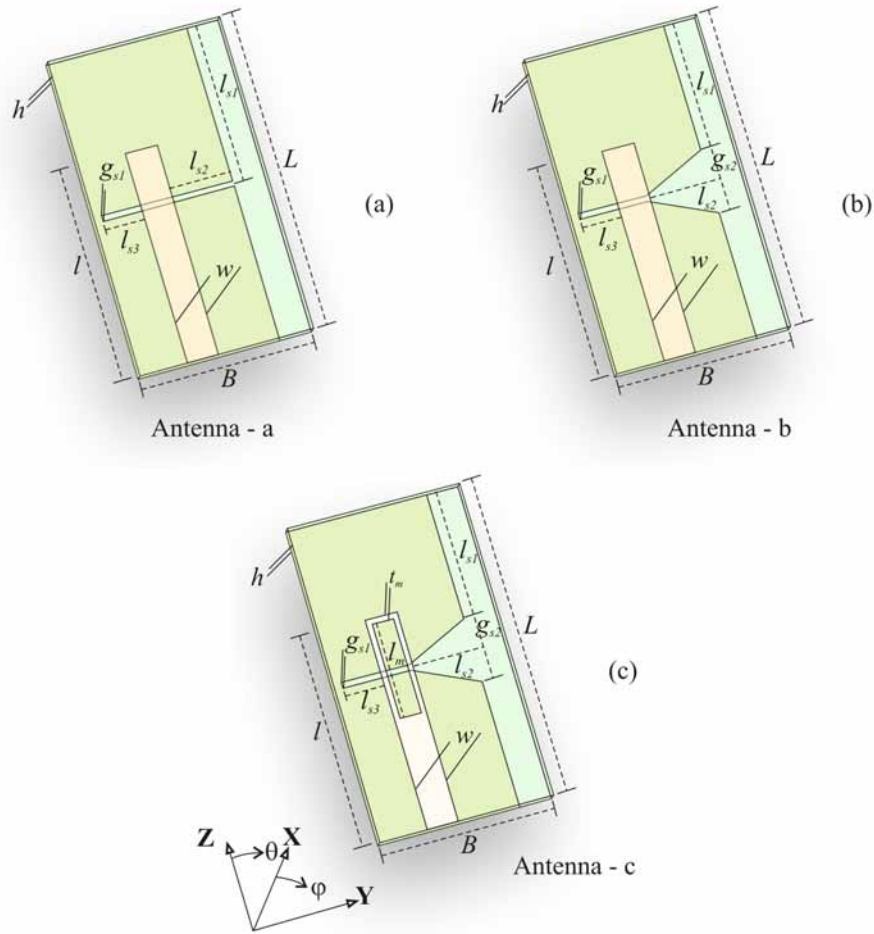
Figure 5.9: Design evolution of the tapered slot antenna.
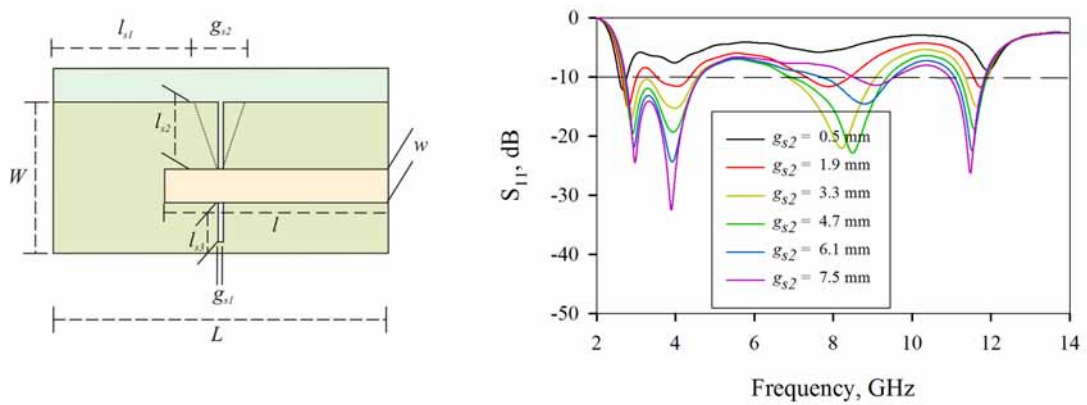
Figure 5.10: Variation in S_{11} with variation in g_{s2} for Antenna–a

Table 5.3: Geometric parameters of the linear tapered slot antennas in Figure 5.9

Parameter	Antenna–a	Antenna–b	Antenna–c
ε_r	4.4	4.4	4.4
$tan(\delta)$	0.02	0.02	0.02
$h(mm)$	1.6	1.6	1.6
$g_{s1}(mm)$	0.5	0.5	0.5
$g_{s2}(mm)$	–	6	6
$l_{s1}(mm)$	14.75	12	12
$l_{s2}(mm)$	5.98	5.98	5.98
$l_{s3}(mm)$	3.5	3.5	3.5
$l(mm)$	25.5	25.5	20
$l_m(mm)$	–	–	9
$t_m(mm)$	0.5	0.5	0.5
$L \times B \ (mm^2)$	30 x 13.5	30 x 13.5	30 x 13.5
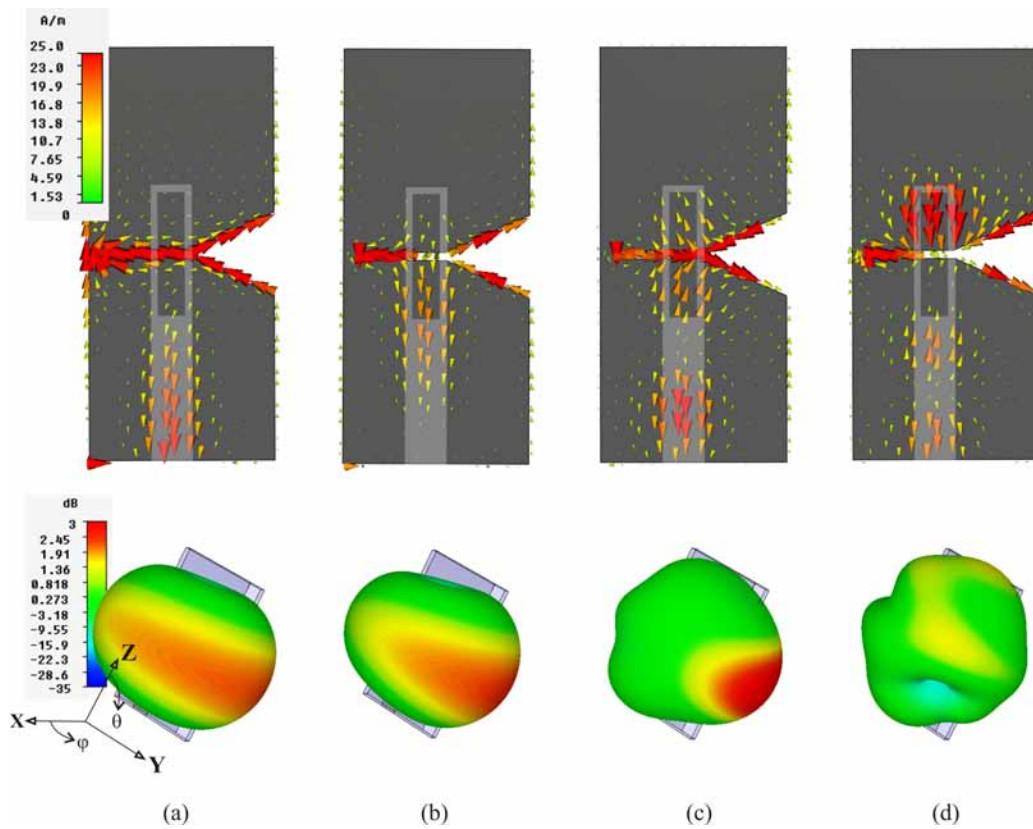
Figure 5.11: Surface current distribution and radiation patterns at (a) 2.9 (b) 3.95 (c) 8 and (d) 11.2 GHz (Antenna–a)

Table 5.4: Computed and optimized geometric parameters of the linear tapered slot antennas (also see Table 3.2)

Parameter (mm)	Antenna−1 (Rogers 5880)		Antenna−2 (Taconic RF-30)		Antenna−3 (FR4 Epoxy)		Antenna−4 (Rogers RO3006)	
	Computed	Optimized	Computed	Optimized	Computed	Optimized	Computed	Optimized
l_{s1}	15.11	15.11	14.25	14	12	12	11	11
l_{s2}	7.4	7.4	6.87	6.87	6.12	5.98	5.73	5.73
l_{s3}	2.95	4.95	2.83	3.6	2.64	3.5	3.5	4.05
g_{s1}	0.5	0.5	0.5	0.5	0.5	0.5	0.5	0.5
g_{s2}	6	6.5	6	6	6	6	6	6
l	25.77	25.77	23.6	23.6	20.3	20	18.9	18.6
l_m	12.82	10.8	11.2	11.2	9.6	9	9.6	9
t_m	1	1	1	1	0.5	0.5	0.1	0.1
LxB	36.7 x 17.5	36.7 x 18.9	34 x 15	34 x 15.8	30 x 13.6	30 x 13.5	28 x 12.13	28 x 12.7
f_1, f_2, f_3, f_4 (GHz)	3.3, 7.35, 10.7	3.3, 4.67, 7.65, 10.2	3.25, 4.64, 7.68, 10	3.31, 5, 8, 10.25	3.1, 3.92, 7.8, 11.35	2.9, 3.9, 8, 11.2	3.56, 8.1, 10.58	3, 3.77, 8.9, 10.6

Figure 5.12: Return loss of the linear tapered slot antenna with (a) computed (b) optimized geometric parameters.

The fourth resonance in the antenna cannot be empirically accounted and it resembles a some higher order mode inherent with the present design.

Equations (5.6)–(5.7) are validated by designing the linear tapered slot antenna on substrates with different permittivity and the computed and optimized values are shown in Table 5.4. The observed return losses of the antennas are plotted in Figure 5.12. This figure ind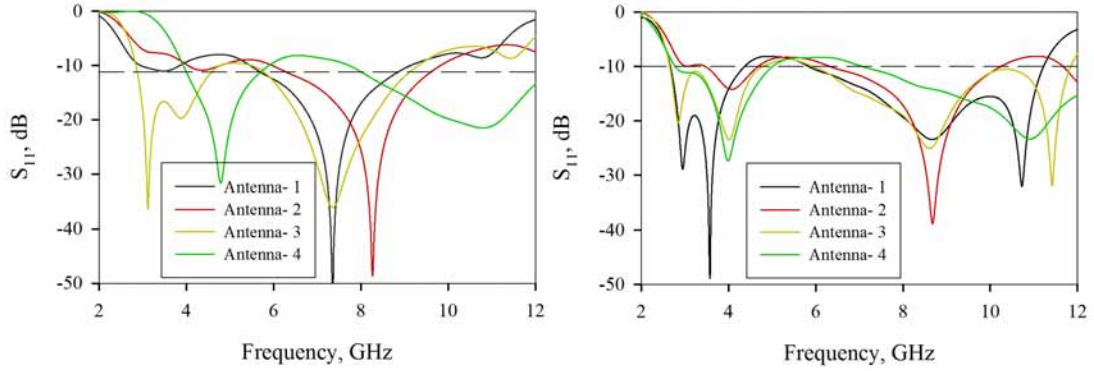icates that the linear tapered slot antenna design is sensitive to variation in design parameters unlike the other antennas discussed in this thesis and hence optimization through simulation is essential.

Results of the parametric studies further conducted is shown in Figure 5.13. It is seen from Figure 5.13 (a) that the length of the ground plane l_{s1} has to be optimum for the resonances to have proper matching. Variation in l_{s2} results in a significant shift in the third resonance than the second resonance as shown in Figure 5.13(b). As seen in Figure 5.13(c), the parameter l_{s3} affects the fourth resonance as in a shift and the first resonance in matching. Effect of the parameter t_m and l_m is at the higher frequencies as seen in Figure 5.13(d). These parameters can be set for the impedance bandwidth to cover the 3.1-10.6 UWB.

5.4   Experimental results

Measured return loss of the antenna indicate a wide bandwidth from 2.95- 14 GHz with close correspondence with the simulation as in Fig 5.14. The measured radiation pattern of the antenna is shown in Figure 5.15 at the resonant frequencies. These are omni directional in the H-plane (X-Z plane) and bi-directional in the
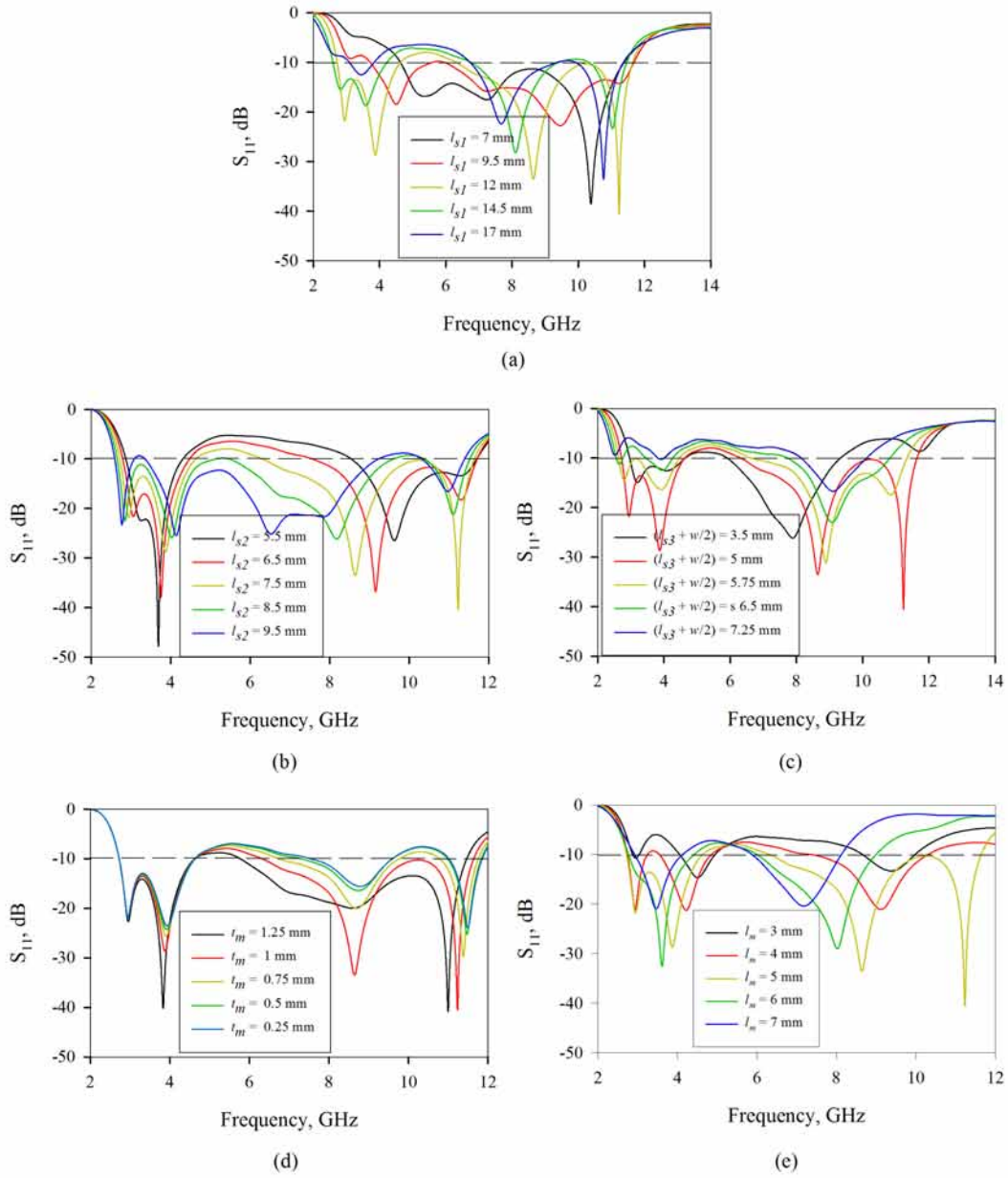
Figure 5.13: Variation in S_{11} with variation in the geometric parameters for Antenna–c.

E-planes (X-Y and Y-Z). Peak gain of the antenna remains constant throughout the band as shown in Figure 5.16 with polarization in the Y-direction. The antenna also exhibits decent radiation efficiency, validated by simulation and is shown in the same figure.
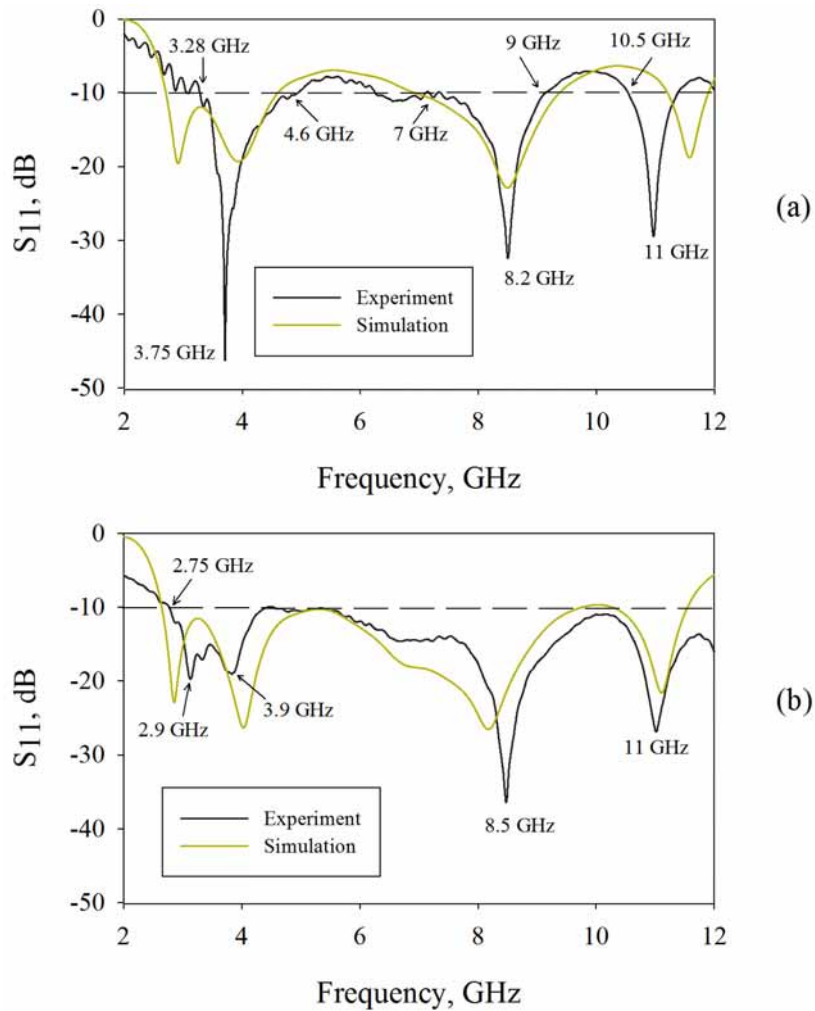
Figure 5.14: Return loss of the antenna (a) without MS feed modification (b) with modified MS feed.
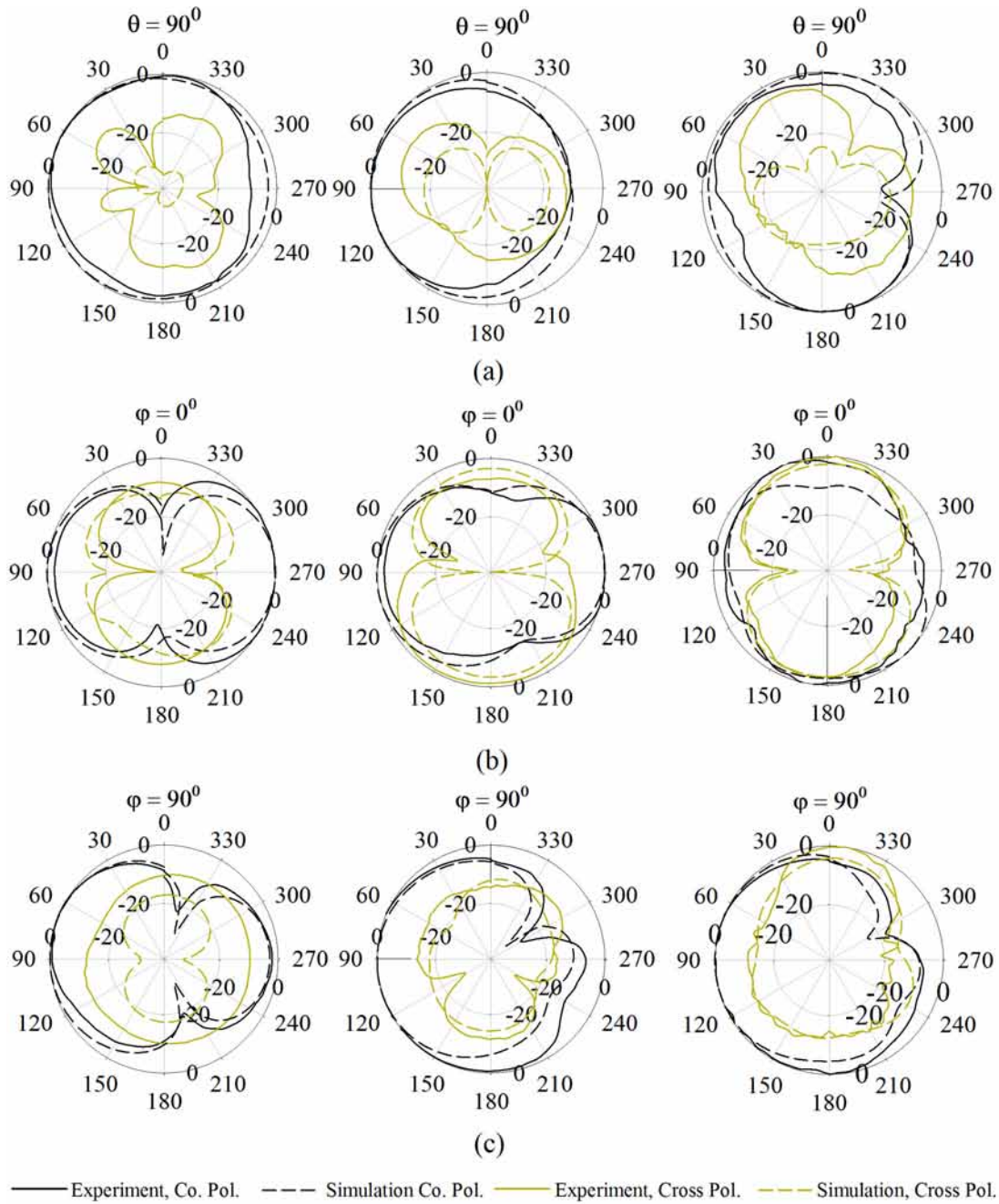
Figure 5.15: Radiation patterns of the tapered slot antenna in the (a) y-z plane: 3.58, 5.18, 10.37 GHz (b) x-z plane: 3.58, 5.18, 10.37 GHz (c) x-y plane: 3.58, 5.18, 10.37 GHz
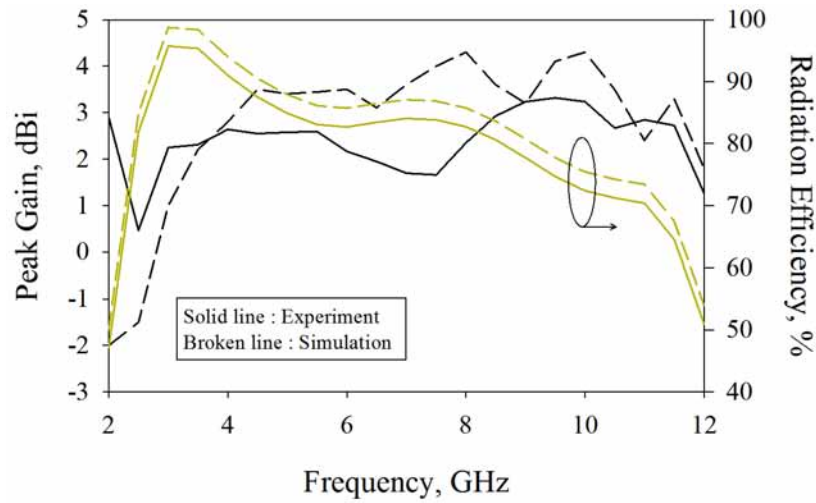
Figure 5.16: Measured and simulated peak gain and radiation efficiency of the linear tapered slot antenna

5.5   Conclusion

Chapters 3 and 4 demonstrated that a proper design of the patch–ground interface, on either side of the transmission line, can minimize pernicious reflections inside the antenna geometry by smooth impedance transformation from 50 Ω–377 Ω. Designs presented in this chapter have transmission line and transformer as a single entity. Even though the impedance bandwidth is less compared to that of the Square Monopole and Semi Elliptic Slot, the operational band covers the communication band allocated for UWB in both Step Slot and Tapered Slot antennas. Radiation patterns are slightly directive with peak gains on any plane along this direction.

References

AMIN M. ABBOSH, H. K. KAN, M. E. BIALKOWSKI. 2006. Compact ultra–wideband planar tapered slot antenna for use in a microwave imaging system. *Microwave and Optical Technology Letters*, **48**(11), 2212–2216. 84

BEHDAD, NADER, & SARABANDI, KAMAL. 2004. A multiresonant single–element wideband slot antenna. *IEEE Antennas and Wireless Propagation Letters*, **3**(March), 5–8. 85

CHAMBER, D. 1970. *Microwave Active Network Synthesis.* Semiannual Report, Stanford Research Institute. 83

CHEN, WEN-SHAN, & KU, KUANG-YUAN. 2006 (14, July). Bandwidth enhancement of open slot antenna for UWB applications. *Pages 2563– 2566 of: IEEE Antennas and Propagation Society International Symposium.* 85

CHRAMIEC, J. 1989. Reactances of slotline short and open circuits on alumina substrate. *IEEE Transactions*, **MTT–37**, 1638–1641. 83

DO-HOON KWON, EVGENY V. BALZOVSKY, YURI I. BUYANOV YONGJIN KIM VLADIMIR I. KOSHELEV. 2008. Small printed combined electric–magnetic type ultrawideband antenna with directive radiation characteristics. *IEEE Transaction on Antennas and Propagation*, **56**(1), 1163–1169. 85

E. GUILLANTON, J. Y. DAUVIGNAC, CH. PICHOT J. CASHMAN. 1998. A new design tapered slot antenna for ultra–wideband applications. *Microwave and Optical Technology Letters*, **19**(4), 286–289. 84

GARCYA E., E. DE LERA, E. RAJO. 2007. Tapered slotline antenna modification for radiation pattern improving. *Microwave and Optical Technology Letters*, **49**(10), 2590–2595. 84

GAZIT, E. 1988. Improved design of the vivaldi antenna. *IEE proceedings H, Microwave Antennas and Propagation*, **135**(2), 89–92. 84

GIBSON, P. J. 1979. The Vivaldi Aerial. *Pages 101–105 of: Proceedings of the 9th European Microwave Conference.* 83

GUPTA K. C., RAMESH GARG, INDER BAHL PRAKASH BHARTIA. 1996. *Microstrip Lines and Slotlines, 2nd Edition.* 685, Canon Street, Norwood, MA 02062: Artech House. 83

KNOTT P., A. BELL. 2001. Coaxially–fed tapered slot antenna. *IEE Electronics Letters*, **37**(18), 1103–1104. 84

LANGLEY J. D. S., P. S. HALL, P. NEWHAM. 1993. Novel ultrawide–bandwidth vivaldi antenna and low cross–polarisation. *IEE Electronics Letters*, **29**(23), 2004–2005. 84

LEI ZHU, RONG FU, KE-LI WU. 2003. A novel broadband microstrip–fed wide slot antenna with double rejection zeros. *IEEE Antennas and Wireless Propgation Letters*, **2**, 194–196. 85

MATSUI, AKINORI. 2004 (June). Experimental consideration on tapered slot antenna divided into radiator and feeding circuit. *Pages 1010–1013 of: IEEE Transaction on Antennas and Propagation*, vol. 1. 84

R. JANASWAMY, D. H. SCHAUBERT. 1987. Analysis of the tapered slot antenna. *IEEE Transaction on Antennas and Propagation*, **AP–35**(9), 1058–1065. 83

RAINEE N. SIMONS, NIHAD I . DIB, RICHARD Q. LEE LINDA P. B. KATEHI. 1995. Integrated uniplanar transition for linearly tapered slot antenna. *IEEE Transactions on Antennas and Propagation*, **43**(9), 998–1002. 83

SAEED I. LATIF, LOTFOLLAH SHAFAI, SATISH KUMAR SHARMA. 2005. Bandwidth enhancement and size reduction of microstrip slot antennas. *IEEE Tranactions on Antennas and Propagation*, **53**(3), 994–1003. 85

SATISH KUMAR SHARMA, LOTFOLLAH SHAFAI, N. JACOB. 2004. Investigation of wide-band microstrip slot antenna. *IEEE Transactions on Antennas and Propagation*, **52**(3), 865–872. 85

SCHIEK B., KOHLER J. 1976. An improved microstrip–to–microslot transition. *IEEE Transactions*, **MTT-24**, 231–233. 83

SUNIL KUMAR RAJGOPAL, SATISH KUMAR SHARMA. 2009. Investigations on ultrawideband pentagon shape microstrip slot antenna for wireless communications. *IEEE Transactions on Antennas and Propagation*, **57**(5), 1353–1359. 87

SYMEON NIKOLAOU, GEORGE E. PONCHAK, JOHN PAPAPOLYMEROU MANOS M. TENTZERIS. 2006. Conformal double exponentially tapered slot antenna (DETSA) on LCP for UWB applications. *IEEE Transactions on Antennas and Propagation*, **54**(6), 1163–1169. 85

TZYH-GHUANG MA, C. H. TSENG. 2006. An ultra wideband coplanar waveguide–fed tapered ring slot antenna. *IEEE Transaction on Antennas and Propagation*, **54**(4), 1105–1110. 84

TZYH-GHUANG MA, SHYH-KANG JENG. 2005a. Planar miniature tapered–slot–fed annular slot antennas for ultrawide–band radios. *IEEE Transaction on Antennas and Propagation*, **53**(3), 1194–1202. 84

TZYH-GHUANG MA, SHYH-KANG JENG. 2005b. A printed dipole antenna with tapered slot for ultra wide band applications. *IEEE Transaction on Antennas and Propagation*, **53**(11), 3833–3836. 84

WANG REN, ZHIGUO SHI, HAIWEN LIU KANGSHENG CHEN. Novel compact 2.4/5–Ghz dualband T–slot antenna for WLAN] Operations, volume = 49, year = 2007. *Microwave and Optical Technology Letters*, June, 1236–1238. 85

WEN-SHAN CHEN, KUANG-YUAN KU. 2008. Bandwidth enhancement of open slot antenna for UWB applications. *Microwave and Optical Technology Letters*, **50**(2), 438–439. 87

YOON I. J., KIM H., CHANG K. YOON Y. J. KIM Y. H. 2005. Ultra wideband tapered slot antenna with band–cut off characteristic. *IEE Electronics Letters*, **41**(11). 84

YUAN YAO, WENHUA CHEN, BIN HUANG ZHENGHE FENG. 2008. Novel planar tapered–slot–fed UWB antenna. *Microwave and Optical Technology Letters*, **50**(9), 2280–2283. 85

Chapter 6

Transfer Property Characterizations

In this chapter, transfer properties of the planar UWB antennas discussed in the previous chapters are investigated and compared. Well–matched antennas may behave differently while transmitting/receiving non–sinusoidal waveforms and hence studies performed in this chapter are of atmost importance for UWB antennas. The measurement set up and the underlying theory are discussed in Chapter 2. Measurements are performed for the azimuthal and elevation planes and are verified using the time domain capabilities of CST Microwave Studio.

6.1   Simulation Studies

Magnitude of the transfer function $\overrightarrow{h}_{Rx}(\omega, \theta, \varphi)$ simulated in CST for the azimuthal plane of the antennas are shown in Figure 6.1 (Using Equation 2.8). It is seen that the intensity plots for $\overrightarrow{h}_{Rx}(\omega, \theta, \varphi)$ and $\overrightarrow{h}_{Tx}(\omega, \theta, \varphi)$ differ only in their relative amplitudes. As shown in Figure 6.1 (a)–(d), transfer functions of Square Monopole and Semi-Elliptic slot antennas are similar, with approximately linear decay in magnitude as a function of frequency over most of the azimuth angles. Effect of the band-notch at 5.5 GHz can be seen in Figures 6.1(b) and (d). Omni-directionality is lost in these antennas at frequencies above 8 GHz where relatively low amplitudes are observed at certain angles. There are sharp nulls between 30^0–50^0, 130^0–150^0, 210^0–230^0 and 320^0–330^0 for the Square Monopole antenna while the effect is less pronounced for the Semi-Elliptic slot antenna. The Step Slot antenna behaves similarly between 0^0–150^0 and at other angles, the

Figure 6.1: Simulated antenna transfer function in the azimuthal plane for (a) Square Monopole (b) Square Monopole with Band Notch (c) Semi-Elliptic Slot (d) Semi-Elliptic Slot with Band Notch (e) Step Slot and (f) Tapered Slot Antennas

Figure 6.2: Simulated antenna impulse response in the azimuthal plane for (a) Square Monopole (b) Square Monopole with Band Notch (c) Semi-Elliptic Slot (d) Semi-Elliptic Slot with Band Notch (e) Step Slot and (f) Tapered Slot Antennas

degradation starts at lower frequencies. As seen in Figure 6.1, transfer function of the linear tapered slot antenna remains constant up to 10 GHz and the amplitude decay begins only after 10 GHz.

The corresponding impulse responses are well formed with good peak value over almost all the angular regions as shown in Figure 6.2. Amplitude degradation beyond 8 GHz in the Square Monopole and Semi-Elliptic Slot is reflected in their corresponding impulse responses between 30^0–120^0 and 200^0–330^0. This can be seen in Figure 6.2(a)–(d) where the impulse response peak show intensity variations at these angles. Antennas with band notch resonators exhibit pronounced rippling in their impulse responses as shown in Figure 6.2 (b) and (d). In the Step Slot, the impulse response behave differently between 150^0–355^0 while that for the Tapered Slot Antenna is sharp and well formed at all angular regions. Among the four antennas investigated, superior azimuthal radiation is found to be that of the Tapered slot.

Transfer functions in the elevation planes of the antennas are shown in Figure 6.3. The nulls in the radiation pattern at 180^0 can be seen in the transfer functions which show intensity variations. Transfer functions in the elevation planes are almost similar for all the antennas. Corresponding impulse responses are shown in Figure 6.4. Excluding the nulls at 180^0, well formed amplitude peaks belong to the linear tapered slot antenna.

6.2 Measurements with prototype antennas

Procedure for the transfer property measurements are as explained in sections 2.3.7 and 2.3.8 in Chapter 2. The transmitting and receiving antennas are positioned in their far field, at a distance of 25 cm for measurements. Source power level in the VNA is set at 10 dB to improve signal to noise ratio in the measured data.

Measured antenna transfer functions in the azimuthal planes are shown in Figure 6.5 and the corresponding impulse response in Figure 6.6. Intensity variations in the antenna transfer function shown in Figure 6.5 agree well with simulations across the azimuthal angles and frequencies. For all the antennas, measured phase is linear across all planes shown in the same figure. It can be seen Figure 6.6 that peak of the impulse response show variation along the azimuthal
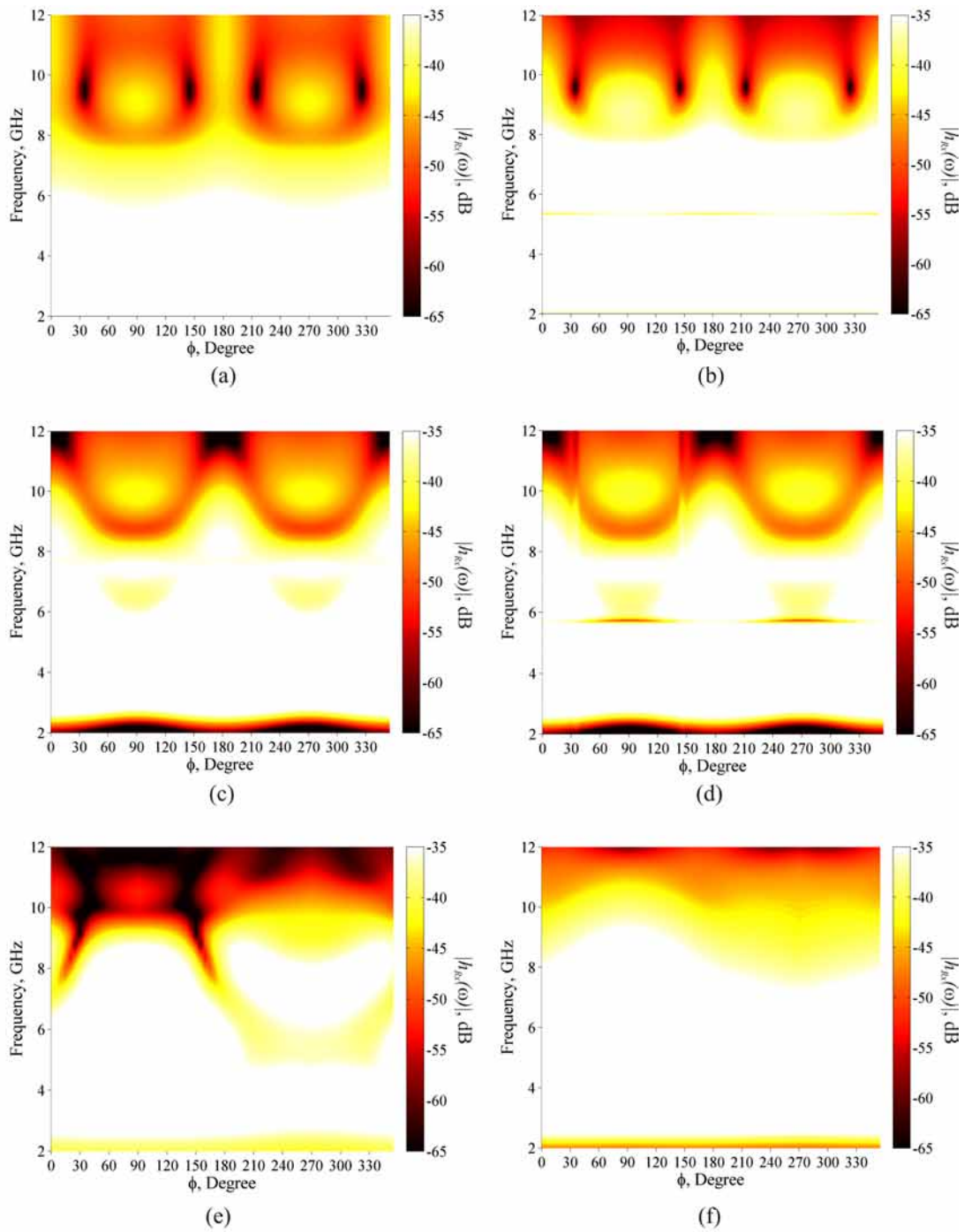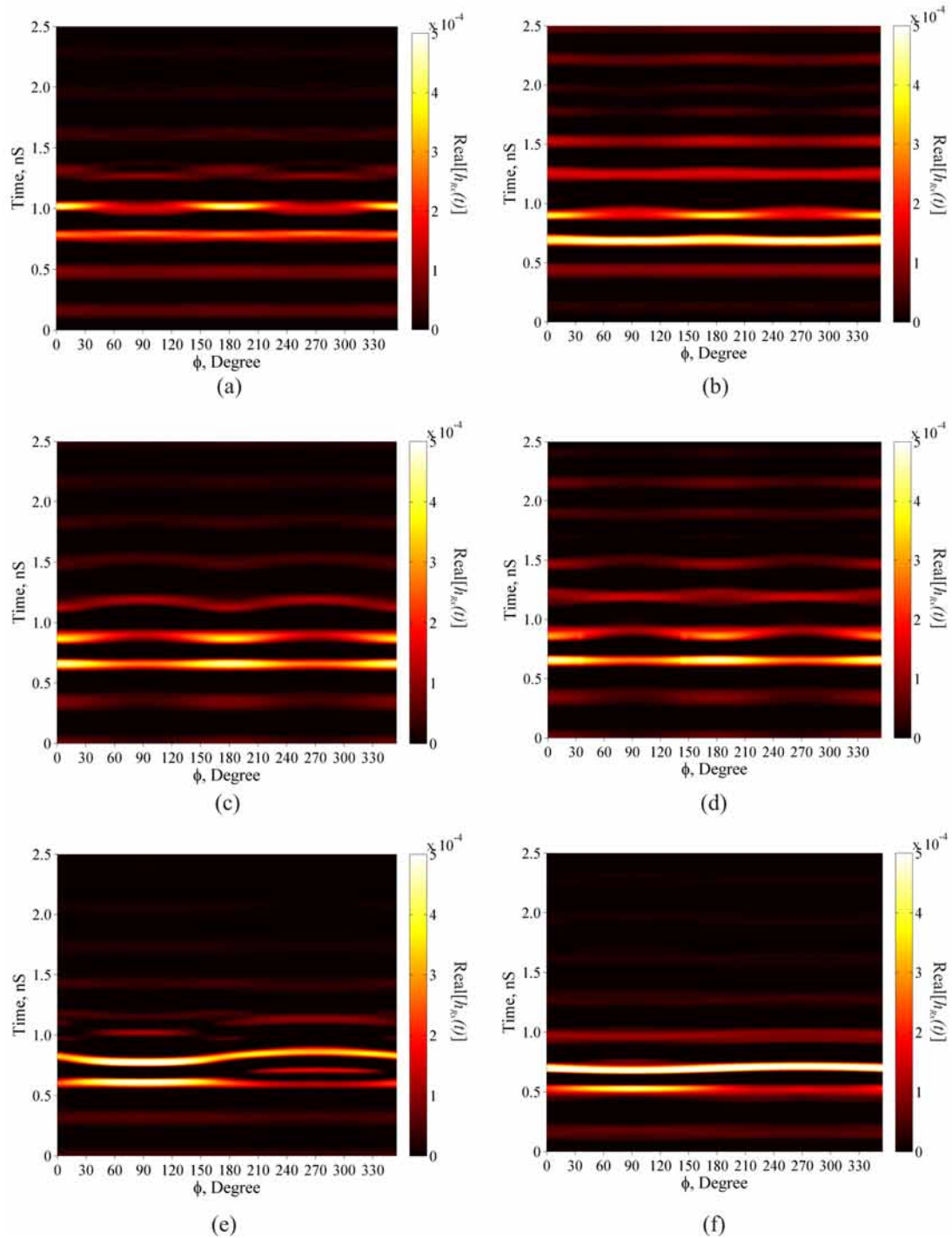
Figure 6.3: Simulated antenna transfer function in the elevation plane for (a) Square Monopole (b) Square Monopole with Band Notch (c) Semi-Elliptic Slot (d) Semi-Elliptic Slot with Band Notch (e) Step Slot and (f) Tapered Slot Antennas.
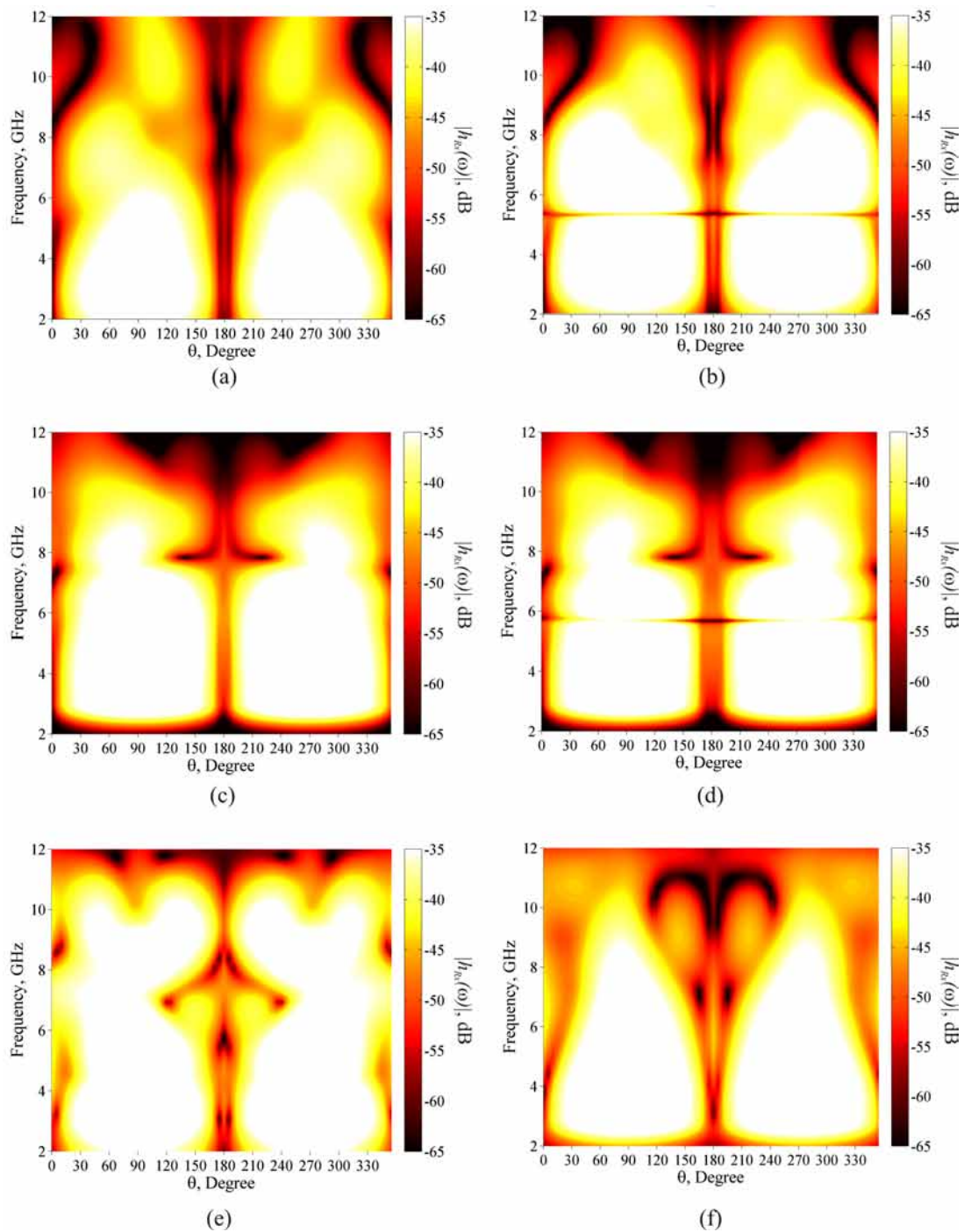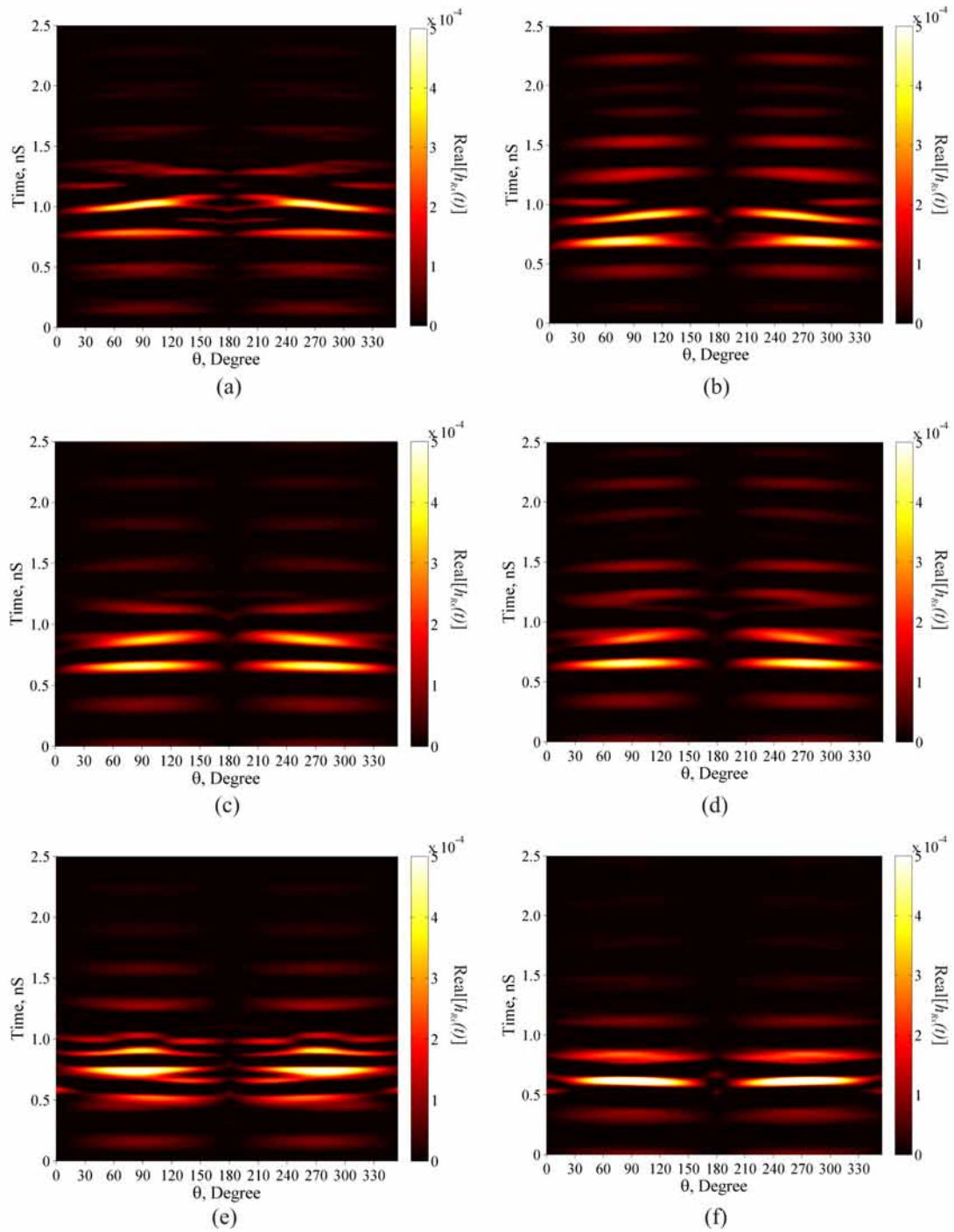
Figure 6.4: Simulated antenna impulse response in the elevation plane for (a) Square Monopole (b) Square Monopole with Band Notch (c) Semi-Elliptic Slot (d) Semi-Elliptic Slot with Band Notch (e) Step Slot and (f) Tapered Slot Antennas.

angle. Amplitude of the impulse response is maximum at $\theta = 90^0$, $\varphi = 0^0$ and $\theta = 90^0$, $\varphi = 180^0$ and minimum at $\theta = 90^0$, $\varphi = 90^0$ for the square monopole and semi-elliptic slot antennas. This can be attributed to the shift in the peak gain which is shown in Figure 3.6 and Figure 4.2. For the step slot and linear tapered slot, the amplitude peaks are maximum at $\theta = 90^0$, $\varphi = 90^0$ and minimum at $\theta = 90^0$, $\varphi = 180^0$. All impulse responses resemble delta function across all angles especially along the spatial angles where the amplitude peaks are maximum.

Measured transfer functions and impulse responses along the elevation planes are shown in Figures 6.7 and 6.8 respectively, which is found to replicate the simulation results.

6.3 Pulse analysis

Antenna effects on the nano second pulses are studied by method outlined in section 2.3.10. The template pulse chosen is fourth derivative of the Gaussian as shown in Figure 2.4. Figure 6.9 shows the measured and simulated pulses in the azimuthal and elevation planes for the square monopole antenna without and with band notch; Figure 6.10, that of the Semi-elliptic slot antenna without and with band notch; Figure 6.11, that of the step slot and linear tapered slot antennas. It is observed that the measurements and simulation agree well with each other for all the antennas. Among all the antennas, superior wave form reproduction is that of the linear tapered slot antenna.

6.4 Quantification of measured and simulated results

Measured and simulated impulse response and waveforms are quantified by methods outlined in section 2.3.9 and 2.3.11 and the results are shown in Table 6.1. It is found that measured and simulated data are more consistent with each other in the azimuthal plane, where the pattern is omni-directional, than in the elevation plane.
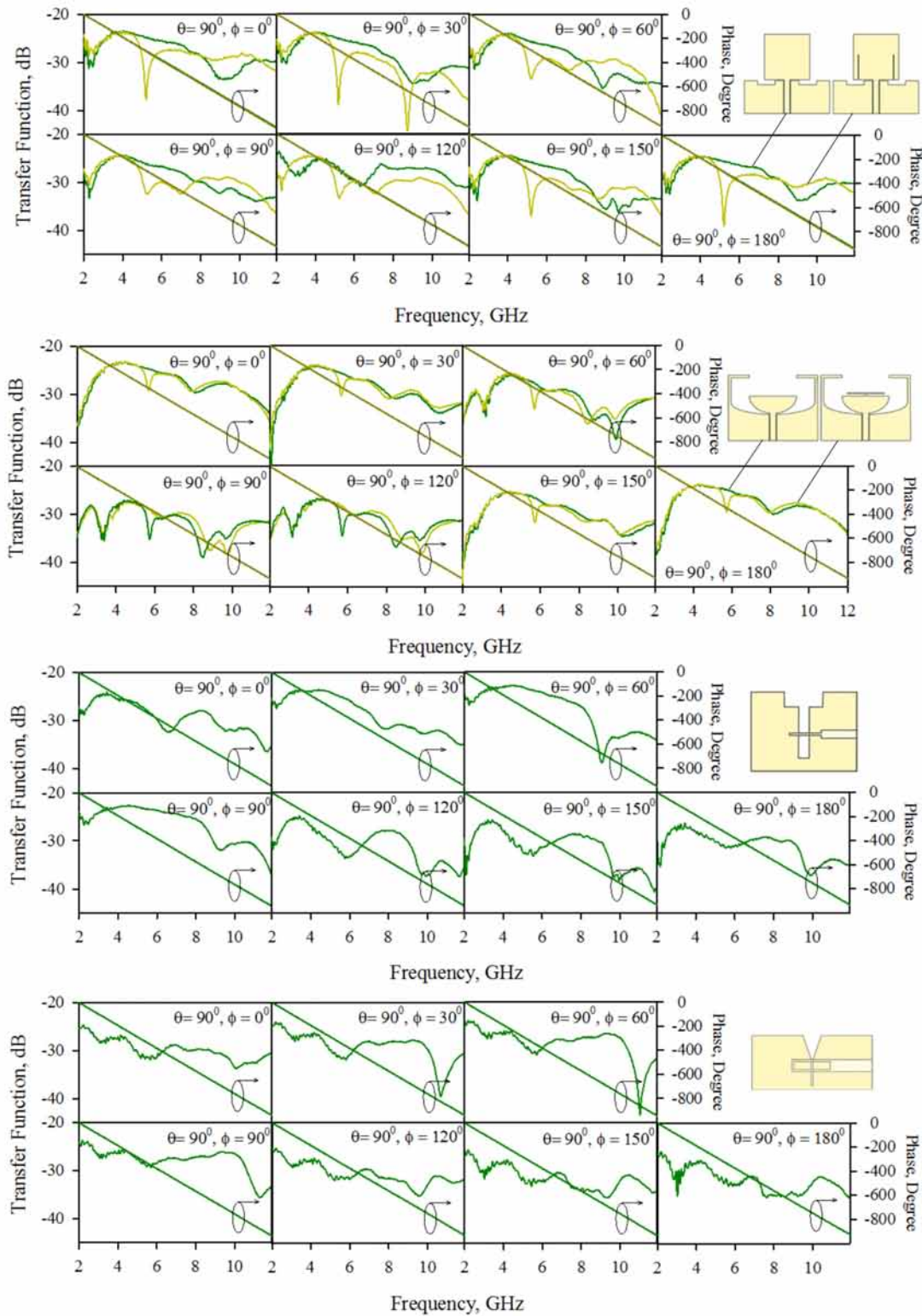
Figure 6.5: Measured antenna transfer function in the azimuthal plane.

Figure 6.6: Measured impulse response in the azimuthal plane.
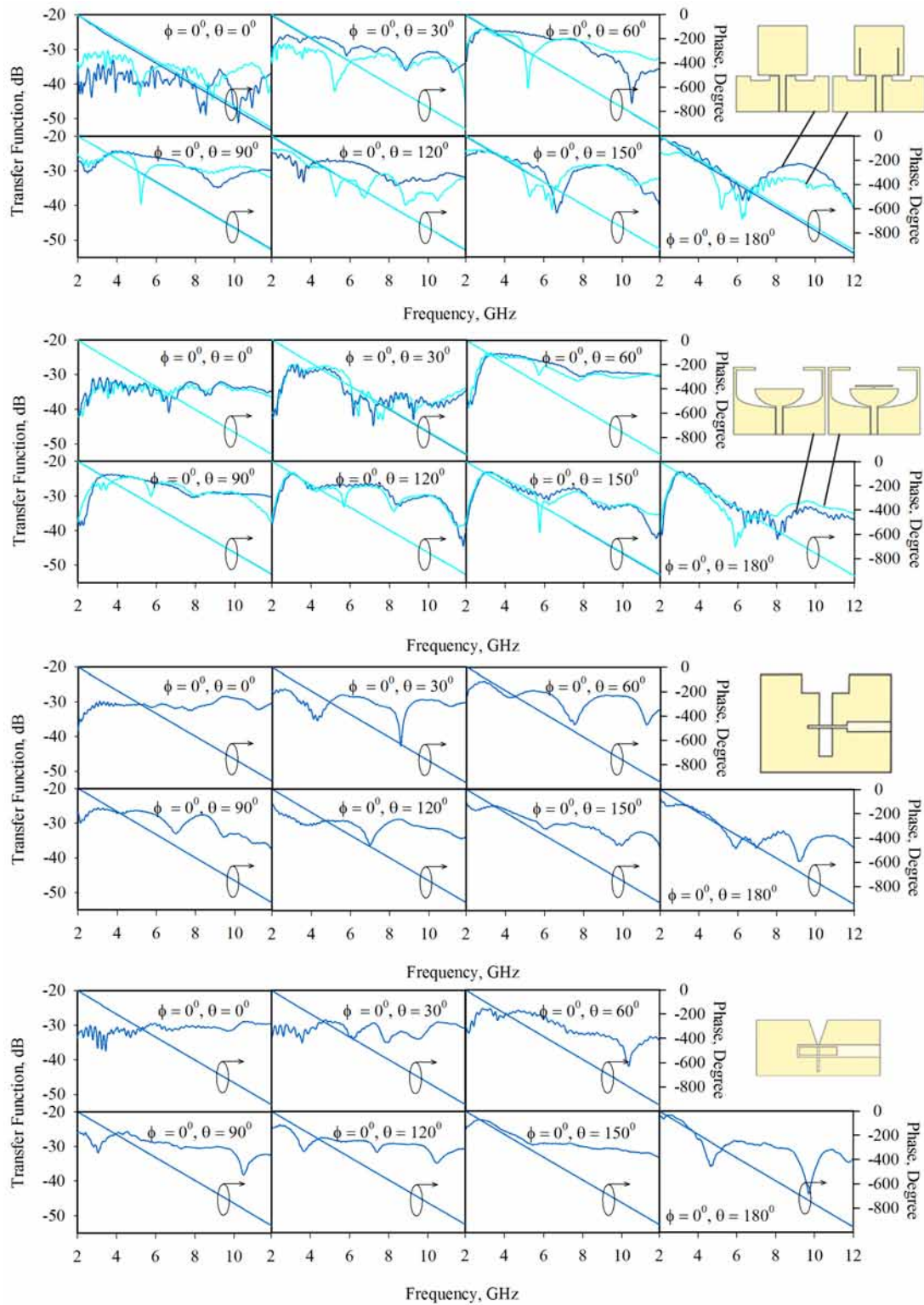
Figure 6.7: Measured antenna transfer function in the elevation plane.

Figure 6.8: Measured impulse response in the elevation plane.
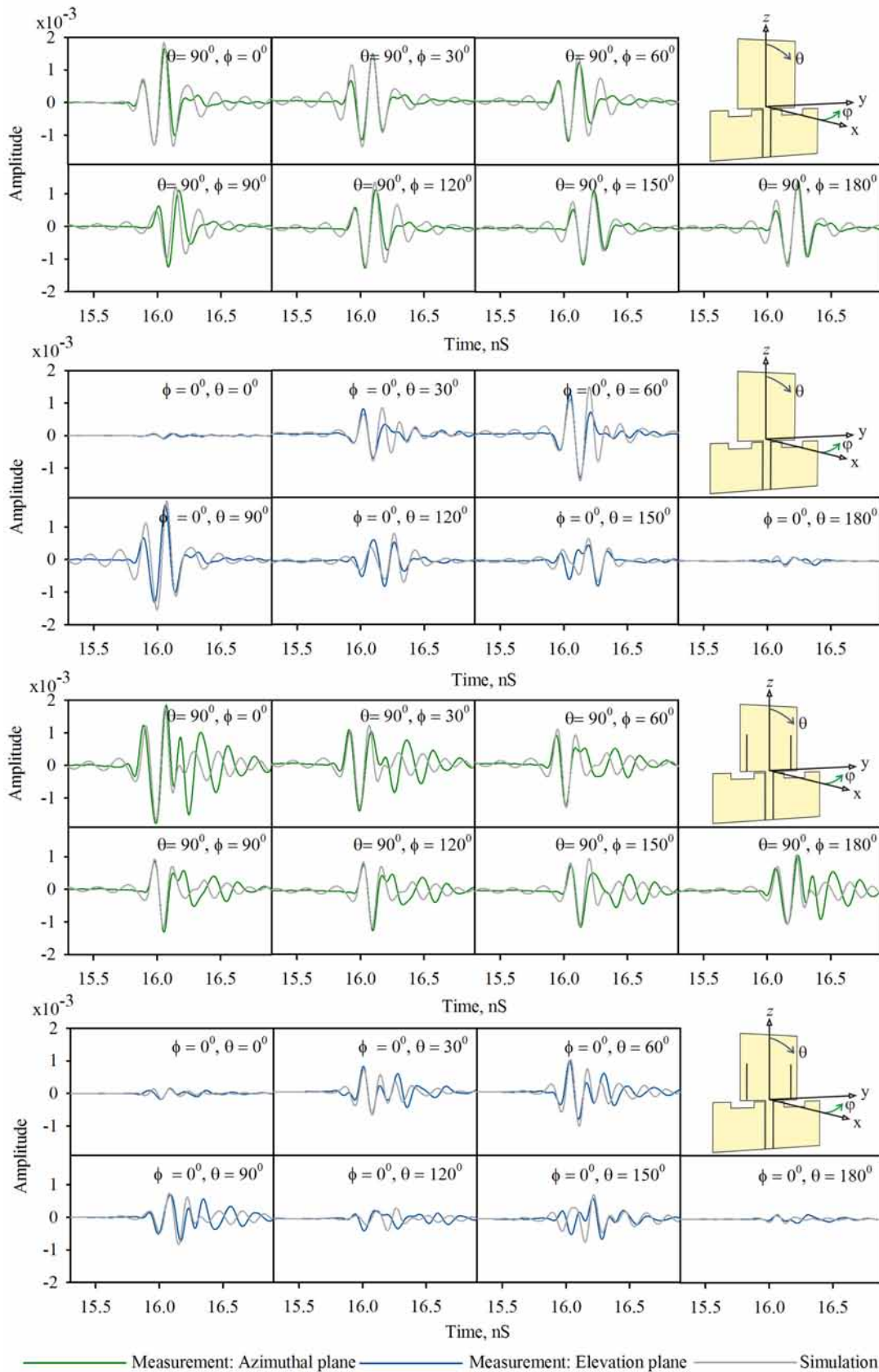
Figure 6.9: Measured and simulated pulses in the azimuthal and elevation planes: Square Monopole antenna without notch and with notch
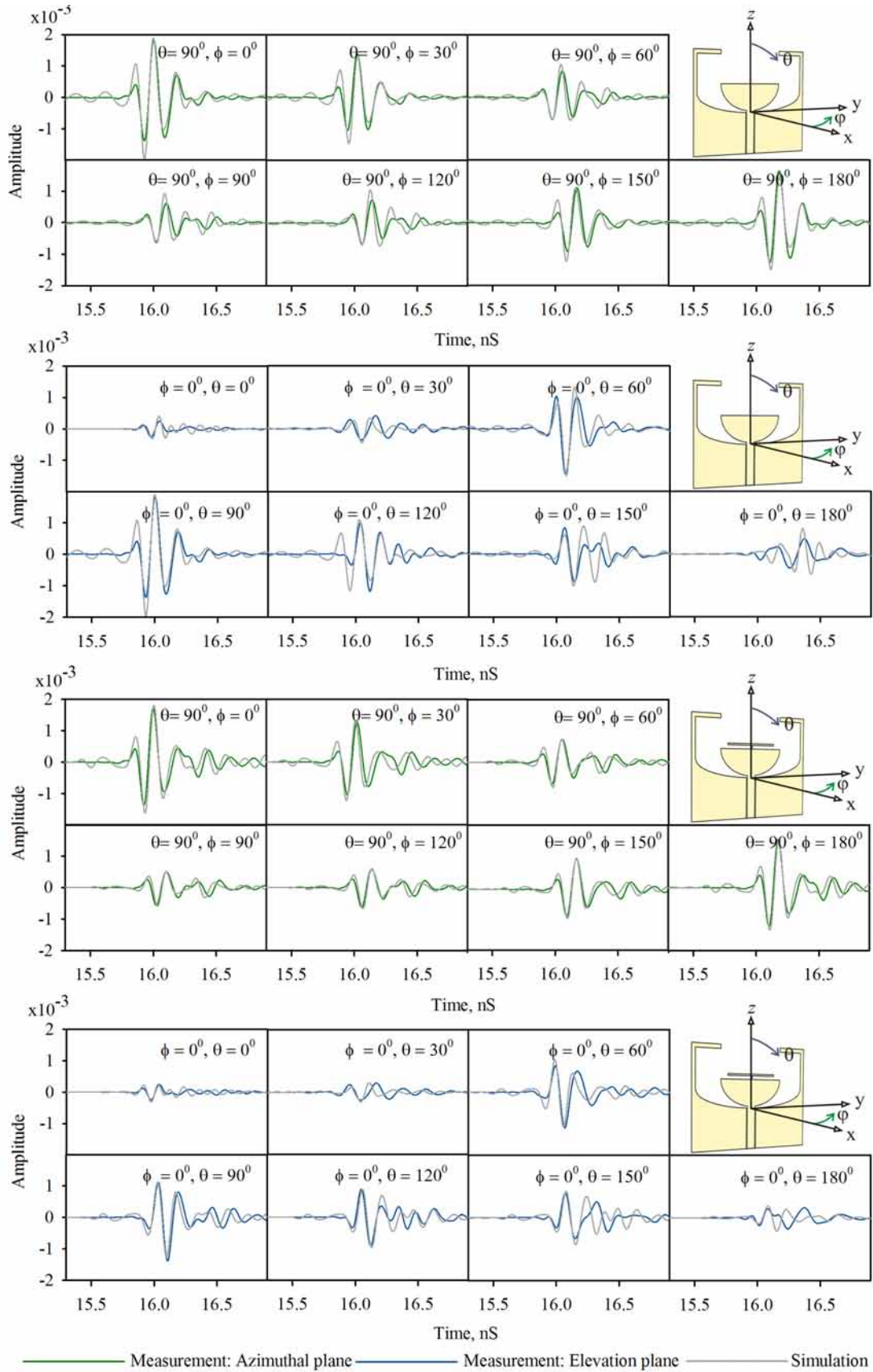
Figure 6.10: Measured and simulated pulses in the azimuthal and elevation planes: Semi–Elliptic Slot antenna without notch and with notch
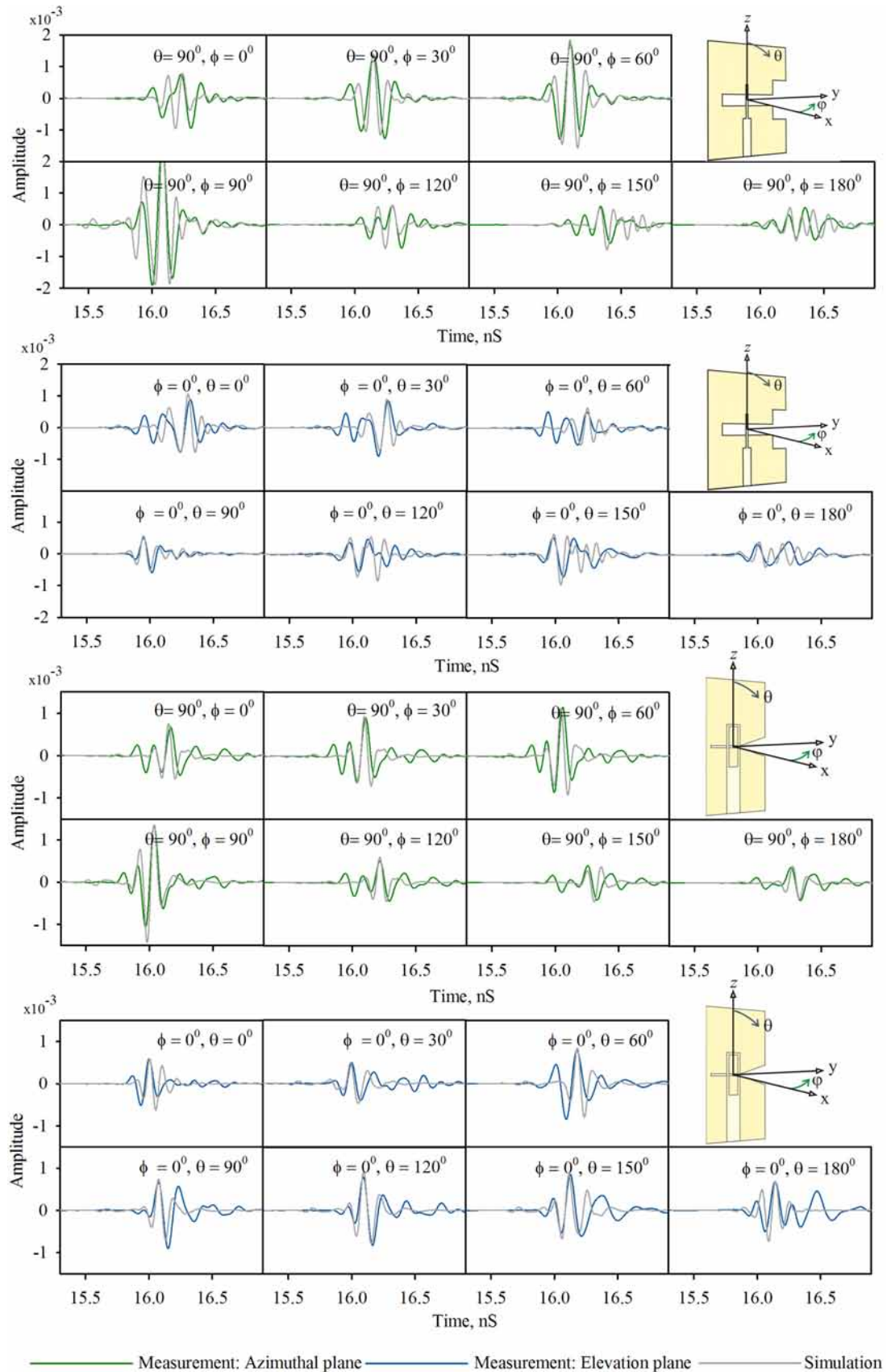
Figure 6.11: Measured and simulated pulses in the azimuthal elevation planes: Step Slot and Tapered Slot antennas

Table 6.1: Measured FWHM, ringing and fidelity in the azimuthal and elevation planes

Angle (φ or θ)	Azimuthal (θ = 90°)						Elevation (φ = 0°)					
	FWHM (pS)		Ringing (pS)		Fidelity (%)		FWHM (pS)		Ringing (pS)		Fidelity (%)	
	Sim.	Meas.	Sim.	Meas.	Sim.	Meas.	Sim.	Meas.	Sim.	Meas.	Sim.	Meas.
Square Monopole												
0°	128.9	176	156.3	296	92	92	189.2	268	289.2	168	79	63
30°	263.2	200	238.5	272	90	89	115.1	208	227.5	272	89	84
60°	159	208	290.6	208	85	83	106.9	168	148	248	85	86.8
90°	142.6	184	298.8	248	84	83.1	128.9	184	156.3	128	92	91.8
120°	159	120	290.6	408	85	83	172.7	272	222	312	74	75
150°	263.2	208	238.5	216	90	88.9	82.25	192	54	136	48	45
180°	128.9	176	156.3	136	92	91.8	175.5	128	104	328	38	28
Sq. Mono. with notch												
0°	274.2	280.3	625.3	654	73	73	587.9	534	394.3	405	58	54
30°	277.2	300.5	631.5	651.7	70	68	415.8	426	320.4	412	60	58
60°	234.1	263	542.1	576	65	63	249.5	265	526.7	589	64	64
90°	203.3	244	539.1	589	60	53	274.2	287.54	625.3	636.5	73	73
120°	234.1	240	542.1	554	65	64	295.7	326	609.9	600	64	51
150°	277.2	312	631.5	650	70	65	338.8	345	594.5	607.43	53	42
180°	274.2	277	625.3	652	73	72	569.4	600	425.1	456	34	27

Table 6.1 – continued from previous page

Angle (φ or θ)	Azimuthal (θ = 90°)						Elevation (φ = 0°)					
	FWHM		Ringing		Fidelity		FWHM		Ringing		Fidelity	
	Sim.	Meas.	Sim.	Meas.	Sim.	Meas.	Sim.	Meas.	Sim.	Meas.	Sim.	Meas.
Semi-Elliptic Slot												
0°	240.2	224	278.7	288	92.5	91.8	169	280	361.8	320	60	60
30°	263.9	248	290.6	312	92	91.7	172	330	284.7	520	61	61.3
60°	281.7	224	279.6	416	91.42	91.8	195.7	232	290.6	416	69	67.7
90°	266.9	248	403.3	456	90.7	90.5	240.2	236	278.7	295	92.5	92
120°	281.7	224	379.6	416	91.42	91.88	364.7	420	243.2	648	70	68
150°	263.9	240	290.6	304	92	91.67	376.6	528	246.1	504	65	64
180°	240.2	208	278.7	264	92.5	91.7	216.5	568	160.1	504	60	58
Semi–Ellip. Slot with notch												
0°	217.6	216	521.7	380	91	91	268.3	340	277.2	560	57	58
30°	232.5	232	521.7	384	90	90	169.9	392	542.5	560	64	64
60°	184.8	232	539.5	464	88	87	187.8	288	530.6	600	86	85
90°	491.9	528	304.1	216	83	80	226.5	200	524.6	384	91	91
120°	184.8	216	539.5	488	88	87	304.1	284	572.3	672	49	51
150°	238.5	240	521.7	392	90	89	357.7	408	554.4	608	45	45
180°	217.6	216	521.7	360	91	91	193.8	520	408.4	504	40	28

Table 6.1 – continued from previous page

Angle (φ or θ)	Azimuthal ($\theta = 90^0$)						Elevation ($\varphi = 0^0$)					
	FWHM		Ringing		Fidelity		FWHM		Ringing		Fidelity	
	Sim.	Meas.	Sim.	Meas.	Sim.	Meas.	Sim.	Meas.	Sim.	Meas.	Sim.	Meas.
Step slot												
0^0	344.4	476	337	320	68	61	166.7	128	396.3	216	82	79.6
30^0	274.1	348	185.2	286	88	76.5	166.7	416	222.2	496	89	88.4
60^0	233.3	304	163	186	92	90.8	288.9	408	170.4	528	82	61.2
90^0	229.6	304	163	178	94	95	344.4	288	337	320	68	61
120^0	233.3	320	163	344	92	91	340.7	264	192.6	488	59	56
150^0	274.1	456	185.2	456	88	76.3	455.6	432	277.8	456	58	55
180^0	344.4	528	337	456	68	60	351.9	432	411.1	440	57.4	54
Linear tapered slot												
0^0	199.6	428	250.5	392	96	95	195.7	128	262.2	96	93	95.73
30^0	191.8	224	262.2	340	97	97.3	266.2	400	387.5	488	91	92
60^0	184	256	262.2	352	97.5	97.45	191.8	264	266.2	680	94	93
90^0	180.1	296	258.3	292	98.5	98	199.6	200	250.5	568	96	95
120^0	184	336	262.2	302	97.5	97.32	262.2	424	293.6	552	94	92
150^0	191.8	344	262.2	412	97	97.28	328.8	504	340.5	496	92	86
180^0	199.6	496	250.5	456	96	95.1	227	560	203.5	544	90	80

The values in Table 6.1 suggests narrow FWHM and low ringing for the linear tapered slot antenna which manifests in high fidelity factor for this antenna. Pulse dispersion and ringing is higher in antennas with band notch resonator due to scattering occurring in the antenna. Of all antennas studied, linear tapered slot antenna has the smallest and simplest configuration and consequently, scattering in the geometry is minimal. From this part of the study it is revealed that simple radiator designs covering the operating band can be preferred for UWB systems than super bandwidth structures with complex impedance matching techniques since they can minimize scattering in the radiator and dispersion of the transmitted/ received waveform.

6.5   Conclusion

In this chapter, transfer properties of the antennas which are studied in the previous chapters are presented. The study reveals a close correspondence between size of the antenna and its performance in the time domain. As the size of the antenna increases, surface currents on different parts of the antenna tend to go out of phase while receiving/ transmitting a signal depending on the spatial orientation of the transmitter/receiver. Electrical length of antennas are larger and the transfer function is no longer flat at the higher operating band (for those spatial orientations). This reflects in the impulse response as a dispersion. Full Width Half Maxima (FWHM) and Ringing quantify dispersion; Fidelity, the cross–correlation between transmitted and received pulses. A comparison reveals minimum FWHM, Ringing and reasonably good Fidelity for the linear Tapered Slot antenna. Square monopole and Semi–Elliptic slot antennas have fractional bandwidth of $\sim 150\%$, while that of the Step slot and Linear Tapered Slot are 114 and 130 respectively. Wider impedance bandwidths are realized in the first two designs at the cost of spatial efficiency. Hence, it can be concluded from the present chapter that, for UWB systems, small element antennas that cover the specified operating band would be a better option than antennas with bandwidth in large excess to the operating band and that consume PCB space.

Chapter 7

Summary and Conclusions

This chapter summarizes and highlights the conclusions drawn from the present study.

7.1   Thesis Summary and conclusions

In this thesis, a comprehensive study on the design, simulation, testing and characterization of UWB antennas is presented taking in to account the extra constraints placed on the antenna design for pulse based operations. Parameters in the frequency and time domains were taken into account in analyzing strengths and weaknesses of the antenna designs.

The four novel antenna designs presented in this thesis, whose impedance bandwidths cover the FCC allocated 3.1–10.6 GHz UWB are: Square Monopole, Semi–Elliptic Slot, Step Slot and Linear Tapered Slot. The study reveals that, key to Ultra Wide Bandwidth lies in the ground–patch interaction and hence, the ground planes are suitably modified to allow a smooth impedance transition from 50Ω to 377Ω.

Square Monopole Antenna This UWB monopole design is arrived from an existing narrow band design by a geometric manipulation of the ground plane, whose design aspects are presented in Chapter 3. As mentioned in the detailed literature review at the beginning of this chapter, there are several design practices to realize UWB in such antennas, which may even complicate the antenna design. In the present work a novel method

is proposed which include inserting cuts in the ground plane which can be mathematically accounted to design the Square Monopole antenna on laminates with any permittivity. In addition, a technique to address the narrow band interference (NBI) issue at the antenna level it self is also presented in this chapter.

Semi–Elliptic Slot Antenna This antenna is a printed version of typical aperture antennas and wide impedance bandwidth and compact size is arrived in this structure by redesigning its the ground plane. Design aspects of this antenna is presented in Chapter 4. Resonances in this geometry is mathematically accounted to allow designing in any microwave laminate and in addition, a technique to avoid NBI is also available.

Step Slot Antenna In the antennas in Chapter 3 and 4, radiation is constituted by both sections on the z–axis of symmetry. Chapter 5 of the thesis analyzes whether radiation is possible if only a single section is present. Two possible geometries titled Step Slot and Linear Tapered slot are presented in Chapter 5. The Step slot antenna is designed with a step like slot aperture at the end of a end shorted slot line, which is fed by a modified microstrip feed.

Linear Tapered Slot Antenna is a modification of the Step slot geometry where the slot aperture and feed architecture are modified to result in a compact as well as radiation efficient structure.

A comparison of the radiation characteristics of the above antennas is presented in Table 7.1. Antennas with band notch resonators have not been included for comparison since their transient characteristics cannot be directly compared with other designs. Widest impedance bandwidth belong to the Semi–Elliptic Slot antenna, which can be attributed to the curved ground–patch design. All antennas are found to offer omnidirectional coverage. However, peak radiation of the step and linear tapered slot geometries are along $\theta = 90^0, \phi = 90^0$, by virtue of their design. Average Gain and Radiation Efficiency in the 3.1–10.6 GHz operating band are almost similar in all cases. Even then, the lowest values

obtained fort the Linear Tapered slot geometry can be justified by its smaller size.

FWHM, Ringing and Fidelity values indicated in the table are for the azimuthal plane of the antennas where radiation is omnidirectional. Nulls in the elevation plane plane patterns have found to impair measurements and due to this, measurements taken in this plane have not been included for comparison. The study reveals that FWHM and Ringing are minimum and Fidelity is maximum in the spatial orientation where the antennas have peak radiation in the plane. For Square monopole and Semi–Elliptic Slot, the maxima and minima in the azimuthal plane are along $\theta = 90^0, \phi = 0^0$ and $\theta = 90^0, \phi = 90^0$. For Step Slot and Linear Tapered Slot, these are along $\theta = 90^0, \phi = 90^0$ and $\theta = 90^0, \phi = 0^0$. Of all antennas, a consistent Fidelity in the azimuthal radiation plane is possessed by the linear tapered slot antenna. For other antennas, there is large difference between the maxima and minima.

This study also reveals that size of the antenna has close correspondence with its time domain performance. A possible reason for this is that as size decreases, phase difference between the surface currents at different parts of the antenna is minimum. Hence, antenna effects on a transmitted/ received pulse is minimum. This is again confirmed by the antenna design presented in Appendix A, which is a monopole design derived from the Square monopole and Semi–Elliptic Slot and which occupies the least PCB space when compared to the designs presented in this thesis.

7.2 Suggestions for Future Work

Based on the conclusions and limitations of the present study, prospects for future works are identified as below.

In this thesis, transient response of the UWB antennas are studied by measurements in the frequency domain followed by a Fourier Transform. The measurements have been performed for discrete steps of 30^0 because of the limitations of the measurement set up. An automated measurement set up may be deviced to take measurements for lesser angles to cover the 3D radiation pattern of the antenna. Also, direct time domain measurements may be performed with a pulse generator and and spectrum analyzer.

Table 7.1: Features of the designed antennas

	Band width (%)	Pattern	Av. Gain (dBi)	Av. Rad. Eff. (%)	FWHM Min.	FWHM Max.	Ringing Min.	Ringing Max.	Fidelity Min.	Fidelity Max.	Size (mm^2)
Sq. Mono.	145	Omni dire.	3.75	86	176	184	248	296	83	92	29.5x32
Semi Ellip.	150	Omni dire.	3.64	87	224	248	288	456	90.5	91.8	34x25
Step Slot	114	Omni dire.	3.16	82	304	476	178	456	60	95	40x33.4
Linear Tap. Slot	130	Omni dire.	2.5	83	296	496	292	456	95	98	30x13.5

All antennas in the thesis have been designed on the lossy Epoxy laminate. Antennas on LTCC substrates may be studied which has the advantage of direct integration with monolithic microwave circuits.

Another interesting work will be the designing of pulse generator and it's integration with the antenna. Prospects of a generator–antenna co–design may be investigated as this approach does away with the need for intermediate transmission lines placed between the RF device/generator and the antenna. This prevents the excitation of common–mode currents and eliminates the need of a balun. The antenna and generator has to be designed taking into account both impedance matching and the generator's influence on the antenna's radiation properties.

Since UWB systems operate with very low power levels, a typical UWB receiver has to have a Low–Noise Amplifier to detect these signals. LNA comes next to the UWB antenna in the system and it has to provide a flat gain response from DC to up-to several GHz, very low signal distortion, low current consumption and high signal voltage gain transfer. Antenna integration with a LNA can be taken as a future investigation.

Using the theory explained in this thesis, channel characterization may be

performed. The antennas presented in this thesis may be redesigned or used as such for applications such as microwave imaging which has full fledged facility available at our research center.

Appendix A

The Rectangular Strip Monopole Antenna

Antenna geometries affect the radiated pulse wave forms according to the propagation of surface currents on them. Significant phase differences in the surface currents during transmission or reception spread a nano second pulse in the time domain. Studies presented in this thesis reveals the superior characteristics of electrically small antennas in handling nano second pulses due to their stable radiation patterns with minimum and distortion at higher frequencies. In addition, they fit perfectly well to space constrained applications such as a wireless dongle or the emerging WiMedia systems [Jinwoo Jung, 2008], [Jung J., 2008], [Wu & Ronghong Jin, 2008], [Jaewoong Shin, 2009].

Here, we present the design of a novel UWB monopole antenna and its characterization in the frequency and time domains. Design aspects and radiation mechanisms [Gopikrishna M., 2007] and [Gopikrishna M., 2009] have been contemplated in designing the present structure. To generate multiple resonances in this small element radiator, a wide gap is set between the patch and the ground plane. An impedance transformer designed in the ground plane prevent standing waves in the feeding structure allowing wide impedance bandwidth from 2.85 – 14.25 GHz.

A.1 Antenna Structure

The schematic diagram of the rectangular strip monopole antenna is shown in Figure A.1(a).
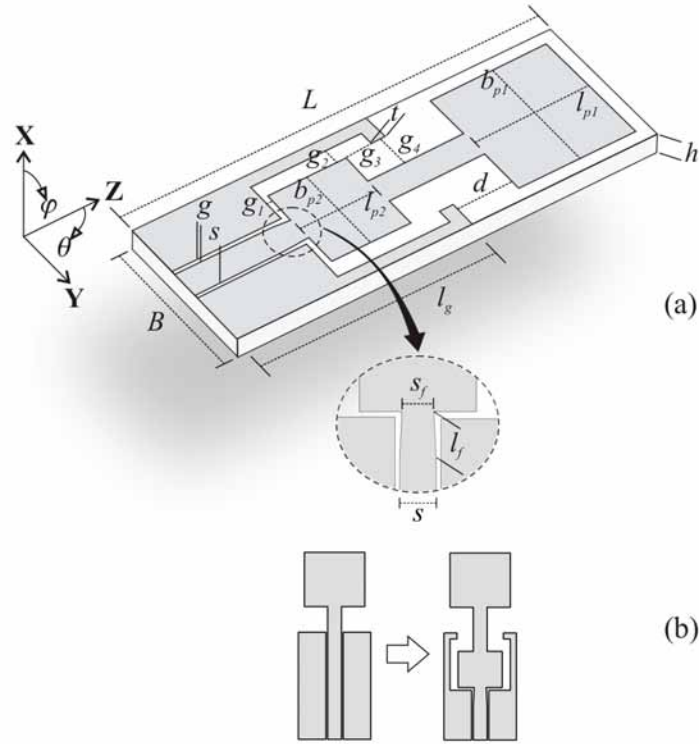

Figure A.1: (a) Configuration of the proposed antenna (b) design evolution

The basic rectangular strip monopole is shown in Figure A.1(b), where the dimensions are l_{p1}= 9 mm, b_{p1}= 10 mm, d= 4.25 mm and l_g = 17.75 mm when designed on a substrate with permittivity ε_r = 4.4 and height h = 1.6 mm and loss tangent 0.02. The coplanar feed dimensions for 50 Ω impedance are s = 2.3 mm and g = 0.28 mm. This configuration exhibits three resonances as shown in Table A.1. A variation study in d indicates that coupling to the radiator is strongly depended on this parameter. To facilitate a gradual impedance transformation that result in broadband impedance matching between the CPW line and the patch, the ground plane is designed with increasing slot widths g_1, g_2, g_3 and g_4. A slight mismatch at the lower frequencies is attended by designing a taper with parameters s_p and l_f. The geometric parameters of the proposed UWB design is :
l_{p2} = 6 mm, b_{p2} = 7.3 mm, g_1 = 0.45 mm, g_2 = 1.35 mm, g_3 = 2 mm, g_4 = 2.7

mm, $t = 1\ mm$, $s_f = 2\ mm$ and $l_f = 3\ mm$. With these, the antenna geometry is restricted to 30x12 mm^2.

A.2 Results

The reflection coefficient measurement indicate broad impedance bandwidth from 2.85-14.25 GHz and is shown in Figure A.2. The simulated resonances are in good agreement with the measurement.

Measured radiation patterns at 3.15, 6.77, 10 and 13.3 GHz are shown in Figure A.3(a) and (b). The radiation patterns remain stable and omni–directional throughout the available bandwidth and pattern degradation at the higher frequency bands is minimal. Cross–polar level is better than –20 dB in the 3.1–10.6 GHz band and the antenna polarization is in the Z direction. In this band, an average gain of 2.24 dBi is observed with ≈0.75 dBi of gain fluctuation.

High fidelity reception or transmission of a wide–band signal is dependent upon the antenna geometry and due this, antennas that are well matched in the frequency domain may behave differently in the time domain. The time domain characterization of the rectangular strip monopole antenna is performed after measurements in the frequency domain, a detailed account of which can be referred in Duroc & Tedjini [2007]. The reference antenna is a wide band ridged horn, which is standardized using an identical pair. Once this is done, the transmitter is fixed and the wide band ridged horn at the receiving end is replaced with the test antenna and the transmission coefficient is measured for its multiple orientations. The measured antenna transfer function of the test antenna in the azimuthal and elevation planes are respectively shown in Figure A.4(a) and (b). The azimuthal transfer functions are constant with variation remaining within 10 dB while that measured for the elevation plane shows large variations at certain frequencies. The corresponding impulse responses are shown in Figure A.5(a) and (b) which is obtained by performing an inverse fourier transform of the measured antenna transfer function. Full Width Half Maxima (FWHM) of the impulse response is constant at all angles in the azimuthal plane and ringing is minimal as shown in Table A.2.

To study the waveform distortion caused by the antenna, measured impulse response is convoluted with the fourth derivative of a gaussian pulse which complies
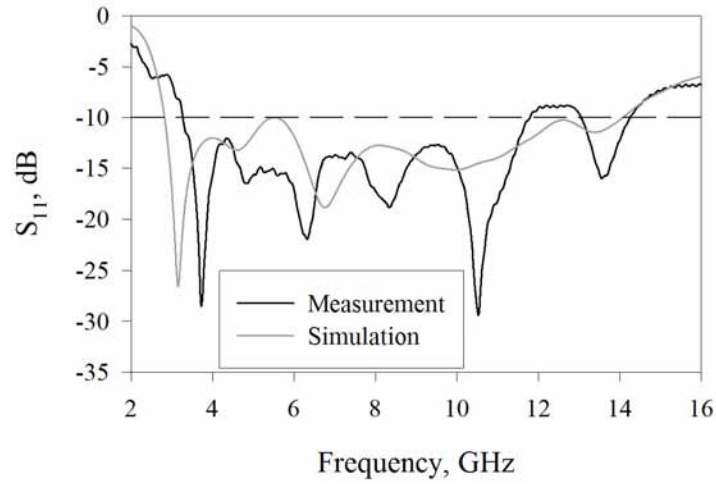
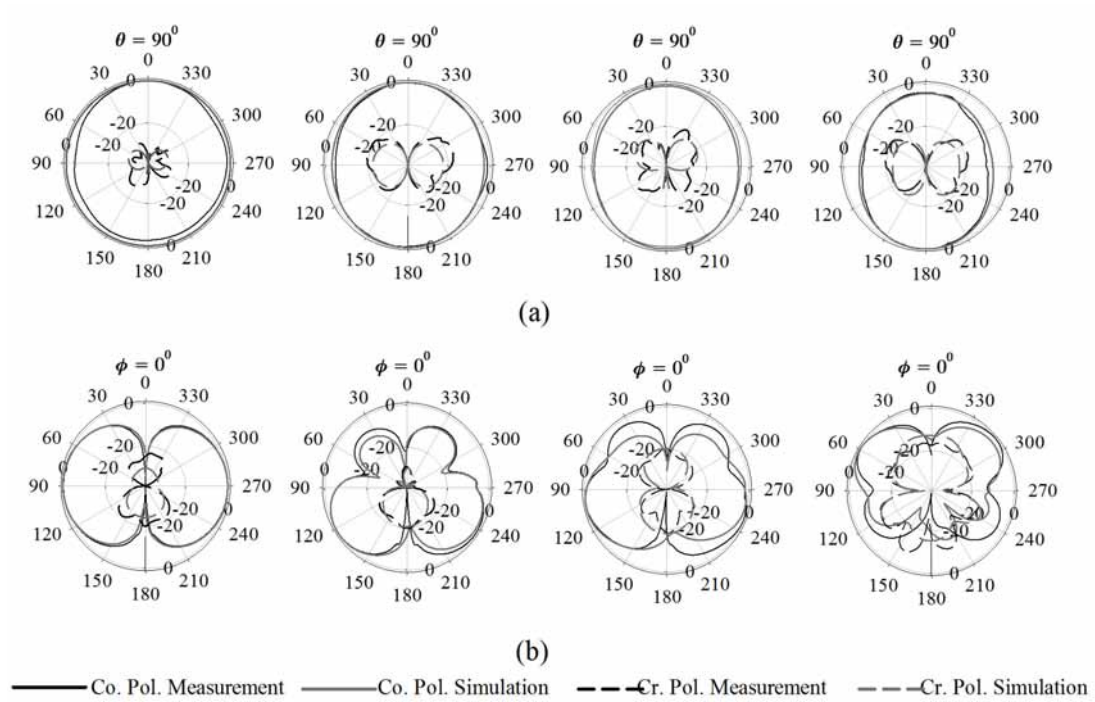Figure A.2: Measured and simulated reflection coefficient $|S_{11}|$

Figure A.3: Measured and simulated radiation patterns in the (a) azimuthal (X-Y) (b) elevation (X-Z) plane at 3.15, 6.77, 10 and 13.3 GHz
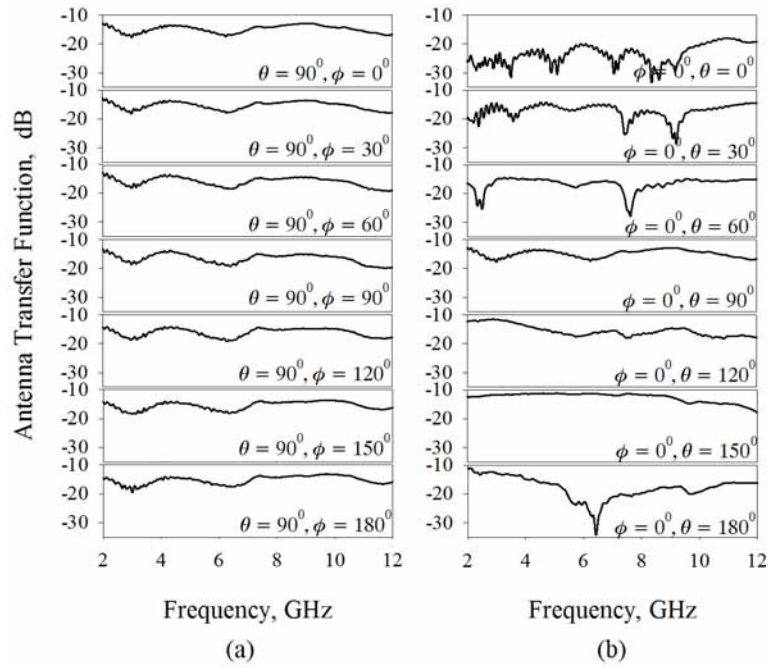
Figure A.4: Antenna transfer function measured in the (a) azimuthal (X-Y) (b) elevation (X-Z) planes for multiple orientations of the test antenna
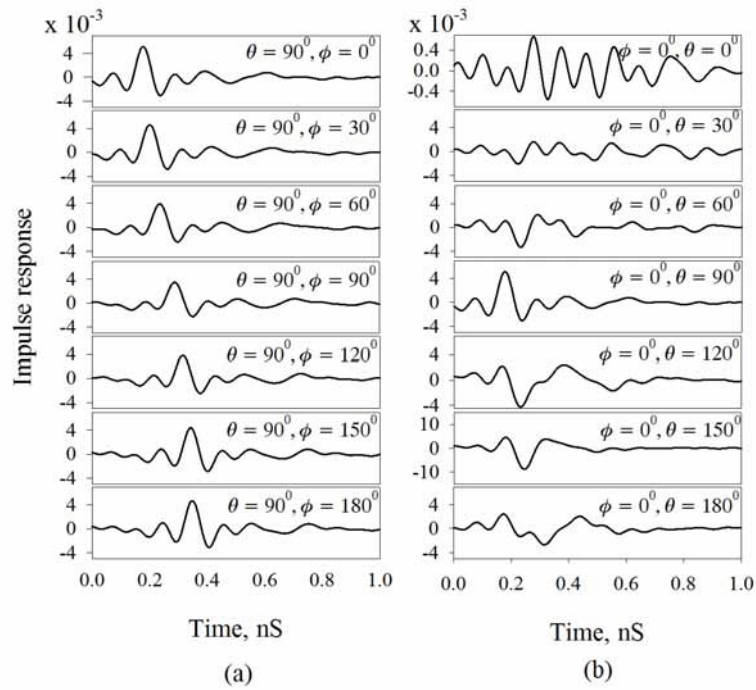

Figure A.5: Antenna impulse response measured in the (a) azimuthal (X-Y) (b) elevation (X-Z) planes for multiple orientations of the test antenna

Table A.1: Dependence of the resonances on parameter d (*Fig.A.1(b)*)

d	Resonances	Matching
(mm)	(GHz)	(dB)
0.25	4.16	–6.8
	8.6	–6
2.25	3.77	–12.7
	7	–25.76
	9.6	–17
4.25	3.34	–13.4
	6.3	–10.85
	9.6	–7.8
6.25	3	–13.4
	6	–6.4
	9.6	–5.4

Table A.2: Measured FWHM, ringing and fidelity in the azimuthal and elevation planes for the rectangular strip monopole antenna

Angle	Azimuthal ($\theta = 90^0$)			Elevation ($\varphi = 0^0$)		
(φ or θ)	FWHM	Ringing	Fidelity	FWHM	Ringing	Fidelity
	(pS)	(pS)	(%)	(pS)	(pS)	(%)
0^0	128	88	94	200	304	38
30^0	120	88	93.57	104	176	32
60^0	128	88	93	128	208	62.5
90^0	120	72	92.1	128	88	94
120^0	128	88	92	376	224	85.57
150^0	128	88	92.6	144	120	78.39
180^0	136	88	93.77	216	144	50.27

with the FCC spectral emission mask. Good cross–correlation is observed between the template and received pulses as indicated by the fidelity values in Table A.2.

A.3 Conclusion

In this work, we have designed a small element UWB antenna with superior radiation characteristics. The present work unearths a connection between the size of a monopole antenna and it's far field radiation. As the antenna size shrinked, the radiation pattern remained omni–directional even at it's highest frequencies of operation which again reflected in it's time domain performance. Measured FWHM is narrow, ringing is less compared to other antennas in this thesis and the pulse fidelity is constant in the entire azimuthal plane. Even though small element antennas have these advantages compared to their larger counter parts, the design of such antennas has to be done with special care, otherwise the finite ground plane effects of the antenna may become an issue during measurements in the lab or practical installation in an equipment.

References

DUROC, Y., GHIOTTO A. VUONG T. P., & TEDJINI, S. 2007. Uwb antennas: Systems with transfer function and impulse response. *IEEE Transaction on Antennas and Propagation*, **55**(5), 1449–1451. 133

GOPIKRISHNA M., DEEPTI DAS KRISHNA, ANUPAM R. CHANDRAN C. K. AANANDAN. 2007. Square monopole antenna for ultra wide band communication applications journal of electromagnetic waves and applications. *Journal of Electromagnetic Waves and Applications*, **21**(11), 1525–1537. 131

GOPIKRISHNA M., DEEPTI DAS KRISHNA, C. K. AANANDAN P. MOHANAN K. VASUDEVAN. 2009. Design of a compact semi-elliptic monopole slot antenna for UWB systems. *IEEE Transactions on Antennas and Propagation*, **57**(6), 1834–1837. 131

JAEWOONG SHIN, SEOKJIN HONG, JAEHOON CHOI. 2009. A compact ultrawideband monopole antenna for wireless communication application. *Ieee tranactions on antennas and propagation*, **57**(9), 2875–2788. 131

JINWOO JUNG, HYEONJIN LEE, YEONGSEOG LIM. 2008. Band notched ultra wideband internal antenna for USB dongle application. *Microwave and Optical Technology Letters*, **50**(7), 1789–1793. 131

JUNG J., H. LEE, Y. LIM. 2008. Compact band–notched ultra–wideband antenna. *IEE Electronics Letters*, **44**(6). 131

Wu, Qi, & Ronghong Jin, Junping Geng, Min Ding. 2008. Printed omni–directional
   UWB monopole antenna with very compact size. *IEEE Transactions on Antennas and
   Propagation*, **56**(3), 896–899. 131

Publications relevant to the thesis

Chapter 3

M. GOPIKRISHNA, DEEPTI DAS KRISHNA, A. R. CHANDRAN and C. K. AANAN-DAN *Square monopole antenna for ultra wide band communication applications* Journal of Electromagnetic Waves and Applications, 21(11), 2007, 1525-1537

M. GOPIKRISHNA, DEEPTI DAS KRISHNA, ANUPAM R. CHANDRAN and C. K. AANANDAN *5GHz WLAN band notched square monopole antenna for UWB systems* Proceedings of the National Symposium on Antennas and Propagation (APSYM 2006), 2006, 47-50

Chapter 4

GOPIKRISHNA M., DEEPTI DAS KRISHNA, C. K. AANANDAN, P. MOHANAN and K. VASUDEVAN *Design of a Compact Semi-elliptic Monopole Slot Antenna for UWB Systems* IEEE Transactions on Antennas and Propagation, 57(6), June 2009, 1834-1837

M. GOPIKRISHNA, DEEPTI DAS KRISHNA and C. K. AANANDAN *A Semi-Elliptic Slot Antenna for UWB Applications* 5th IASTED International Conference on Antennas, Radar and Wave Propagation, 2008, 431-435

M. GOPIKRISHNA, DEEPTI DAS KRISHNA and C . K. AANANDAN *Band Notched Semi-elliptic Slot Antenna for UWB Systems* 38th European Microwave Conference (EuMC), 2008, 889-892

Chapter 5

GOPIKRISHNA M., DEEPTI DAS KRISHNA, C. K. AANANDAN, P. MOHANAN and K. VASUDEVAN *Design of a microstrip fed step slot antenna for UWB communications* Microwave and Optical Technology Letters, Wiley Interscience, 51(4), April 2009, 1126-1129

M. GOPIKRISHNA, DEEPTI DAS KRISHNA and C. K. AANANDAN *Design of a Microstrip-fed stepped slot for UWB Communications* IEEE Antennas and Propagation Symposium (IEEE-APS), 2008, 1098-1102

GOPIKRISHNA M., DEEPTI DAS KRISHNA, C. K. AANANDAN, P. MOHANAN and K. VASUDEVAN *Compact Linear Tapered Slot Antenna for UWB Applications* Electronics letters, Institution of Engineering and Technology, 44(20), 25th Sept. 2008

Publications by the Author

<u>In International Journals</u>

ANUPAM R. CHANDRAN, **M. GOPIKRISHNA**, C. K. AANANDAN, P. MOHANAN and K. VASUDEVAN *Radar cross section enhancement of dihedral corner reflector using fractal based metallo-dielectric structures* Electronics letters, 42(20), Sept., 2006

DEEPTI DAS KRISHNA, **M. GOPIKRISHNA**, C. K. AANANDAN, P. MOHANAN and K. VASUDEVAN *Compact Dual-Polarized Square Microstrip Antenna with Triangular Slots for Wireless Communication* Electronics letters, Institution of Engineering and Technology, 42(16), Aug., 2006

ANUPAM R. CHANDRAN, **M. GOPIKRISHNA**, C. K. AANANDAN, P. MOHANAN and K. VASUDEVAN *Scattering Behavior of Fractal Based Metallo-Dielectric Structures* Progress in Electromagnetic Research, 63, 2007, 323-339

M. GOPIKRISHNA, DEEPTI DAS KRISHNA, A. R. CHANDRAN and C. K. AANANDAN *Square monopole antenna for ultra wide band communication applications* Journal of Electromagnetic Waves and Applications, 21(11), 2007, 1525-1537

DEEPTI DAS KRISHNA, **M. GOPIKRISHNA**, C. K. AANANDAN, P. MOHANAN and K. VASUDEVAN *Planar Elliptic UWB antenna with Band-Notch Characteristics* International Journal on Wireless & Optical Communications (IJWOC), World Scientific, 4, 2007, 1-12

GOPIKRISHNA M., DEEPTI DAS KRISHNA, C. K. AANANDAN, P. MOHANAN and K. VASUDEVAN *Design of a Compact Semi-elliptic Monopole Slot Antenna for UWB Systems* IEEE Transactions on Antennas and Propagation, 57(6), June 2009, 1834-1837

DEEPTI DAS KRISHNA, **M. GOPIKRISHNA**, C. K. AANANDAN, P. MOHANAN and K. VASUDEVAN *Compact Wide Band Koch Fractal Printed Slot Antenna* Microwaves Antennas & Propagation, Institution of Engineering Technology (IET), 3(5), 2009, 782-789

GOPIKRISHNA M., DEEPTI DAS KRISHNA, C. K. AANANDAN, P. MOHANAN and

K. VASUDEVAN *Compact Linear Tapered Slot Antenna for UWB Applications* Electronics letters, Institution of Engineering and Technology, 44(20), 25th Sept. 2008

R. GAYATHRI, T. U. JISNEY, DEEPTI DAS KRISHNA, **M. GOPIKRISHNA** and C. K. AANANDAN *Band-notched inverted-cone monopole antenna for compact UWB systems* Electronics letters, Institution of Engineering and Technology, 44(20), 25th Sept. 2008, 1170-1171

DEEPTI DAS KRISHNA, **M. GOPIKRISHNA**, C. K. AANANDAN, P. MOHANAN and K. VASUDEVAN *Ultra-wideband slot antenna for wireless USB dongle applications* Electronics letters, Institution of Engineering and Technology, 44(18), 28th Aug. 2008

GOPIKRISHNA M., DEEPTI DAS KRISHNA, C. K. AANANDAN, P. MOHANAN and K. VASUDEVAN *Design of a microstrip fed step slot antenna for UWB communications* Microwave and Optical Technology Letters, Wiley Interscience, 51(4), April 2009, 1126-1129

DEEPTI DAS KRISHNA, **M. GOPIKRISHNA**, C. K. AANANDAN, P. MOHANAN and K. VASUDEVAN *CPW-Fed Koch Fractal Slot Antenna for WLAN/WiMAX Applications* Antennas and Wireless Propagation Letters (AWPL), 7, 2008, 389-392

DEEPTI DAS KRISHNA, **M. GOPIKRISHNA**, C. K. AANANDAN, P. MOHANAN and K. VASUDEVAN *Ultra-wideband Slot Antenna with Band-notch Characteristics for Wireless USB Dongle Applications* Microwave and Optical Technology Letters (MOTL), Wiley Interscience, 51(6), 2009, 1500-1504

<div align="center">In International Conferences</div>

DEEPTI DAS KRISHNA, **M. GOPIKRISHNA**, C. K. AANANDAN, P. MOHANAN and K. VASUDEVAN *Square Patch Antenna with a Bow-Tie Slot for Dual Port Operation* International Conference on Microwaves, Antenna, Propagation and Remote Sensing (ICMARS), 2006, 14-18

M. GOPIKRISHNA, DEEPTI DAS KRISHNA and C. K. AANANDAN *A Semi-Elliptic Slot Antenna for UWB Applications* 5th IASTED International Conference on Antennas, Radar and Wave Propagation, 2008, 431-435

M. GOPIKRISHNA, DEEPTI DAS KRISHNA and C. K. AANANDAN *A Compact Wide-band Koch Fractal Printed Slot Antenna for WLAN Applications* 5th IASTED International Conference on Antennas, Radar and Wave Propagation, 2008, 444-448

M. GOPIKRISHNA, DEEPTI DAS KRISHNA and C . K. AANANDAN *Band Notched Semi-elliptic Slot Antenna for UWB Systems* 38th European Microwave Conference (EuMC), 2008, 889-892

DEEPTI DAS KRISHNA, **M. GOPIKRISHNA** and C. K. AANANDAN *A CPW-fed Triple Band Monopole Antenna for WiMAX/WLAN Applications* 38th European Microwave Conference (EuMC), 2008, 897-900

M. GOPIKRISHNA, DEEPTI DAS KRISHNA and C. K. AANANDAN *Design of a Microstrip-fed stepped slot for UWB Communications* IEEE Antennas and Propagation Symposium (IEEE-APS), 2008, 1098-1102

<u>In National Conferences</u>

DEEPTI DAS KRISHNA, **M. GOPIKRISHNA**, C. K. AANANDAN, P. MOHANAN, and K. VASUDEVAN *Electronically Switchable Compact Microstrip Antenna with Triangular Slots for Dual port operation* Proceedings of the National Symposium on Antennas and Propagation (APSYM 2006), 2006, 55-58

M. GOPIKRISHNA, DEEPTI DAS KRISHNA, ANUPAM R. CHANDRAN and C. K. AANANDAN *5GHz WLAN band notched square monopole antenna for UWB systems* Proceedings of the National Symposium on Antennas and Propagation (APSYM 2006), 2006, 47-50

Resume of the Author

EDUCATION

2005-, Cochin University of Science and Technology, Cochin
Doctoral degree in Microwave Electronics

2003 -2004 , Cochin University of Science and Technology, Cochin
M Phil in Physics

1999 - 2002, Cochin University of Science and Technology, Cochin
M Sc in Physics with specialization in Electronics

1996 - 1999, Union Christian College, Aluva
BSc in Physics

1994 - 1996, Union Christian College, Aluva
Pre - Degree in Group 2 with optional Mathematics

1993 - 1994, Govt. Model High School, Thiruvanathapuram, SSLC

AWARDS RECEIVED

Received Junior Research Fellowship (JRF) from UGC-CSIR in 2004

PROFICIENCY IN COMPUTERS

Operating system- Windows
Languages- Fortran, C, C++
Softwares- Matlab, Mathematica, Visual C++
EM Simulation Tools- Ansoft HFSS, CST Microwave Studio, Zeland IE3D,
Agilent ADS

RESEARCH INTERESTS

Design and characterization of antennas for WLAN, UWB; RCS measurements.

Finite Difference Time Domain (FDTD) techniques for antenna problems.

BST based microwave devices (Have been part of a UKIERI (UK India Education Research Initiative, funded by the British Council) project between University of Surrey, UK and CUSAT to design a novel millimeter wave phase shifter for beam steering.)

PUBLICATIONS

Journals – 13
Conferences – 7
Monographs – Co–Authored "A Course in Information Technology for Graduates"

PERSONAL DETAILS

Nationality- Indian
Father's Name and Occupation- K. V. Madanan, Director of Public Instructions (Retd.)
Religion- Hindu
Date of Birth- 26/08/1978
Passport No.- E7480653
Languages - English, Malayalam, Hindi
Place of permanent residence- Aluva, Ernakulam (Dist.), India

REFERENCES

Dr. C. K. Aanandan (Supervisor)
Professor
Dept. of Electronics
Cochin University of Science and Technology
Cochin, India 682 022
E Mail: anand@cusat.ac.in
Mob: +91-09447667267
Tel: +91-484-2576418
Fax: +91-484-2575800

Dr. P. Mohanan
Professor
Dept. of Electronics
Cochin University of Science and Technology
E Mail: drmohan@cusat.ac.in
Mob: +91-09447325765
Tel: +91-484-2576418

	Cochin, India 682 022	Fax: +91-484-2575800
Dr. K. Vasudevan	Professor	E Mail: vasuvevan@cusat.ac.in
	Dept. of Electronics	Mob: +91-09447357328
	Cochin University of Science and Technology	Tel: +91-484-2576418
	Cochin, India 682 022	Fax: +91-484-2575800
Dr. Ramesh Babu T.	Professor	E Mail: rbt@cusat.ac.in
	Dept. of Physics	Tel: +91-484-2576418
	Cochin University of Science and Technology	Fax: +91-484-2575800
	Cochin, India 682 022	

Index